In-cycle control of the

extrusion blow molding process

Gino Lalli

Department of Electrical and Computer Engineering
Centre for Intelligent Machines – Systems and Control Group
Industrial Automation Lab
McGill University, Montreal, Canada
December 2004

A thesis submitted to McGill University in partial fulfillment of the requirements of a Masters degree in Electrical and Computer Engineering

Your file Votre référence
ISBN: 978-0-494-25297-0
Our file Notre référence
ISBN: 978-0-494-25297-0

Abstract

Parison length control in extrusion blow molding of plastic parts has been studied and attempted for the past quarter-century. Most methods used involve *cycle-to-cycle* control where the next part shows an improvement over the previous one using either weight measurement of the part or a simple photocell initiating the cutting of the parison. In the present thesis, plant models are developed using a control engineering technique called system identification. Since the process model thus determined is based on experimental data, sag and swell of the parison are implicitly taken into account. Furthermore, an in-cycle robust controller is designed and simulated where the die gap opening and the extrusion speed are adjusted as the parison is being extruded. The outlined control strategy focuses on controlling the parison length against process disturbances and machine drifts. The control system thus obtained is then reduced to two single-input single-output controllers for potential implementation on the extruder machine employed throughout the research.

Résumé

Le contrôle de la longueur de la paraison utilisée dans le moulage par extrusion et soufflage de pièces de plastique a été le sujet de plusieurs études pendant les 25 dernières années. Les méthodes ainsi suggérées sont basées sur un contrôle *cycle-en-cycle* ayant pour objectif d'améliorer la pièce suivante, et ceci en mesurant le poids de la pièce ou en utilisant une cellule photo-électrique qui déclenche le sectionnement de la paraison. Dans la présente thèse, les modèles du procédé sont établis à l'aide de la technique nommée 'identification des systèmes'. Puisque le modèle du processus ainsi déterminé est basé sur des mesures expérimentales, l'affaissement et le gonflement de la paraison sont implicitement inclus. En plus, un contrôleur robuste à deux entrées et une sortie dans lequel l'ouverture de la filière et la vitesse d'extrusion sont ajustées, est comissioné et simulé. La stratégie de la commande aura pour objet d'ajuster la longueur de la paraison en dépit des pertubations et des variations. Finalement, le système de contrôle est réduit à deux systèmes à une entrée, une sortie pour fin d'implémentation sur la machine extrudeuse utilisée dans cette recherche.

Acknowledgements

First and foremost, I would like to thank Professor Benoit Boulet, whose patience and guidance have been invaluable throughout my graduate career. He was successful in providing direction while encouraging independence. I am indebted to him. This work would also not have been possible without the help of Ammar Haurani. He was selfless in sharing with me his wealth of knowledge in control theory.

I am grateful to the CNRC-NRC IMI for providing me with all the tools necessary to perform the experimental tests. I owe a great deal to many of the IMI employees Dr. Robert Di Raddo for his guidance and experience, Linda Pecora, Benoit Lanctot, Patrick Girard and Mitra Yousefi have all been particularly helpful and generous with their time and expertise. I must not forget Christian DeGrandpre and Marc-Andre Rainville for continuously fielding my numerous questions in the lab.

I would also like to thank all my friends for their continuous support. I'd especially like to thank my dear friend and future business partner Mark Ajersch for his efforts in proofreading my thesis.

Finally, I am forever indebted to my parents, Lise and Orfelio and to my beautiful fiancée Nina for their understanding, endless patience and encouragement when it was most required.

Table of Contents

ABSTRACT II

ACKNOWLEDGEMENTS IV

LIST OF FIGURES VII

LIST OF TABLES IX

NOMENCLATURE X

1 INTRODUCTION 1

1.1 THESIS OBJECTIVE 1
1.2 BENEFITS TO INDUSTRY 2
1.3 LITERATURE REVIEW 3
1.3.1 Modeling of the EBM Process 3
1.3.2 EBM Closed-Loop Control 4
1.3.3 Parison Length Control 5

2 BLOW MOLDING PROCESS 6

2.1 EXTRUSION VS. INJECTION VS. STRETCH 6
2.2 HISTORY 7
2.3 MARKETS 8
2.4 DIFFERENT STAGES OF EBM 10
2.5 EXTRUDER 12
2.5.1 Continuous vs. Intermittent 12
2.5.2 Resin Description 15
2.5.3 Die Head Description 15

3 THEORETICAL MODEL 18

3.1 CONTROL SYSTEM MODELS 18
3.2 MASTER FORMULA DERIVATION 18
3.3 SIMULINK MODEL 'A' 22
3.4 EXPERIMENTAL PROTOCOL 24
3.5 THEORETICAL VS. EXPERIMENTAL 27
3.6 MODEL IMPROVEMENTS NEEDED 28

4 EXPERIMENTAL MODELS 30

4.1 EXPERIMENTAL PROTOCOL 30
4.1.1 Photron Motion Tools Software 32
4.1.2 Input vs. Output 33
4.2 SIMULINK MODEL 'B' 33
4.3 GAIN MATRIX 37
4.4 MODEL 'C' 39
4.4.1 Simulink 39
4.4.2 Model 'C' Validation 40
4.5 OUTPUT ABNORMALITIES 44
4.5.1 Abnormality in Region 1 44
4.5.2 Abnormality in Region 2 47
4.5.3 Abnormalities in Region 3 and 4 48
4.6 INPUT SIGNAL CHANGES 50
4.7 MODEL 'D' 52
4.7.1 Simulink 52
4.7.2 Model 'D' Validation 54
4.8 RPM GAINS 59

4.8.1 'Family' of Inputs *60*
4.8.2 RPM Gain Relationship *64*
4.9 MODEL 'E' 67
5 CONTROLLER DESIGN 68
5.1 CLOSED-LOOP CONTROL 71
5.1.1 Desired Length Profile 1 ..... *76*
5.1.2 Desired Length Profile 2 ..... *78*
5.1.3 Desired Length Profile 3 ..... *80*
5.2 SINGLE-LOOP CONTROL SYSTEMS 83
5.2.1 'Relaxed' Extruder Speed Loop *84*
5.2.2 'Relaxed' Die Gap Loop *87*
5.3 BATTENFELD EBM MACHINE 90
6 CONCLUSION 94
6.1 SUMMARY 94
6.2 RECOMMENDATIONS AND FUTURE WORK 95
7 BIBLIOGRAPHY 97
8 APPENDIX A: BLOW MOLDING TIME LINE 100
9 APPENDIX B: HDPE 1000 PROPERTIES (PETROMONT) 101
10 APPENDIX C: OPTIKON PCI FASTCAM 102
11 APPENDIX D: COMPLETE LIST OF INPUT SIGNALS 103
12 APPENDIX E: PID CONTROLLERS 105

List of Figures

FIGURE 2-1: PARISON FORMATION STAGE 10
FIGURE 2-2: FINAL PART AFTER EBM STAGES 11
FIGURE 2-3: BATTENFELD EXTRUDER 13
FIGURE 2-4: OPERATOR CONSOLE (MACO 8000) 14
FIGURE 2-5: SECTION VIEW OF THE DIE HEAD 16
FIGURE 2-6: TOP VIEW (LEFT), FRONT VIEW (MIDDLE), 3D VIEW (RIGHT) OF A EXTRUSION DIE 17
FIGURE 3-1 'STEEL' PARISON 19
FIGURE 3-2: MASS FLOW RATE VS. RPM 21
FIGURE 3-3: INITIAL SIMULINK MODEL 'A' 22
FIGURE 3-4: THEORETICAL LENGTH OF 'STEEL' PARISON 23
FIGURE 3-5: EXPERIMENTAL SET-UP AT CNRC-NRC IMI 25
FIGURE 3-6: CAMERA VIEW OF THE BATTENFELD MACHINE 26
FIGURE 3-7: THEORETICAL VS. EXPERIMENTAL LENGTH (H_0 = 90%, RPM = 55) 27
FIGURE 3-8: BOTTLES PRODUCED BY THE BATTENFELD EBM MACHINE 29
FIGURE 4-1: EXAMPLE OF INPUT PARISON PROGRAMMING PROFILE 31
FIGURE 4-2: EXPERIMENTAL LENGTH FOR 95% → 20% AND RPM = 55 31
FIGURE 4-3: SNAP SHOT OF VIDEO AT T = 1 SEC 32
FIGURE 4-4: INPUT (95% → 20%) VS. PARISON LENGTH 33
FIGURE 4-5: SIMULINK MODEL 'B' 34
FIGURE 4-6: MODEL 'B' OUTPUT VS EXP LENGTH FOR 95% → 20% AND RPM = 55 34
FIGURE 4-7: MODEL 'B' FOR 20% → 80% INPUT SIGNAL 35
FIGURE 4-8: PARISON PROGRAMMING PROFILE FOR 20% → 80% 36
FIGURE 4-9: MODEL 'B' OUTPUT VS. EXP LENGTH FOR 20% → 80% AND RPM = 55 36
FIGURE 4-10: GAIN MATRIX CURVES 39
FIGURE 4-11: LUT PARAMETER SCREEN 40
FIGURE 4-12: SIMULINK MODEL 'C' 40
FIGURE 4-13: EXP VS. MODEL 'C' OUTPUT FOR 95% → 20% WITH RPM = 55 41
FIGURE 4-14: EXP VS. MODEL 'C' OUTPUT FOR 15% → 75% WITH RPM = 45 42
FIGURE 4-15: EXP VS. MODEL 'C' OUTPUT FOR 55% → 20% WITH RPM = 50 42
FIGURE 4-16: ERROR COMPARISONS FOR MODEL 'C' 43
FIGURE 4-17: EXPERIMENTAL OUTPUT FOR 95% → 20% WITH RPM = 55 44
FIGURE 4-18: REGION 1 ABNORMALITY (CLOSE-UP) 45
FIGURE 4-19: MACHINE RECOIL FOR INPUT OF 95% → 20% WHILE EXTRUDER TURNED OFF 46
FIGURE 4-20: DIE GAP DIFFERENCES 47
FIGURE 4-21: REGION 2 ABNORMALITY (CLOSE-UP) 48
FIGURE 4-22: REGION 3 ABNORMALITY (CLOSE-UP) 49
FIGURE 4-23: REGION 4 ABNORMALITY (CLOSE-UP) 50
FIGURE 4-24: INPUT PARISON PROGRAMMING PROFILE FOR 95% → 20% AND RPM = 55 51
FIGURE 4-25: SLEWED INPUT FOR 95% → 20% 51
FIGURE 4-26: SLEWED VS. SQUARE INPUT SIGNAL FOR 95% → 20% 52
FIGURE 4-27: MORE DETAILED LUT 53
FIGURE 4-28: MODEL 'D' IN SIMULINK 54
FIGURE 4-29: EXP VS. MODEL 'D' FOR 95% → 20% AND RPM = 55 55
FIGURE 4-30: MODEL 'D' ERROR SIGNAL FOR 95% → 20% AND RPM = 55 55
FIGURE 4-31: MODEL 'C' AND MODEL 'D' ERRORS FOR 95% → 20% AND RPM = 55 56
FIGURE 4-32: EXP VS. MODEL 'D' FOR 15% → 75% AND RPM = 45 56
FIGURE 4-33: 'D' ERROR SIGNAL FOR 15% → 75% AND RPM = 45 57
FIGURE 4-34: MODEL 'C' AND MODEL 'D' ERRORS FOR 95% → 20% AND RPM = 55 57
FIGURE 4-35: EXP VS. MODEL 'D' FOR 55% → 20% AND RPM = 50 58
FIGURE 4-36: MODEL 'D' ERROR SIGNAL FOR 55% → 20% AND RPM = 50 58
FIGURE 4-37: MODEL 'C' AND MODEL 'D' ERRORS FOR 95% → 20% AND RPM = 55 59

FIGURE 4-38: EXPERIMENTAL RESULTS FOR 20% → 80% INPUT FAMILY 60
FIGURE 4-39: MODEL 'D' WITH AN ADDED GAIN BLOCK 61
FIGURE 4-40: EXP (RPM = 45) VS. MODEL 'D' OUTPUT WITH RPM GAIN = 1 61
FIGURE 4-41: EXP (RPM = 50) VS. MODEL 'D' OUTPUT WITH RPM GAIN = 1.12 62
FIGURE 4-42: EXP (RPM = 55) VS. MODEL 'D' OUTPUT WITH RPM GAIN = 1.25 63
FIGURE 4-43: EXP (RPM = 60) VS. MODEL 'D' OUTPUT WITH RPM GAIN = 1.38 63
FIGURE 4-44: RPM GAINS VS. EXTRUDER SPEED 64
FIGURE 4-45: RPM GAINS VS. EXTRUDER SPEED FOR FOUR (4) INPUT FAMILIES 65
FIGURE 4-46: MODEL 'E' BLOCK DIAGRAM 67
FIGURE 5-1: MODEL 'F' 68
FIGURE 5-2: EXP VS. MODEL 'E' VS MODEL 'F' FOR 15% → 75% AND RPM = 45 69
FIGURE 5-3: MODEL 'E' AND MODEL 'F' ERROR SIGNALS 70
FIGURE 5-4: SIMPLE FEEDBACK CONTROL SYSTEM 71
FIGURE 5-5: FULL CONTROLLER FOR EBM PROCESS 73
FIGURE 5-6: PID GAINS FOR DIE GAP OPENING (H_0) 74
FIGURE 5-7: PID GAINS FOR EXTRUDER SPEED (RPM) 74
FIGURE 5-8: THREE DESIRED LENGTH PROFILES 75
FIGURE 5-9: DESIRED VS OUTPUT LENGTH PROFILE (#1) 76
FIGURE 5-10: ERROR SIGNAL FOR PROFILE 1 77
FIGURE 5-11: DIE GAP OPENINGS FOR PROFILE 1 77
FIGURE 5-12: EXTRUDER SPEED FOR PROFILE 1 78
FIGURE 5-13: DESIRED VS OUTPUT LENGTH PROFILE (#2) 78
FIGURE 5-14: ERROR SIGNAL FOR PROFILE 2 79
FIGURE 5-15: DIE GAP OPENINGS FOR PROFILE 2 79
FIGURE 5-16: EXTRUDER SPEED FOR PROFILE 2 80
FIGURE 5-17: DESIRED VS OUTPUT LENGTH PROFILE (#3) 80
FIGURE 5-18: ERROR SIGNAL FOR PROFILE 3 81
FIGURE 5-19: GAP OPENINGS FOR PROFILE 3 81
FIGURE 5-20: EXTRUDER SPEED FOR PROFILE 3 82
FIGURE 5-21: EXTRUDER SPEED PROFILE WITHOUT SATURATION BLOCK 83
FIGURE 5-23: SISO CONTROL SYSTEM WITH RELAXED EXTRUDER SPEED LOOP 85
FIGURE 5-24: DESIRED PARISON LENGTH FOR RELAXED RPM LOOP 85
FIGURE 5-25: DIE GAP PROFILE WITH RELAXED RPM LOOP 86
FIGURE 5-26: ERROR SIGNAL FOR RELAXED RPM LOOP 86
FIGURE 5-27: ERROR SIGNAL FOR RELAXED RPM LOOP (100RPM) 87
FIGURE 5-28: SISO CONTROL SYSTEM WITH RELAXED DIE GAP LOOP 88
FIGURE 5-29: EXTRUDER SPEED PROFILE WITH RELAXED DIE GAP LOOP 88
FIGURE 5-30: ERROR SIGNAL FOR RELAXED DIE GAP LOOP 89
FIGURE 5-31: ERROR SIGNAL FOR 10% DIE GAP OPENING 90
FIGURE 5-32: SISO RPM-CONTROLLER BLOCK DIAGRAM 91
FIGURE 5-33: DESIRED PARISON EVOLUTION BASED ON INITIAL PROGRAMMING PROFILE 92
FIGURE 5-34: ERROR SIGNAL FOR SISO RPM-CONTROLLER 92
FIGURE 5-35: EXTRUDER SPEED PROFILE FOR SISO RPM-CONTROLLER 93

List of Tables

TABLE 2-1: POLYMER PROCESSES AND THEIR PRODUCTS 7
TABLE 2-2: ADVANTAGES AND DISADVANTAGES TO HDPE 15
TABLE 3-1: THEORETICAL LENGTHS OF 'STEEL' PARISON FOR T_{EXT} = 10SEC 24
TABLE 3-2: EXPERIMENTAL LENGTHS OF 'STEEL' PARISON FOR T_{EXT} = 10SEC 27
TABLE 3-3: MAXIMUM PERCENT ERRORS 28
TABLE 4-1: GAIN MATRIX 38
TABLE 4-2: INPUT SIGNALS ANALYZED 54
TABLE 4-3: RPM GAINS FOR FOUR (4) DIFFERENT INPUT FAMILIES 65
TABLE 9-1: HDPE 1000 PROPERTIES 101
TABLE 11-1: LIST OF INPUT SIGNALS FILMED 103
TABLE 12-1: LIST OF CONTROLLERS 105

Nomenclature

CNRC-NRC – Conseil National de Recherches Canada – National Research Council

EBM – Extrusion Blow Molding

FEM – Finite Element Model

HDPE – High-Density Polyethylene

IMI – Industrial Materials Institute

K_d – Derivative Controller Gain

K_i – Integral Controller Gain

K_p – Proportional Controller Gain

LDPE – Low-Density Polyethylene

LUT – Look-Up Table

MIMO – Multiple Input/Multiple Output

MISO – Multiple Input/Single Output

PET – Polyethylene Terephthalate

PP – Polypropylene

PVC – Polyvinyl Chloride

RPM – Revolutions Per Minute

SISO – Single Input/Single Output

1 Introduction

The extrusion blow molding process (EBM) is widely used in the plastics forming industry. Along with thermoforming and injection blow molding processes, EBM requires heating and subsequent shaping of a polymer using a mold into useful consumer parts. More specifically, EBM involves the formation of the parison, the clamping of the mold, the part formation using blown air and the cooling stage. The EBM process is described in more detail in the Chapter 2.

1.1 Thesis Objective

This thesis will focus exclusively on the parison formation stage of the EBM process. The goal of this research is to develop a control strategy capable of tracking a desired parison length profile during the parison formation stage. The control strategy can further be divided into two objectives. The first objective is to obtain dynamic system models able to predict the evolution of the parison length. Basic System Identification methods will be used to develop these models. The second objective is to design a robust model-based in-cycle controller. During the parison formation stage, there are two parameters that can directly affect the parison length. These inputs are the extruder speed (rpm) and die gap opening (h_o). By definition, an in-cycle controller is capable of adjusting the input parameters to correctly track the desired output within one cycle of the process. Therefore, for a desired parison length profile, an in-cycle controller is required to perform sensor measurements and process projections before the end of an extrusion cycle. More widely used cycle-to-cycle (CTC) controllers only adjust the input parameters once the cycle is complete as a goal to improve the next part. An immediate advantage for in-cycle over CTC controllers is the reduction of scrap. A CTC controller might require several cycles before reaching steady-state whereas a robust in-cycle controller should attain steady-state within one cycle of the process.

The scope of this thesis is the design and simulation of a robust in-cycle controller for the EBM MISO process based on models developed from experimental work on the

Battenfeld extruder located at the CNRC-NRC IMI in Boucherville, Quebec. The Battenfeld extruder is described in more detail in Chapter 2.

1.2 Benefits to Industry

The design and eventual implementation of an in-cycle controller on an EBM machine will be beneficial to industry in many ways.

Traditional EBM machines employ a parison programming unit requiring open-loop control. Using trial-and-error, an operator must tweak the machine parameters after every cycle until the final blown part meets specifications such as thickness distributions, impact resistance, minimum weight, etc. [1]. This method can be time-consuming and costly.

Closing the loop involves a feedback signal that can correct for unexpected disturbance or noise that enters the process [2]. These disturbances include periodic flow rate changes caused by uneven melting and signal noise from the die gap transducer [3]. In addition, as previously mentioned, the in-cycle controller will attempt to adjust the input parameters to counter these disturbances in order to track the desired parison length evolution within one cycle of the process.

Scrap reduction has become an integral part in the blow molding industry [4]. Controlling the evolution of the parison length will minimize the parison tail thus reducing scrap. The parison tail is the bottom part of the parison that exceeds the mold once it is clamped [5]. Another possible scrap reduction is the flash of the part. The part flash is the melted resin that is forced out the cavity mold and onto the parting line between the molds [5]. A well-designed parison length profile can minimize the flash on the bottom of the mold. Excessive tail and flash will lead to increased cooling times thus increasing the overall cycle time [35].

Finally, controlling the evolution of the parison length will lead eventual parison thickness control. The in-cycle controller designed in this work will be able to increase

parison repeatability. If the parison is consistently able to achieve a pre-determined length in a fixed extrusion time, then it will facilitate the design of a parison thickness controller. The parison thickness distribution is an essential specification for an acceptable part.

1.3 Literature Review

There have been many technological advancements in the EBM industry over the past quarter century. However, over the past decade, there has been a major development in the parison prediction field. The goal of predictive parison behavior is to model the effects of sag and swell during the parison extrusion using finite-element models (FEM). Prior to predictive modeling, the mid to late 1980s brought upon several attempts to control specific parameters such as parison thickness and diameter control. However, less work has been done on parison length control. Furthermore, to the author's knowledge, there is no record of in-cycle parison length control.

1.3.1 Modeling of the EBM Process

The first recorded study on parison behavior was Sheptak and Beyer in the mid-1960s [6]. Using a pinch-off mold consisting of several blades, their goal was to determine the rheological effects of sag and swell on the parison. Many years later, Kalyon et al. [7] attempted to continue Sheptak and Beyer's work by improving the measuring techniques. The resulting measurement methods were time consuming and thus limited in their practical usefulness. Ryan and Dutta [8] developed a simple model based on mathematical descriptions of the parison shape and length due to the competing influences of sag and swell.

The first model reference system for parison length acquisition was developed by Dormeier [9] in 1986. Dormeier used photocells fixed on a stepper-motor adjusting mechanism capable of following the lower edge of the extruded parison. A mathematical

description of the parison length with respect to second-order time equations was formulated and compared to experimental results.

Finally, based on swell data from experiments and rheological data of the resin, Dealy and Orbey [10] were able to develop a lumped parameter model to predict the length of the parison. Different experiments were done to isolate the effects of sag and swell. The final model considered the parison as a group of segments each of a finite length.

There are many other references available; however, very few describe a model for the parison length. The vast majority of the articles read offered models based on the rheological properties of the resin during the extrusion. This research will present models based on experimental results. The rheological effects will be included in the system dynamics.

1.3.2 EBM Closed-Loop Control

Closed-loop control has been applied to the EBM process in the past. DiRaddo, Patterson and Kamal [2] developed a control strategy describing the on-line measurement and closed loop control of parison dimension profiles in EBM. A cycle-to-cycle controller was designed to control the parison thickness profile against disturbances introduced to the process such as a 10°C drop in melt temperature. The strategy was able to successfully control the percent error to within acceptable limits in less than ten cycles.

DiRaddo and Garcia-Rejon [3] experimentally developed deterministic and stochastic models using an extrusion blow molding machine. A first order ARMA noise model was found to describe the process. Finally, an in-cycle controller was simulated to control the thickness distribution of the extruded parison. However, due to difficulties in measuring the thickness profile on-line, the in-cycle controller proved difficult to implement.

1.3.3 Parison Length Control

In addition to the thickness distribution controller, there have been some past attempts to design parison length controllers. However, these controllers all appear to be cycle-to-cycle controllers. The first on-line length acquisition for process control was produced by Dormeier [9]. His model was described in Section 1.3.1. The velocity of the parison drop was measured using a stationary photocell and analyzed in the model. The stored speed values are then updated during each measurement cycle. Similarly, Schrand [4] also used a photocell to detect the parison length in his cycle-to-cycle controller. Schrand proposed three different types of length control; parison length control, modified parison length control and extruder rpm control for an intermittent extruder (see Section 2.5.1).

Finally, Noguchi et al. hold a 1995 United States patent called "Parison Length Control Method for Blow Molding Machine" [11]. Again, like Dormeier and Schrand, Noguchi et al., developed a cycle-to-cycle controller. The extruder screw rotation speed of the next cycle is determined by measuring the difference between the actual and desired parison lengths of the previous cycle. This scheme is acceptable for reducing scrap and lowering cycle time, but does not maximize yield time.

Chapter 2 describes the EBM process in more detail and gives the reader an idea of the equipment used throughout the research. A theoretical model describing the parison length is derived in Chapter 3 neglecting any rheological effects of sag and swell. Chapter 4 focuses on developing deterministic models based on experimental results. Furthermore, Chapter 4 explains the abnormalities in the evolution of the parison length during the 10 second extrusion time. A robust SIMO in-cycle controller is designed and simulated in Chapter 5. Derivative SISO controllers are also seen and designed specifically for the Battenfeld machine. Finally, the last chapter offers a summary of the work as well as a look into future work beyond the scope of this research.

2 Blow Molding Process

2.1 Extrusion vs. Injection vs. Stretch

There are many ways to form plastic parts. Usually, the shape of the part determines the appropriate process needed to form it. For example, plastic parts such as dust pans, refrigerator linings, etc., are formed using the thermoforming process where a heated sheet of plastic is pressed against a mold. Hollow parts however are manufactured by the blow molding process. A heated polymer resin is blown into a mold as the name suggests. The blow molding process can be characterized into three different processes. They are: extrusion blow molding, injection blow molding and stretch blow molding [12].

Extrusion blow molding (EBM) is mostly used to produce thick and heavy parts weighing more than 12 ounces [13]. Containers carrying food, laundry, waste or poisonous materials are manufactured by EBM. A major advantage to EBM is the ability to include handles in their parts so that the consumer can easily carry the heavier containers.

Lighter parts weighing less than 12 ounces are typically produced by injection blow molding. Compared to extrusion blow molding, injection blow molding offers a better definition in the final part: more detailed molds are used to make more complex parts. It can give a more accurate wall-thickness distribution as well as a high-quality finish at the neck of the part. Industries such as pharmaceuticals, cosmetics and alcohol rely on the injection blow molding process to produce their containers [13]. In addition to better detail, injection blow molding can create parts out of polymers that otherwise cannot be extruded like polyethylene terephthalate (PET).

Finally, stretch blow molding is used mostly to form parts out of polymers that are difficult to blow such as polypropylene (PP) and PET. Due to the nature of the polymer, stretch blow molded parts have better gas-barrier properties that are important, especially in the carbonated-beverages industry [14].

The scope of this thesis will focus only on the extrusion blow molding process. Table 2.1 shows the different products created from each of the three blow molding processes [15].

Table 2-1: Polymer Processes and their products

Process	Products Made	Resins Used
Extrusion Blow Molding	Bottles, Automotive fuel tanks, Venting ducts, Watering cans, Boat fenders, etc	PP, PE, PET, PVC
Injection Blow Molding	Bottles, Jars, Roll-on containers	LDPE, LLDPE, PP, PET, PVC
Stretch Blow Molding	Carbonated and soft drink bottles, Cooking oil containers, Health and oral hygiene products, Bathroom and toiletry products	PET

2.2 History

The actual blow molding process originated in the first century BC where Syrian glass workers shaped heated bulbs on the end of a blow pipe to create hollow parts [17]. Although evidence shows that the Egyptians and the Babylonians were the first to mold plastics into utensils, the first recorded molded part was a baby rattle in 1880. Its creator, John Wesley Hyatt, established Celluloid Corp. in 1872 and was granted the first US patent for a blow molding process in 1881 [12].

The blow molding industry for fifty years following the first baby rattle remained stagnant mainly due to the lack of development in resins. Celluloid and celluloid acetate were used to mold the backs of hair brushes, ping-pong balls, doll parts, cutlery handles, jewellery and the outer end of a telephone receiver. It was only in the late 1930s that the 'modern' blow molding industry was born [17]. Just prior to the Second World War, there were two major developments in the blow molding industry. The first involved the development of the machinery while the second development was material based.

In 1938, James T. Bailey of Plax Corporation invented the first hot-melt intermittent extrusion machine. This particular machine, using a crosshead die and one-cavity mold, would extrude a hollow tube of melted resin. Once the tube was long enough, the machine would stop, the mold would clamp and air would be blown in to form the part.

Soon after, J.T. Bailey designed the first commercial automatic continuous blow-molding machine capable of handling four molds in sequence [12].

Concurrently, in 1937, low-density polyethylene (LDPE) was patented and used exclusively for the war. After several failed attempts to commercially blow-mold LDPE parts by the Plax Corp. in the early 1940s, it was the Hudson Talcum Powder Co. who successfully produced the "Stoppette" deodorant squeeze bottle [25]. Despite the early failures for LDPE, "the introduction of polyethylene as a thermoplastic raw material was probably as important as equipment inventions in advancing the field of blow molding [12]."

Similar advancements in technology and materials allowed for several growth periods in the blow molding industry since the initial boom in the late 1930s. One of the more notable growths occurred in the late 1950s where two major developments surfaced. The first was the commercial production of blow-molding machines. The second was the introduction of high-density polyethylene (HDPE) to blow-molding processors [12]. Appendix A shows a timeline with the important dates in EBM history up to 1991 [1].

2.3 Markets

According to a Plastics Technology website forecast, the total blow molding output within North America will have increased by 6% this year followed by another 6% in 2005. These increases are encouraging considering that the price per pound of resin has been the highest in many years due to its close correlation to the price of petroleum per barrel [19].

Below is a list of the top ten blow molding companies found in North America with their total sales for 2003 in parentheses (millions US$) [20].

1. Amcor PET Packaging, Manchester, MI (1340.00)
2. Owens-Illinois Inc., Toledo, OH (1100.00)

3. Plastipak Packaging Inc., Plymouth, MI (880.00)

4. Graham Packaging Co. LP, York, PA (809.60)

5. Consolidated Container Co. LLC, Atlanta, GA (800.00)

6. Kautex Textron, Troy, MI (650.00)

7. Inergy Automotive Systems LLC, Troy, MI (622.00)

8. Constar International Inc., Philadelphia, PA (562.80)

9. Silgan Plastics Corp., Chesterfield, MO (528.00)

10. ABC Group Inc, Toronto, Ontario (460.00)

In 2003, the top ten North American blow molding companies generated almost 8 billion USD in total sales.

Table 2.1 states that bottles, automotive fuel tanks, venting ducts, watering cans, and boat fenders are all produced by EBM. Other products such as toys, trash cans, and household chemicals are also important markets for the EBM process. However, of all the EBM markets, bottles are by far the most important in this industry and it will only continue to grow [19]. Plastic Technology predicts that the market for bottles containing potable substances will grow by 8% per year for many years to come. Similarly, bottle containing non-potable liquids are expected to grow at a rate of 6% per year [21].

The plastics industry is a force in today's world and it is slowly becoming an integral part of other major industries. It has already affected the automotive industry making cars lighter, safer, and less expensive and will soon become a major player in the biomedical field.

2.4 Different Stages of EBM

Most sources will inform the reader that there are four stages to the extrusion blow molding process. They are: parison formation, clamping, blowing and cooling [17]. Some references tend to group the middle two stages into one stage and simply call it the clamping/blowing stage. To simplify matters, the description below of the EBM process will be described as four stages.

The first stage consists of forming the parison before it is blown into the mold. A parison is a long hollow tube of melted resin extruded through a narrow annular opening. The length and thickness of the free-hanging parison are crucial in the subsequent inflation and final part thickness distribution. There are rapid advances being made in the development of software programs that will correctly predict the final thickness distribution of a part based on the characteristics of the extruded parison. Figure 2-1 shows the parison formation stage.

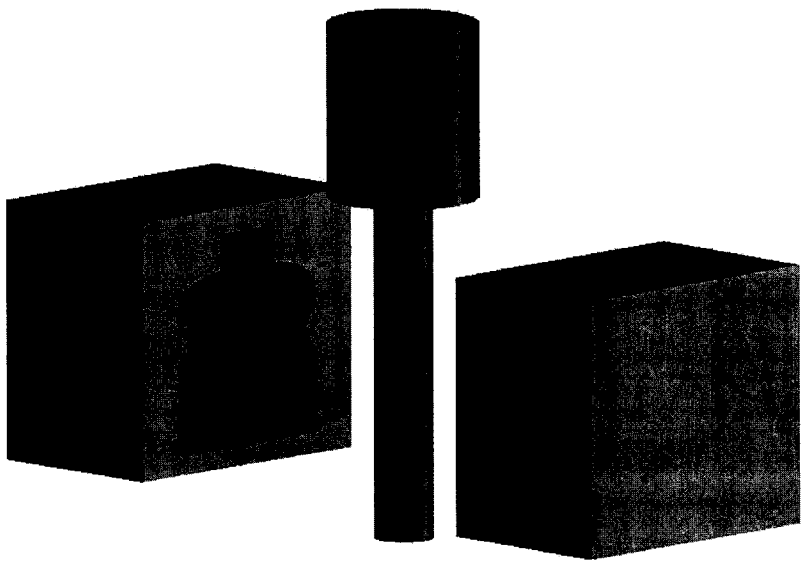

Figure 2-1: Parison Formation Stage

Following the extrusion of the parison, the next step is to clamp the two halves of the mold. Otherwise known as the pinch-off stage, this step will physically detach the parison from the extruder while forming a seal on the bottom edge. The benefits of removing the parison from the extruder are two-fold. First and foremost, it allows for

forming of a new parison while the previous one continues the process. Secondly, depending on the abilities of the blow molding machine, an operator can have up to eight molds working at once in a rotational system to maximize productivity.

The third stage of extrusion blow molding involves blowing air into the parison enclosed in the mold. This increased pressure inside the mold forces the pinched-off parison to take the shape of the mold cavity and for the first time in the extrusion blow molding process, the parison resembles the final part.

Once the parison is inflated, the parison is still too hot to leave the mold. In addition, the blown part is still in a 'melted' state. Although short, the cooling stage is crucial in the final product. This final stage can be performed in various ways. For example, most EBM machines use cold water to cool the mold halves which solidifies the exterior of the part. The inner wall of the blown part is cooled by the convective nature of the blown air inside the mold. Cooling times are also important to optimize. Excessive cooling times decrease productivity while short cooling times increase chance of shrinkage and warpage [17]. Figure 2-2 shows a final part after all the blow molding stages have been completed.

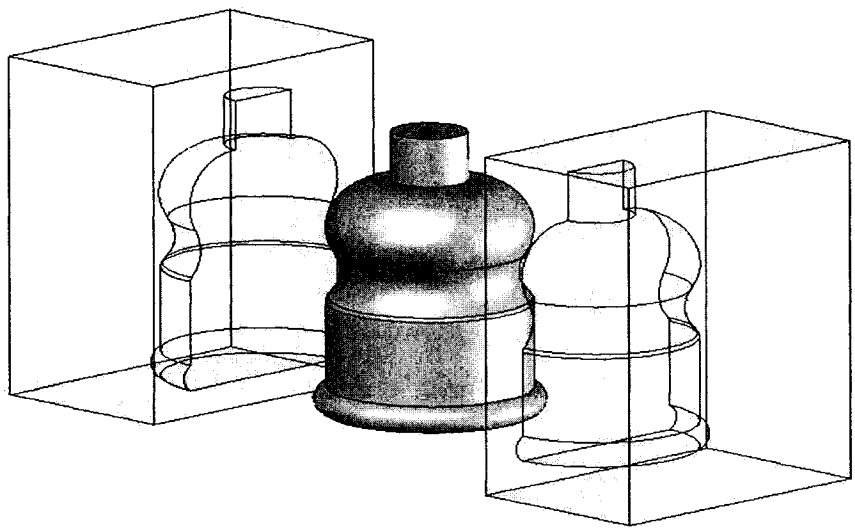

Figure 2-2: Final Part after EBM Stages

2.5 Extruder

As discussed in the previous section, the actual extrusion of the parison plays an important role in the quality of the final blown part. Presently, extensive research is being conducted to correctly predict the parison dimensions extruded from the machine. Due to the continuously changing rheological characteristics of the resin, the parison extrusion is difficult to model. The type of extruder, the description of the die head and the polymer resin being melted are important factors that can affect the behaviour of the parison. The purpose of this section is not to explain the rheological effects of each factor on the parison but rather to describe the different options that are available to the machine operator. Moreover, this section will present to the reader the specific experimental set-up used throughout this research.

2.5.1 Continuous vs. Intermittent

Extrusion blow molding can be divided in two main categories; continuous extrusion and intermittent extrusion [18].

In continuous extrusion blow molding, the melted resin never ceases to be extruded. Since the parsion is continuously being formed, the next three stages of the blow molding process must be performed away from the die head. In the past, some extrusion machines transferred the parison from the die head to the mold before continuing with the process. This process has since become obsolete [16]. Rather than move the malleable parison, today's machines first clamp the mold onto the parison and then move the closed mold to another station to complete the blow molding process. This procedure can be done in three ways: rising mold method, the rotary method and the shuttle method. Each have advantages and disadvantages with respect to cost and productivity and characteristics of the final part.

Intermittent extrusion blow molding can also be referred to as discontinuous extrusion or shot extrusion [16]. As the name implies, this extrusion method extrudes the melted resin

enough for one part and waits until the rest of the process is completed before extruding another 'shot'. An advantage to using intermittent extruders is that the clamped mold does not need to be displaced to continue its process. Clamping, blowing and cooling all take place directly beneath the die head. Similarly to the continuous extruder, the intermittent extrusion process can be divided into three subcategories. However, these divisions are made with respect to how the resin is extruded and not how it is clamped like in the continuous process. In intermittent extrusion, the resin is 'shot' either by a reciprocating screw, a ram accumulator or an accumulator head [18]. Again, each method has advantages and disadvantages depending on the final blown part.

The extruder used throughout this research project is called the Battenfeld-Fischer FBZ 1000 located in the large-scale laboratory at the CNRC-NRC IMI in Boucherville, Quebec, Canada. It was manufactured in 1987 and purchased by the CNRC-NRC IMI the following year. It is a continuous extruder that uses the shuttle method with a single mold. Figure 2-3 shows the Battenfeld as it stands in the research laboratory at the IMI.

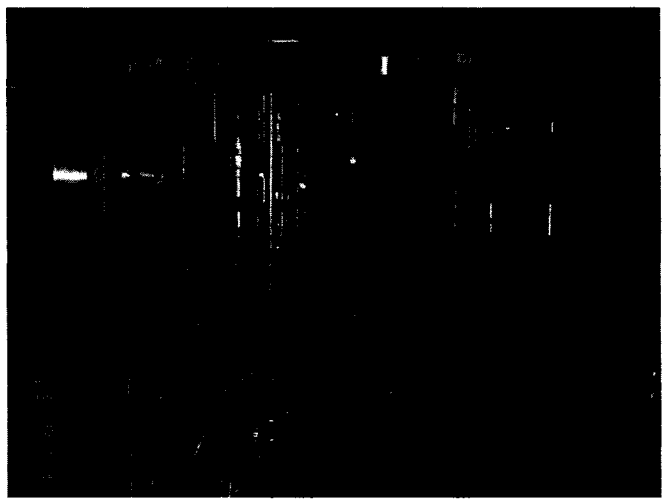

Figure 2-3: Battenfeld Extruder

Figure 2-4 shows the operator console (MACO 8000) that communicates with the Battenfeld machine.

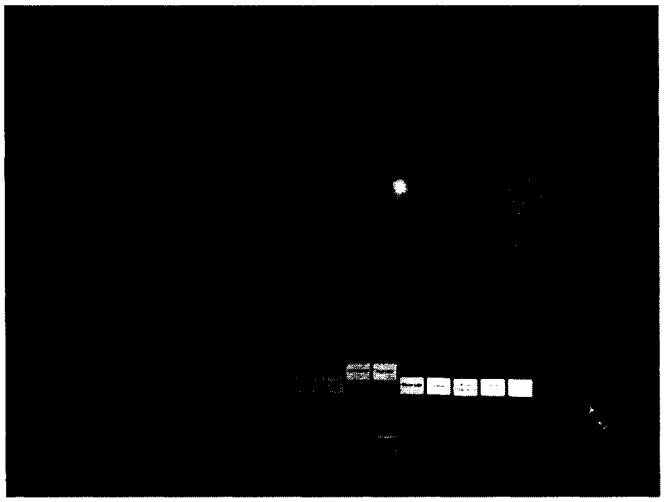

Figure 2-4: Operator Console (MACO 8000)

The screen seen in Figure 2-4 is a touch screen that allows the operator to input the parison profile. Based on a given specific part design, a parison programming profile is required for operation. There are a total of 100 points in a Battenfeld parison profile. However, an operator can only specify the die gap opening for up to 10 points. These are referred to as 'master' set-points. The Battenfeld then interpolates the die gaps between any two master points. The required programming profiles inform the Battenfeld machine how die gap openings vary for a fixed extrusion time. The extrusion time throughout this research was fixed to 10 seconds. Once the extrusion process begins, the parison profile cannot be altered. The operator must wait for the Battenfeld to completely stop before modifying the profile. Also included on the Battenfeld console are the buttons that control the speed of the extrusion. The LED display on the upper left of Figure 2-4 tells the operator exactly how fast the screw is turning in units of revolutions per minute (RPM). Unlike the parison programming profile, the extruder speed could be tuned while the extrusion process is in progress. Determining whether the parison profile and/or the extruder speed could be changed during the extrusion cycle is important in designing a controller for the Battenfeld EBM machine.

2.5.2 Resin Description

The choice of polymer is an integral part of the blow molding process. The rheological properties of a polymer will determine the quality of the end product. For example, suppose an operator runs two Battenfeld EBM machines with identical operating parameters but using different polymer resins. The final blown parts will probably look identical but both will not be necessarily suitable for industry. For example, either bottle might not be shatter-proof or might be susceptible to degradation under higher temperatures. These are important factors to consider when choosing a polymer resin.

In the EBM industry, HDPE is the most widely used polymer resin [18]. A 2001 Plastics News survey showed that over 85% of the responding North American blow molding companies (194 in all) used HDPE as a polymer resin [22]. In addition, a 2001 report shows that in the industrial packaging industry, HDPE accounted for almost 90% of the poundage produced which is equivalent to over 2 billion pounds of resin [23]. Table 2.2 shows the advantages and the disadvantages to using HDPE as a resin in the extrusion blow molding industry [18].

Table 2-2: Advantages and Disadvantages to HDPE

Advantages to using HDPE	Good moisture barrier properties
	Good stiffness for many applications
	Relative chemical inertness
	Good thermal stability over a range of -40 to 316°C
Disadvantages to using HDPE	Relatively high gas transmission rates
	Some chemicals may cause premature failure of HDPE
	Higher temperatures may cause degradation of HDPE

For the reasons mentioned above along with its relatively low cost, HDPE 1000 was used as the resin of choice throughout the research on the Battenfeld EBM machine. Appendix B shows a table containing other HDPE 1000 parameters [24].

2.5.3 Die Head Description

Another parameter that could change the complexion of the extruded parison is the die head description. The three main parts of the die head are the bushing, the mandrel and

the die as shown in Figure 2-5. The bushing is the outside piece that encases the mandrel and the die. The die is attached to the mandrel which is itself a movable pin inside the bushing. Depending on the parison programming profile, a hydraulic system moves the mandrel pin vertically to reach the appropriate die head opening. The parison programming points entered in the Battenfeld is a percentage of the maximum stroke length. A stroke length is defined as the vertical distance between the tip of the die head and the bushing. The maximum stroke length for the Battenfeld machine is 0.536cm. Therefore, the die gap opening in length units (i.e. cm) is shown in Equation 2.1 below.

$$h_o(cm) = \frac{h_o(\%) \cdot \max stroke}{100} = \frac{h_o(\%) \cdot 0.536cm}{100} \tag{2.1}$$

Figure 2-5 shows the cross-section of the components that make up the die head [16].

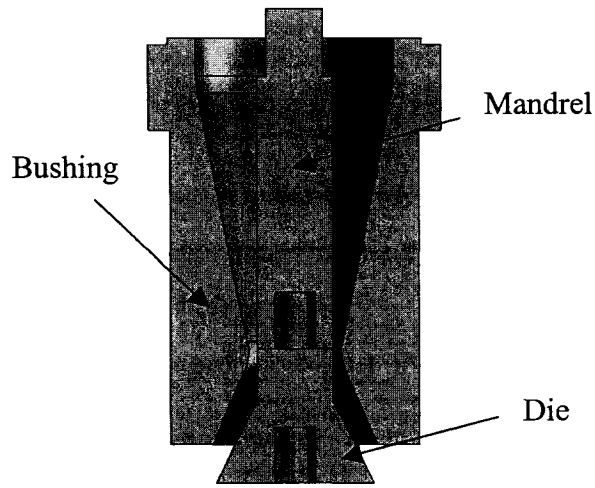

Figure 2-5: Section view of the Die Head

The die used throughout this experiment is a diverging die with a 29mm diameter (see Figure 2-6 (left) – top view). The angle of the diagonal plane with the vertical is 30° (see Figure 2-6 (middle) – front view). Figure 2-6 (right) shows the die in three dimensions. The bushing inner diameter is 30mm. Therefore when the die is flush with the bottom of the bushing (otherwise known as 0% open), there is a mere 0.5mm of space for the melted resin to extrude. This is impractical in any bottle design. In addition, a rule of

thumb in design practices is that die gap openings should never be fully opened (100%) to avoid mechanical failures.

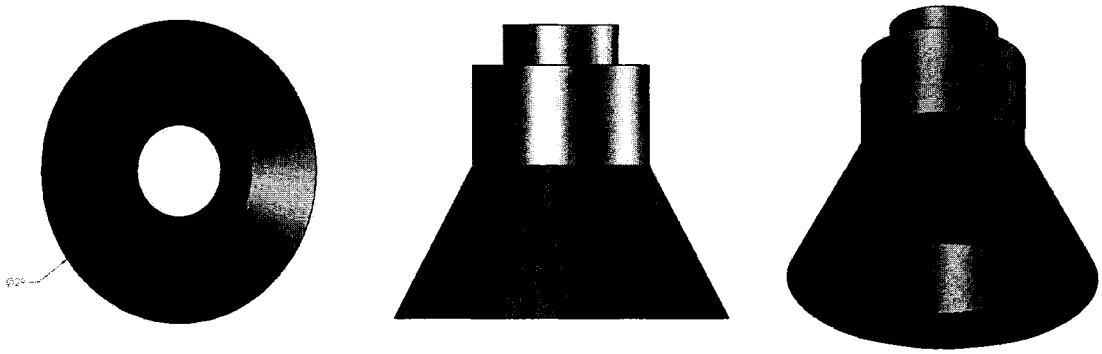

Figure 2-6: Top view (left), Front view (middle), 3D view (right) of a extrusion die

3 Theoretical Model

For any process, a model has to be developed in order to understand the system dynamics. In other words, if the input(s) of a system change, how does it affect the output(s)?

3.1 Control System Models

The model of the system is critical to the design of an effective controller. Whereas the model does not have to be an exact replica of the system studied, its response to the input signal applied to the system must follow the system output as closely as possible. A well-designed controller will then minimize the error between the model and the actual system in closed-loop.

Assuming that the resin and the die parameters do not change, there are two other parameters that can affect the system output. They are the speed of the extruder (rpm) and the die gap opening (h_o). As a result, this chapter will focus on an initial model of the continuous extrusion blow molding process having two inputs (rpm & h_o) and a single output (parison length). Such a system is called a MISO (**m**ultiple **i**nput, single **o**utput) system.

3.2 Master Formula Derivation

For over a quarter of a century, polymer processing experts have tried to model the rheological effects that occur in the EBM process known as swell and sag. The model developed in this chapter will neglect these influences of swell and sag. Therefore, replacing a normal polymer resin by an incompressible, undeformable material such as cold steel in the extrusion process will avoid any swell or sag in the parison. Figure 3.1

shows an example of an extruded 'steel' parison indicated with the variables needed to derive the master formula.

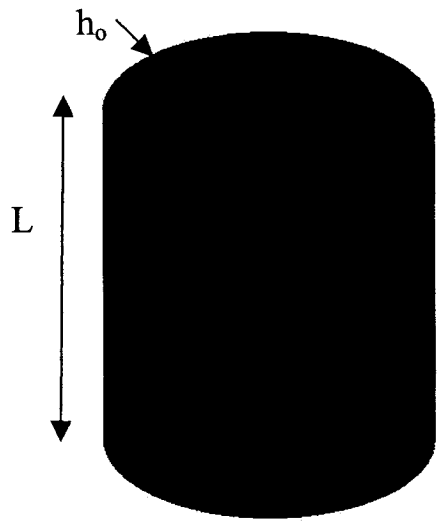

Figure 3-1 'Steel' Parison

Finding a function that determines the parison length (L) is the purpose of this section. The first step is to calculate the parison volume (V) with respect to L. Equation (3.1) represents the volume of a cylinder.

$$V = L \cdot \left(\pi r_2^2 - \pi r_{die}^2 \right) \tag{3.1}$$

From Figure 3-1, the die gap opening (h_o) is shown in the following equation:

$$h_o = r_2 - r_{die} \tag{3.2}$$

Using Equations (3.1) and (3.2), the length of the extruded parison can thus be expressed by Equation (3.3):

$$L = \frac{V}{2\pi r_2 h_o - \pi h_o^2} \tag{3.3}$$

In order for Equation (3.3) to have the correct units (i.e. cm), a change of units is required for the die gap h_o. As explained in Section 2.5.3, the Battenfeld understands the die gap as a percentage opening (%). Recall that the maximum stroke length (100% open) of the die head is 0.536cm. Consequently, any die gap length can be calculated by multiplying the die gap percentage by the maximum stroke length (see Equation 2.1).

The next step is to represent the parison length L as a function of both rpm and die gap (h_o) as they will be the inputs to our model. To do this, the volume V of the extruded parison must be represented in terms of mass flow rate. Equation (3.4) shows how volume is a function of the volumetric flow rate (Q_v) while Equation (3.5) links the volumetric flow rate to the mass flow rate (Q):

$$V(t) = Q_v(t) \cdot t \tag{3.4}$$

$$Q_v(t) = \frac{Q(t)}{\rho} \tag{3.5}$$

where ρ is the melt density of the resin in (g/cm^3). For HDPE 1000, the melt density is $0.763 g/cm^3$ [26]. Inserting Equations (3.4) and (3.5) in (3.3) will give the length L as a function of die gap (h_o) and mass flow rate (Q). Note that L is now time dependent.

$$L(t) = \frac{1}{\pi\rho}\left(\frac{Q \cdot t}{2r_{die}h_o + h_o^2}\right) \tag{3.6}$$

The final step to calculate the 'steel' parison length L(t) is to find the relationship between the mass flow rate (Q) and rpm. Assume that the extruder screw is a tight fit in the barrel minimizing the channel depth [27]. As the melted resin is being propelled through the barrel, no backward flow along the screw axis is assumed because of the minimal channel depth. In other words, the melted resin follows a 'perfect' flow out of the die head. This assumption would lead to the mass flow rate Q being an almost linear function of rpm.

To verify this assumption, a quick experimental test was performed. Four different extruder speeds (*rpm*) were analyzed (rpm = 45, 50, 55 and 60). Similarly, six different die gaps were used (h_o = 10%, 25%, 50%, 75%, 90% and 100%). For each rpm and h_o combination, five samples of polymer resin were extruded for 15 seconds and weighed. As a result, there were a total of 120 samples of extruded plastic. An average flow rate (g/min) for each rpm was calculated, plotted and shown in Figure 3-2.

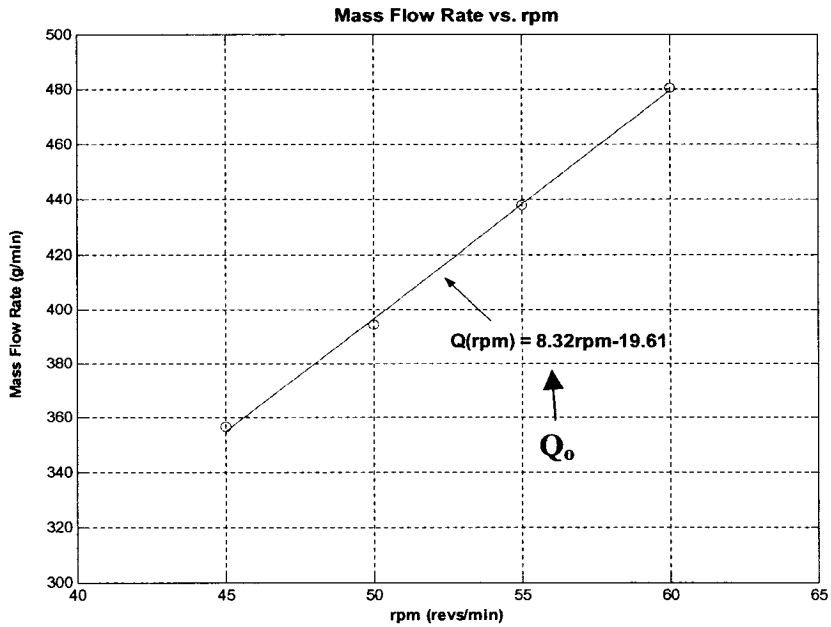

Figure 3-2: Mass Flow Rate vs. rpm

Clearly, Figure 3-2 confirms that the assumption of the mass flow rate being a linear function of rpm is accurate. Equation (3.7) shows the linear relationship between Q and rpm:

$$Q(rpm) = Q_o \cdot rpm = 8.32 \cdot rpm \tag{3.7}$$

where Q_o (g/rev) represents the slope in Figure 3-2.

Inserting Equation (3.7) into Equation (3.6) gives the final expression of an extruded 'steel' parison as shown in Equation (3.8):

$$L(h_o, rpm, t) = \alpha\left(\frac{rpm}{d_{die}h_o + h_o^2}\right)\cdot t \tag{3.8}$$

where $\alpha = \frac{Q_o}{\pi\rho}$. Note that α can be calculated without any knowledge of the inputs.

Equation (3.8) is referred to as the 'master formula' for several reasons. Since the equation is dependent on machine and material parameters, it can be utilized on any extrusion blow molding machine for any choice of resin. As mentioned previously, the value of $\alpha = \frac{Q_o}{\pi\rho}$ can be calculated without any knowledge of the inputs. Therefore, a database could potentially be created listing different values of α for different extruder machine and material combinations. For example, the Battenfeld using HDPE 1000 would have $\alpha = 3.48\text{cm}^3/\text{rev}$. Finally, this 'master' length formula will be the essence of the initial model representing the EBM process described in the next section.

3.3 Simulink Model 'A'

Mathworks is a company that specializes in technical computing (*MATLAB*) and Model-Based Design software (*Simulink*). More specifically, *Simulink* allows the user to design, implement, simulate, test control any type of system in a user-friendly graphic interface [28]. Figure 3-3 shows an example of a *Simulink* model. Figure 3-3 also represents the initial Model 'A'.

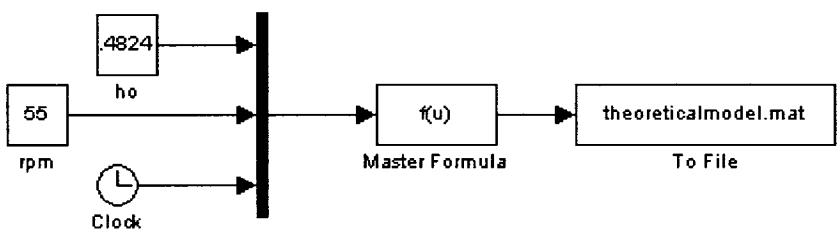

Figure 3-3: Initial Simulink Model 'A'

Figure 3-3 shows that there are three inputs to the system: die gap (h_o), extruder speed (*rpm*) and time (t) all being fed into a multiplexer block which combines several input signals into a vector output signal. The block entitled 'Master Formula' contains Equation (3.8) from the previous section and inserts the given input values. Finally, the last block on the right allows the user to save the output signal into a file which could be plotted using a *MATLAB* program.

Figure 3-4 shows the system output signal for a constant input signal of rpm = 55 and h_o = 90% (or 0.4824cm). The extrusion time throughout the thesis will be 10 seconds. That is, the initial model calculates the length of a 'steel' parison with the die head opened at 90% of its maximum stroke while the extruder is pumping at 55rpm for 10 seconds.

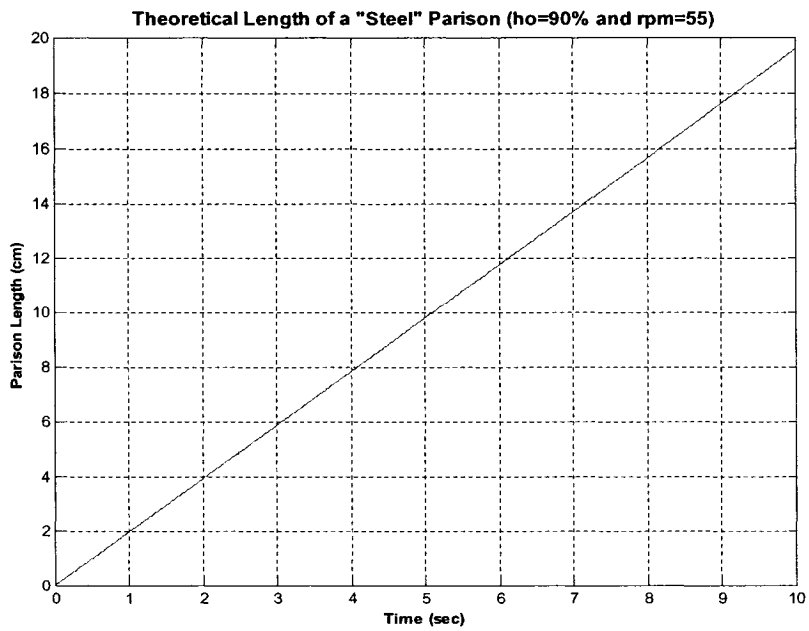

Figure 3-4: Theoretical Length of 'Steel' Parison

Table 3.1 represents the final length (cm) (after t_{ext} = 10sec) for all the different input combinations studied.

Table 3-1: Theoretical Lengths of 'Steel' Parison for t_{ext} = 10sec

$h_o \rightarrow$ RPM	50%	75%	90%	100%
45	30.74cm	19.66cm	16.00cm	14.17cm
50	34.16cm	21.85cm	17.77cm	15.75cm
55	37.57cm	24.03cm	19.55cm	17.32cm
60	40.99cm	26.22cm	21.33cm	18.90cm

There are two patterns of note in Table 3-1. The first observation shows the parison length increasing as the extruder speed increases for a given die gap opening. This is not surprising as there is more polymer resin being extruded. The screw increases in velocity thus producing a longer parison length. The second observation shows the parison length decreasing as the die gap increases for a given rpm value. At first thought, one might be led to believe that decreasing the die gap opening would actually decrease the length of the parison. However, the effect of decreasing the die gap opening is similar to placing one's thumb at the end of a hose with running water. More pressure is created inside the hose and therefore the water sprays further.

3.4 Experimental Protocol

Experimental tests must be performed using the same input signals to validate Model 'A'. Figure 3-5 shows the experimental set-up performed in the large-scale lab at the CNRC-NRC IMI.

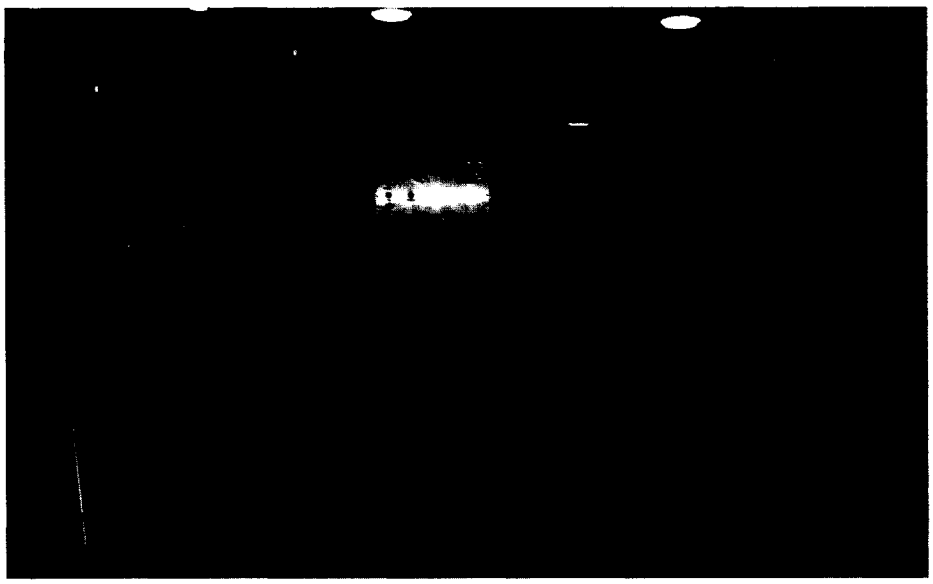

Figure 3-5: Experimental Set-up at CNRC-NRC IMI

The leftmost tripod holds the Fastcam PCI High Speed Camera purchased to capture the length evolution of the parison. The high speed camera is able to take up to 10,000 frames per second (fps) with a 512 x 480 resolution (see Appendix C) [34]. However, since the memory buffer is fixed, decreasing both the frame rate and the resolution will allow for a longer duration of filming. As a result, the camera was set to take 125fps with a resolution of 512 x 240. These settings will ensure the camera to capture a 10 second extrusion time. The tripod immediately to the right of the camera holds the 1000W spotlight directed toward the parison. Figure 3-6 shows the camera view of the Battenfeld machine.

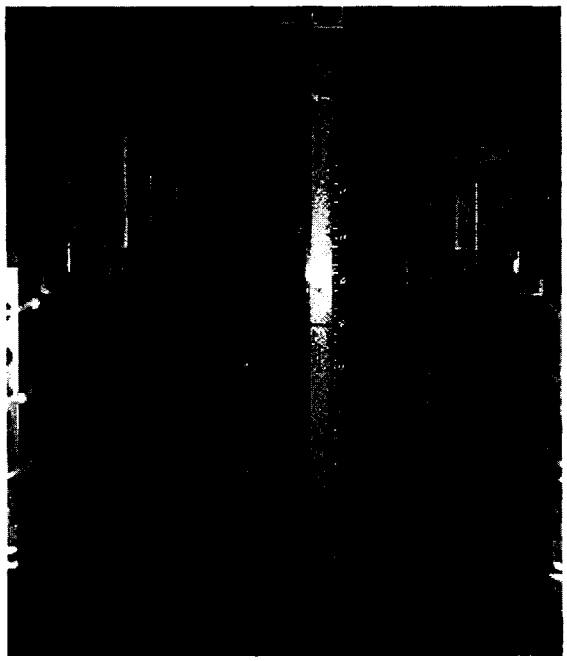

Figure 3-6: Camera view of the Battenfeld machine

Normally, a newly-extruded parison will be translucent due to its high temperature (over 180°C). For optimal filming, a white dye was mixed in the resin before the extrusion. These white dye particles occupied 2% of the volume for a batch of HDPE 1000. Such a small percentage will not affect the overall rheological properties of the polymer. In addition, to maximize the contrast between the extruded parison (now white), a black surface was installed directly behind the extruded parison. A white ruler (60cm) was also glued to the background in order to calibrate the pixel-tracking software included with the purchase of the high speed camera.

Similar combinations of inputs (extruder speeds (rpm) and die gap openings (h_o)) were used to validate Model 'A'. Equation (3.9) represents the vectors used to perform the experiments (four rpm values and four values of h_o). In all, there are 16 different possible combinations of rpm and h_o.

$$\begin{aligned} rpm &= [45, 50, 55, 60] \\ h_o &= [50\%, 75\%, 90\%, 100\%] \end{aligned} \tag{3.9}$$

3.5 Theoretical vs. Experimental

Figure 3.7 represents a comparison between the Model 'A' output and the experimental result for a specific input of 90% die gap opening with 55rpm using an extrusion time of 10 seconds.

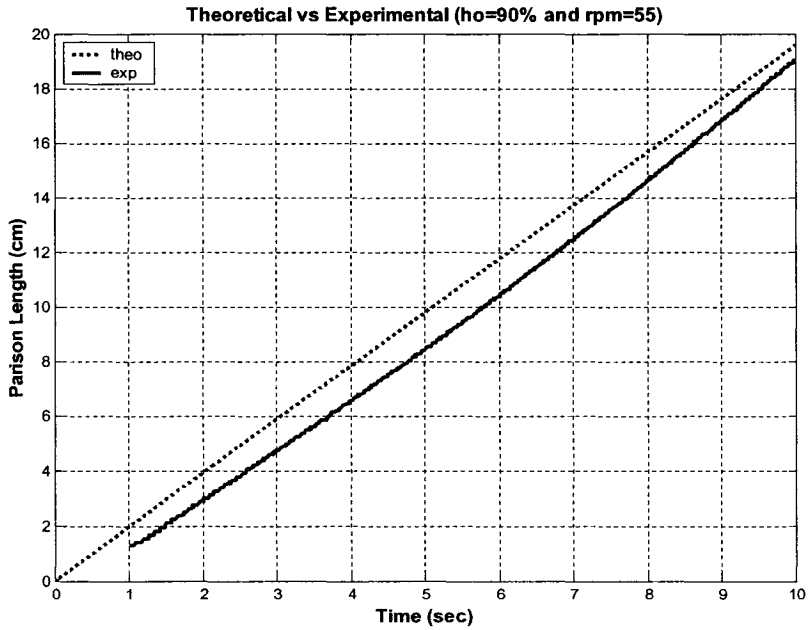

Figure 3-7: Theoretical vs. Experimental Length (h_0 = 90%, rpm = 55)

Similarly to Table 3-1 from Section 3.3, Table 3-2 shows the experimental values of a parison made out of HDPE 1000 after 10 seconds of extrusion time.

Table 3-2: Experimental Lengths of 'Steel' Parison for t_{ext} = 10sec

h_0 → RPM	50%	75%	90%	100%
45	24.20cm	18.46cm	15.59cm	14.29cm
50	27.59cm	20.15cm	17.28cm	15.91cm
55	31.09cm	22.63cm	19.04cm	17.48cm
60	34.57cm	25.37cm	21.72cm	19.04cm

The best way to validate the Model 'A' is to calculate the percent error for each data point. Equation (3.10) shows the expression to calculate the percent error.

$$Error(\%) = \frac{|\text{experimental-theoretical}|}{\text{experimental}} \cdot 100 \tag{3.10}$$

Table 3-3 shows the maximum error from each combination of inputs.

Table 3-3: Maximum Percent Errors

$h_o \rightarrow$ RPM	50%	75%	90%	100%
45	75.24%	44.72%	31.05%	46.31%
50	88.55%	60.80%	49.35%	40.29%
55	43.49%	45.21%	60.68%	21.29%
60	49.67%	36.94%	44.98%	52.32%

Clearly, Table 3-3 confirms that this initial model developed for a 'steel' parison in this chapter is not suitable. Therefore, an efficient control system cannot be designed because of such high model errors. However, this model does prove that swell and sag must be accounted for in models to come.

The next section will provide some suggestions on providing a better modeling scheme and further explain why the initial Model 'A' is not appropriate for the control system.

3.6 Model Improvements Needed

As explained in the previous section, Model 'A' yields very high percent error. Poor models could potentially lead to unstable control systems. Another problem with the initial model is that both inputs ($rpm \,\&\, h_o$) are constant values. This restriction is not suitable for industry as final part designs require changes in die gap openings to achieve optimal thickness distributions.

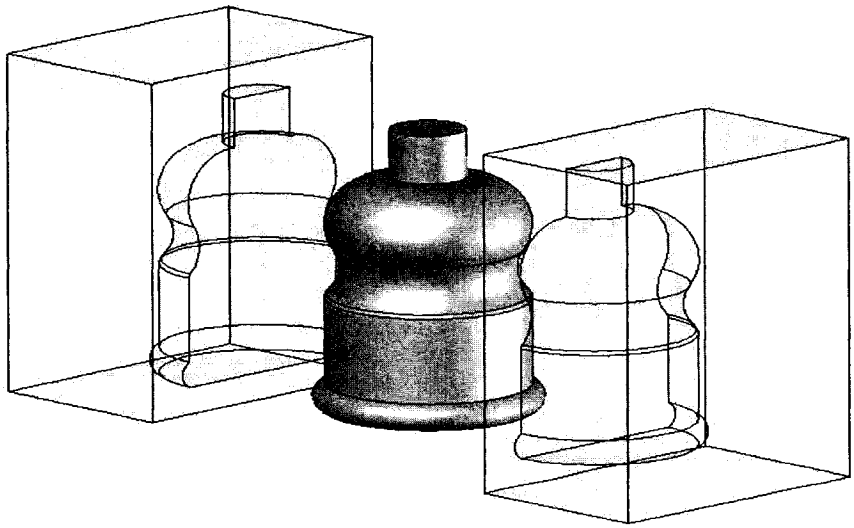

Figure 3-8: Bottles Produced by the Battenfeld EBM Machine

Figure 3-8 shows an example of a final part created by the mold installed on the Battenfeld. The parison programming points needed to produce such a bottle will have a variation of die gaps to achieve a suitable thickness distribution.

By varying these input parameters, any model improvement should be able to include the system dynamics. That is, these models should be able to determine how changes in the die gap opening affect the parison length and similarly, determine what effects changing the extruder speed (*rpm*) will have on the parison length. Consequently, the improved models in the next chapter will focus on tracking the parison length evolution as the input parameters vary.

Despite the sub-par results of the initial model, Model 'A' shows the behaviour of the parison length as the inputs are changed from cycle to cycle thus allowing for a better understanding of the EBM process. Furthermore, outputs from Model 'A' could be used as a 'first guess' for future models.

4 Experimental Models

Whereas the previous chapter focused on creating a model based on theoretical derivations, this chapter will create models based on experimental results. This method is called system identification. Models based on experimental identification are called black box models and are used here for the purpose of a MISO in-cycle controller design. Rather than entering constant values of extruder speed (rpm) and die gap openings (h_o), these inputs will be incrementally changed one at a time to see their respective effects on the parison length. In other words, the system dynamics will be embedded in the experimental results and therefore included in the proposed models.

4.1 Experimental Protocol

The protocol for this experiment is as follows:

1) Create parison programming profiles that cover almost the entire range of die gap openings (h_o) from 10% to 95%.

2) Film using the PCI high speed camera each programming profile for extruder speeds (rpm) of 45, 50, 55 and 60rpms.

3) Determine the parison length using the pixel tracking software Photron Motion Tools.

4) Analyze results and propose different models.

Although an infinite number of parison programming profiles can be designed, the profiles created for this experiment are simple step functions with a period of 4 seconds alternating between two different h_o values. Figure 4-1 shows an example of such an input profile using 95% and 20% die gap openings.

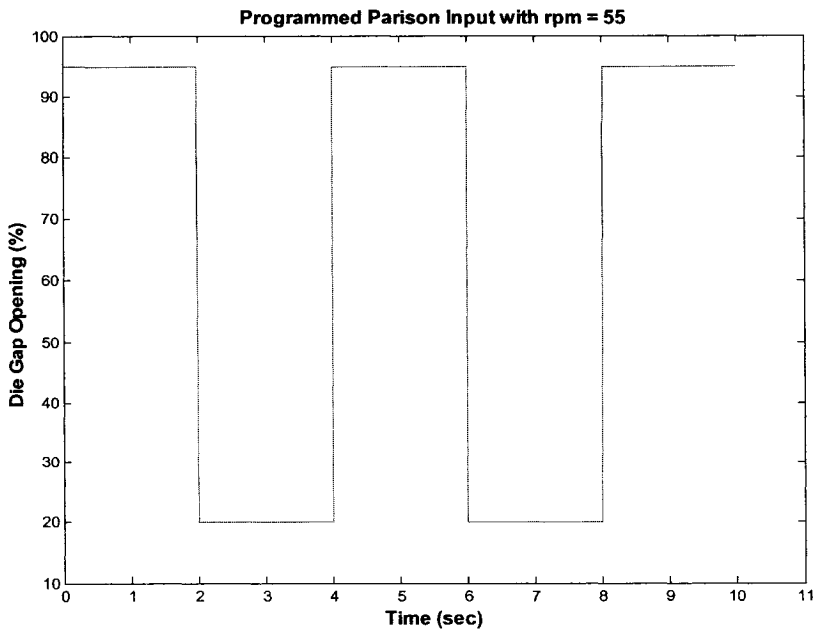

Figure 4-1: Example of input parison programming profile

Figure 4-2 shows the resulting parison length evolution with the above parison programming profile and an extruder speed of 55rpms.

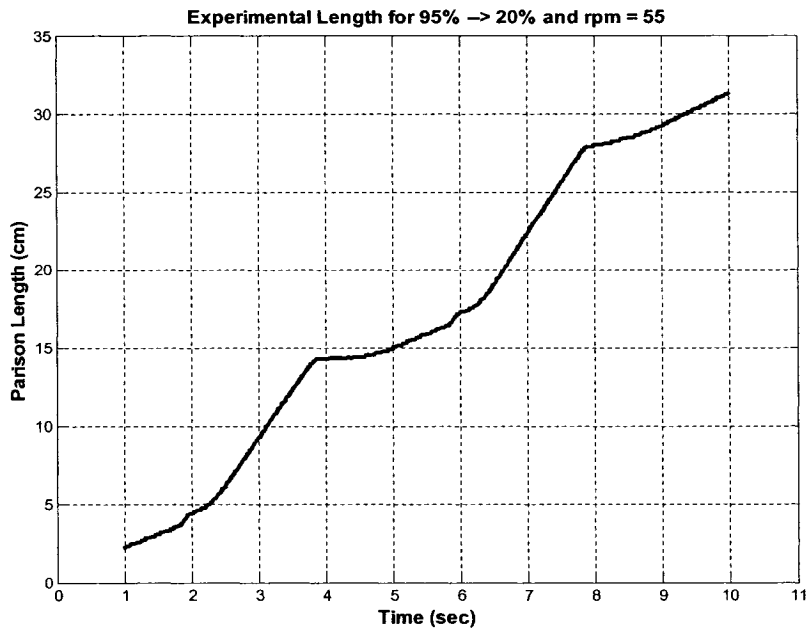

Figure 4-2: Experimental Length for 95% → 20% and rpm = 55

4.1.1 Photron Motion Tools Software

From Figures 4-1 and 4-2, the extrusion time of the parison appears to be 9 seconds. However, the Battenfeld machine is programmed to have an extrusion time of 10 seconds before the clamping stage commences. The pixel-tracking software accompanying the Fastcam PCI restricts the length evolution analysis by one second. The Photron Motion Tools software must have a reference region to successfully to track a region of pixels. An acceptable reference region is only attainable after the first second of extrusion. That is, there is enough melted resin coming out of the die head to be able to track for the following 9 seconds. Figure 4-3 shows a frame at t = 1 second (the parison segment is shown faintly on the right). The white box on the right of Figure 4-3 is the region that the software will use to track the evolution of the parison length. As was mentioned in Section 2.4, the ruler at the bottom of the frame is used as a calibration tool. The origin is located where the knife cuts the parison. Please note that the camera was placed on its side to allow filming of the entire extrusion process in order to maximize the resolution in the direction of increasing parison length (i.e. vertical). As a result, the parison in Figure 4-3 flows from right to left.

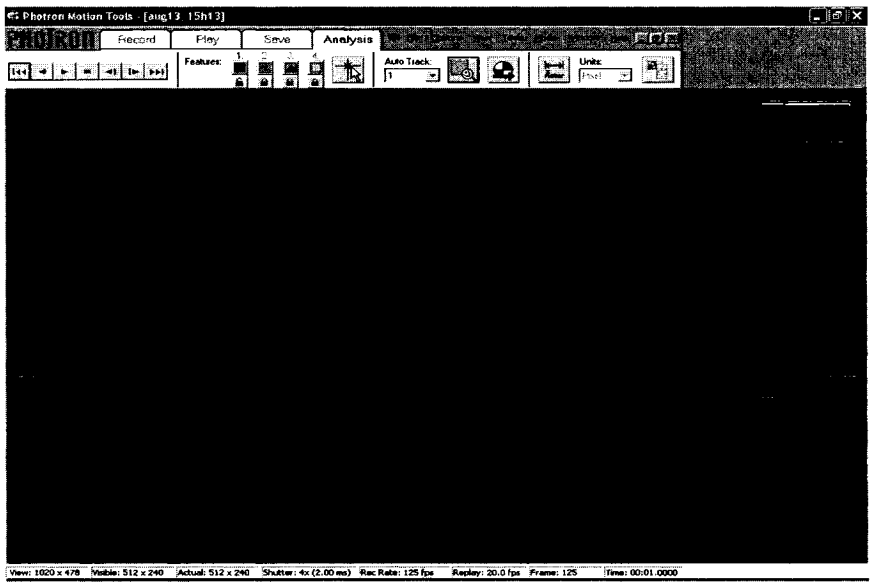

Figure 4-3: Snap shot of video at t = 1 sec

4.1.2 Input vs. Output

Figure 4-4 shows the evolution of the parison length vs. the programming profile used to achieve it.

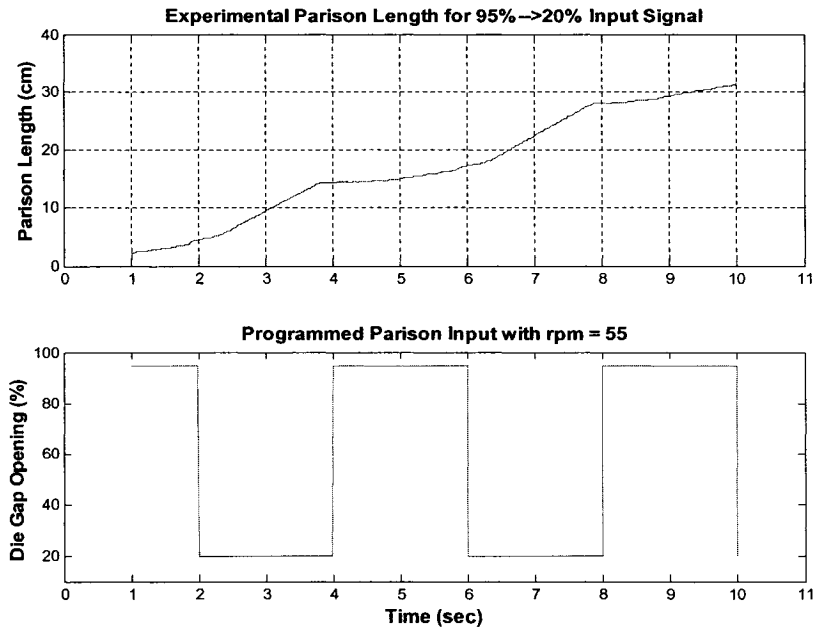

Figure 4-4: Input (95% → 20%) vs. Parison Length

Figure 4-4 concludes that as the die gap changes from 95% to 20% or vice versa, the evolution of the parison length changes accordingly. That is, where the input toggles values at t = 2, 4, 6, 8 seconds, the parison lengths become affected at approximately the same times. This observation will be useful in developing the model in the sections to come.

4.2 Simulink Model 'B'

Another observation from Figure 4-4 is that for a constant portion of the input signal, the output behaves in a linear manner. This observation strongly suggests that the next model (Model 'B') should contain a simple integrator block. As a result, Figure 4-5 represents a simple model using an integrator block.

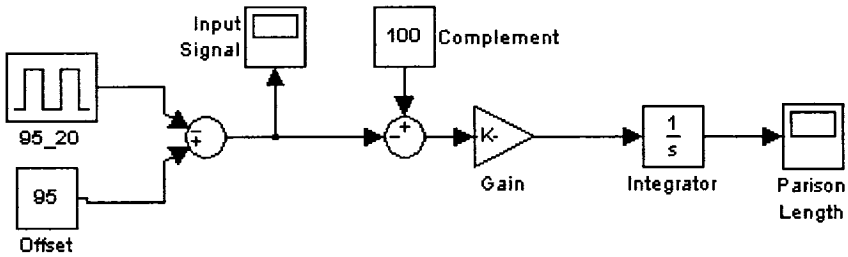

Figure 4-5: Simulink Model 'B'

The left hand side of Figure 4-5 duplicates the parison programming profile that is entered in the Battenfeld and described in the previous section. The 'compliment' block is necessary due to the inverse behaviour of the parison flow rate as the die gap increases. Recall from Section 3.3 that the rate at which the melted resin flows out of the die head decreases as the die gap increases. Normally, the integrator block output will want to increase as the input increases. Finally, the 'Gain' block is present to allow for the model output to best fit the experimental result.

Figure 4-6 compares the output of the model seen in Figure 4-5 to the experimental result for the input signal shown in Figure 4-4 (bottom).

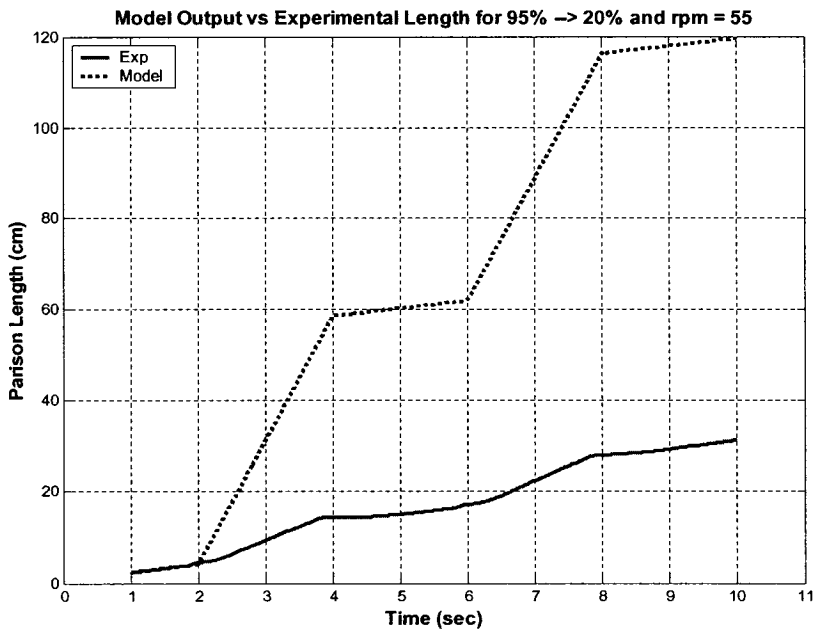

Figure 4-6: Model 'B' output vs Exp Length for 95% → 20% and rpm = 55

Although Model 'B' does not seem to track the experimental result very well, the goal of Model 'B' was to find the appropriate gain such that the curves before the first die gap change (from 95% to 20% at t = 2sec) would coincide. For a 95% die gap opening at rpm = 55, the gain needed was 0.34.

Figure 4-6 also shows that the system is causal. A system is causal "if the output at any time depends only on values of the input at the present time and in the past" [29]. The gain block in the model affects the slope of the parison length evolution for a specific die gap opening. In the example provided, the die head is open at 95% of its maximum stroke length between the time intervals [1, 2], [4, 6] and [8, 10]. With a gain of 0.34, the slopes of the model output are comparable to the slopes of the experimental result for an h_o = 95%. This proves that the model output is affected only by present input values and not by future input values.

The next figures show a similar model (Figure 4-7) and results (Figure 4-9) but for a different input signal (Figure 4-8) programmed in the Battenfeld machine.

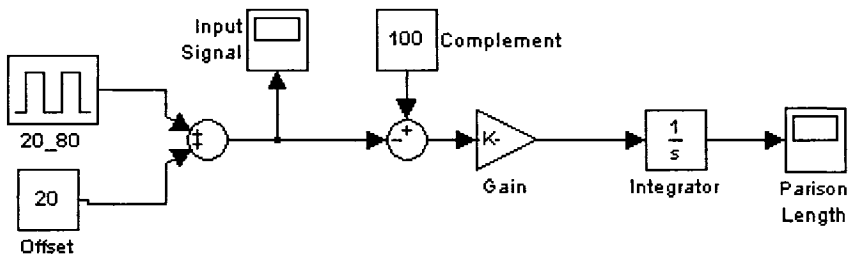

Figure 4-7: Model 'B' for 20% → 80% Input Signal

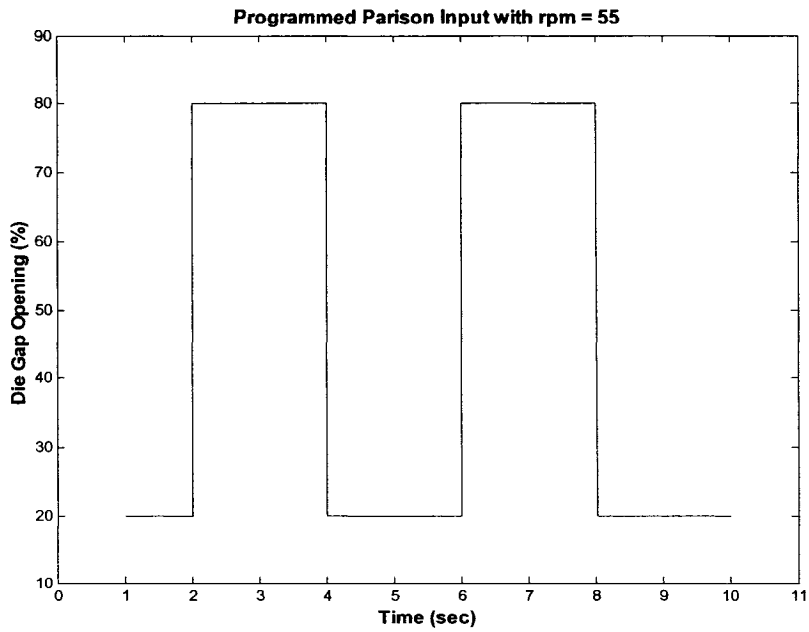

Figure 4-8: Parison Programming Profile for 20% → 80%

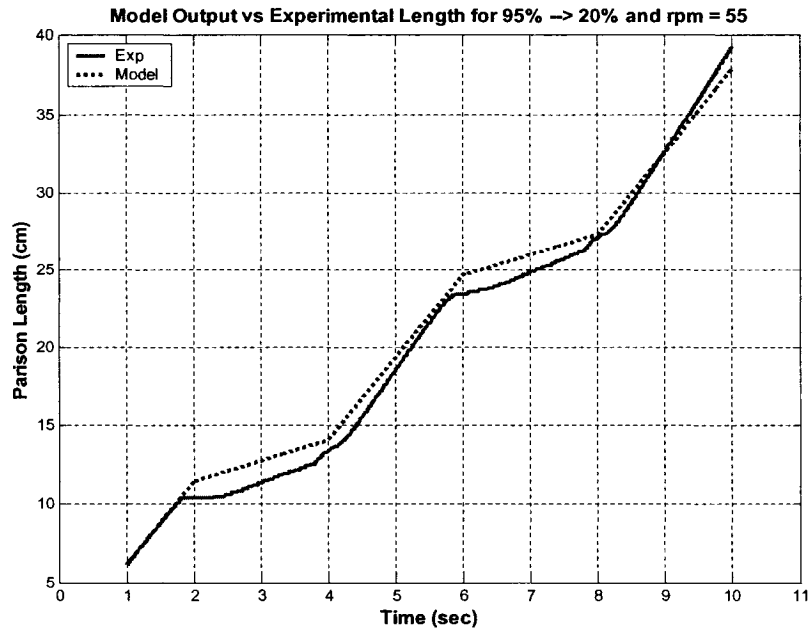

Figure 4-9: Model 'B' output vs. Exp Length for 20% → 80% and rpm = 55

In order to have both curves coincide before the first die gap change at t = 1 second, the gain value in Model 'B' is 0.066. Unlike the first example where the model output varies greatly from the experimental result, Figure 4-9 shows that Model 'B' with a gain of

0.066 does track the experimental result for a 20% → 80% input signal. However, a model must be able to perform adequately for any input. Improvements must therefore be made.

4.3 Gain Matrix

The next step to improving Model 'B' is to create a gain matrix such that numerical gain values are found for several input combinations. For example, one of the gains found in the previous section of 0.34 is specifically for a die gap opening of 95% with a 55 rpm extruder speed. Similarly, for a 20% die gap opening and a 50 rpm extruder speed, the gain proved to be 0.066.

Using the tuning method developed in Section 4.2, gain values are calculated for the other 70 input combinations of die gap openings (18 different h_o) and extruder speeds (4 different rpm). Appendix D shows the list of all the parison programming profiles filmed throughout the entire experiment.

Table 4.1 shows the gain magnitudes for all the possible input combinations. The columns represent the varying die gap openings, while the rows represent the extruder speeds.

Table 4-1: Gain Matrix

	10%	15%	20%	25%	30%	35%	40%	45%	50%	55%	60%	65%	70%	75%	80%	85%	90%	95%
45	0.075	0.062	0.054	0.051	0.046	0.043	0.042	0.042	0.042	0.042	0.050	0.050	0.052	0.056	0.076	0.086	0.128	0.270
50	0.075	0.070	0.066	0.063	0.054	0.050	0.046	0.046	0.047	0.050	0.052	0.052	0.058	0.068	0.075	0.092	0.130	0.300
55	0.083	0.076	0.066	0.060	0.057	0.052	0.052	0.052	0.050	0.051	0.057	0.057	0.063	0.073	0.088	0.106	0.170	0.340
60	0.090	0.078	0.072	0.065	0.061	0.058	0.057	0.054	0.053	0.056	0.062	0.063	0.072	0.078	0.097	0.108	0.200	0.360

The values from Table 4.1 are plotted in Figure 4-10. The gains for each extruder speed are well behaved. Increasing the extruder speed appears to shift the gain curve upwards.

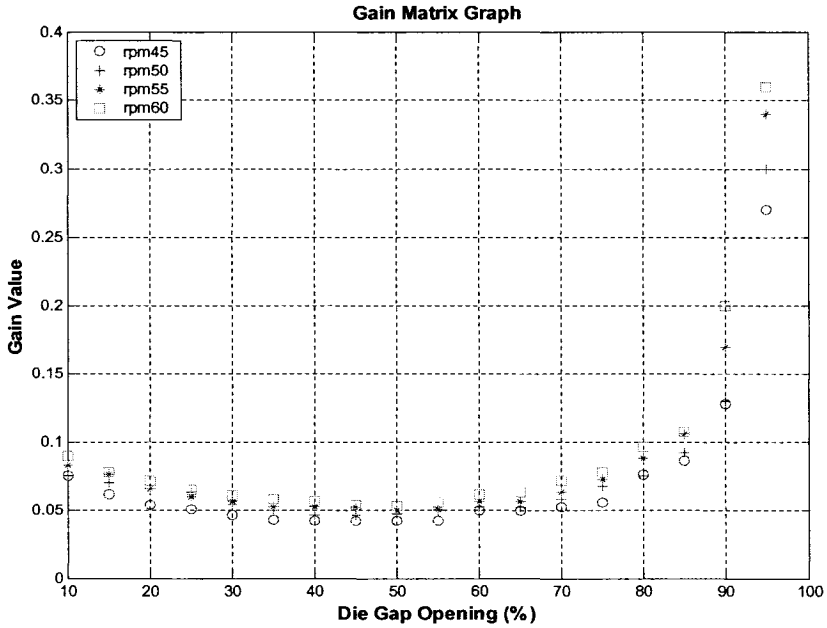

Figure 4-10: Gain Matrix Curves

These gains will be used to improve Model 'B' seen in the next section as Model 'C'.

4.4 Model 'C'

4.4.1 Simulink

Similarly to Model 'A', Model 'B' needs to be improved before designing a MISO in-cycle controller for the continuous EBM process. The easiest way to implement the gains from Table 4.1 is to replace the simple gain block from Figure 4-7 with a look-up table (LUT). Depending on the input, the LUT assigns an output (a gain) to be used throughout the simulation. For example, suppose that the input is a step signal where the die gap openings vary from 95% to 20% as seen in Figure 4-1 with a 55rpm extruder speed. Within the LUT block, the input vector will be [20, 95]. Based on Table 4-1, the corresponding output vector for the LUT is [0.066, 0.34]. The LUT will output a gain of

0.066 if the die gap is at 20%, 0.34 is the die gap is 95% and will interpolate the gains for all die gap openings in between. Figure 4-11 shows the LUT parameter screen as seen in the Simulink software. Below it, Figure 4-12 shows Model 'C' with the LUT block included.

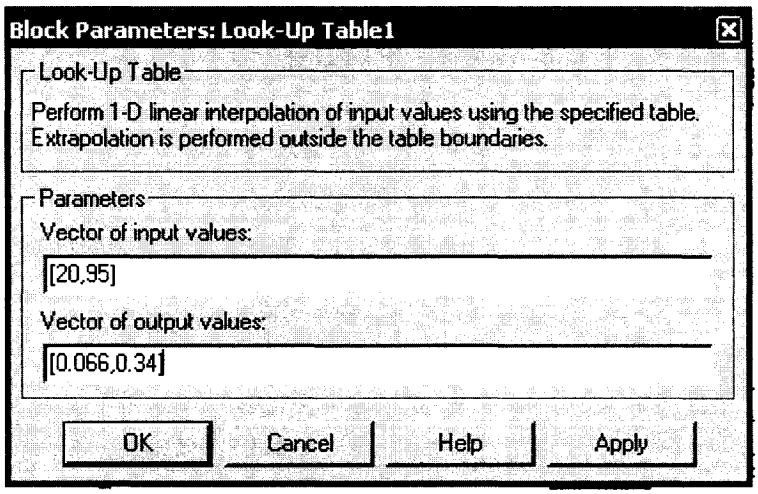

Figure 4-11: LUT Parameter Screen

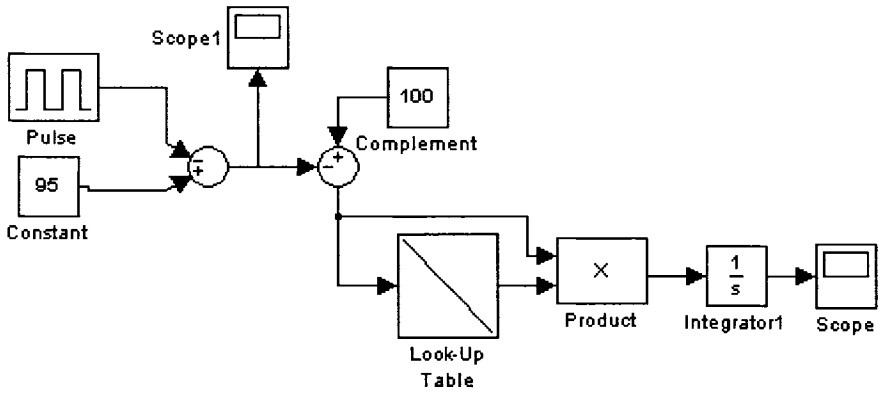

Figure 4-12: Simulink Model 'C'

4.4.2 Model 'C' Validation

Figure 4-13 shows a typical 10 second simulation.

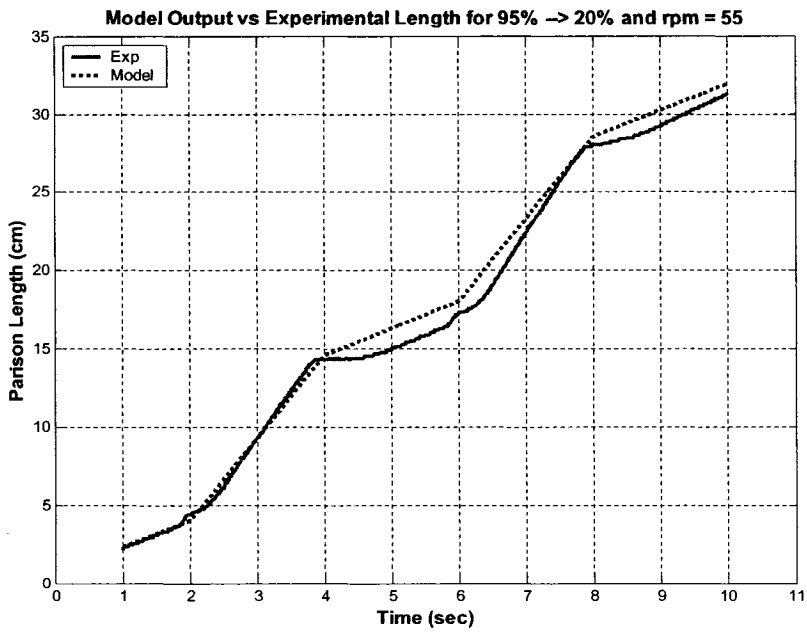

Figure 4-13: Exp vs. Model 'C' Output for 95% → 20% with rpm = 55

To further help validate Model 'C', two more inputs will be simulated. The input values are given below:

- Step signal with h_o varying from 15% to 75% and rpm = 45
- Step signal with h_o varying from 55% to 20% and rpm = 50

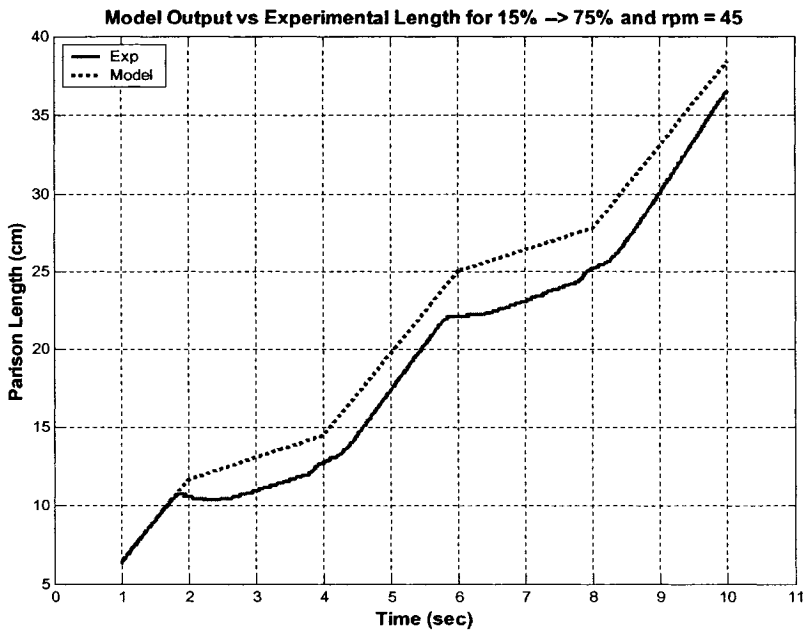

Figure 4-14: Exp vs. Model 'C' Output for 15% → 75% with rpm = 45

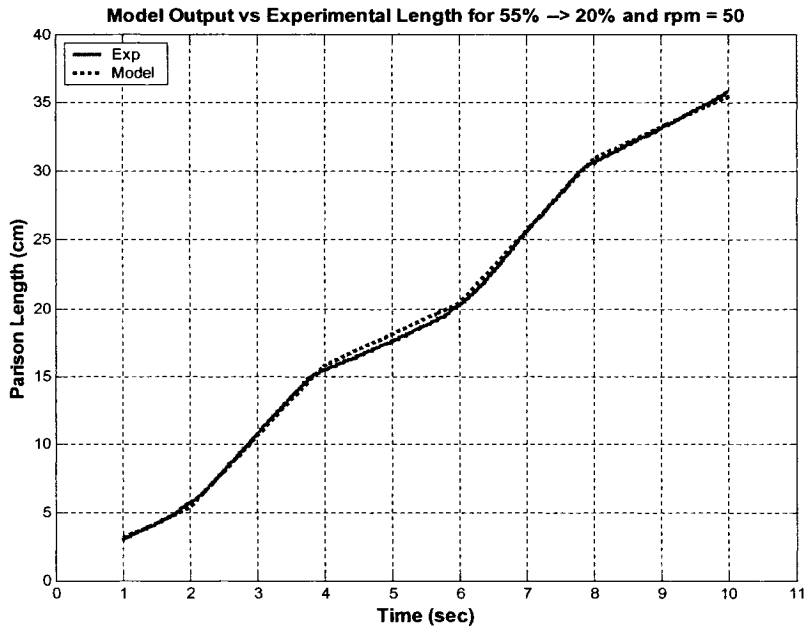

Figure 4-15: Exp vs. Model 'C' Output for 55% → 20% with rpm = 50

The three examples shown in this section offer a wide range of parison programming input signals. Each have a different starting h_o (high, low, medium, resp.), different

changes in amplitudes (75, 60, 35 resp.) and different extruder speeds (45, 55, 50, resp.). An effective method to validate Model 'C' is to compare the error between the experimental and model outputs for each of the three cases. Figure 4-16 represents the error signals.

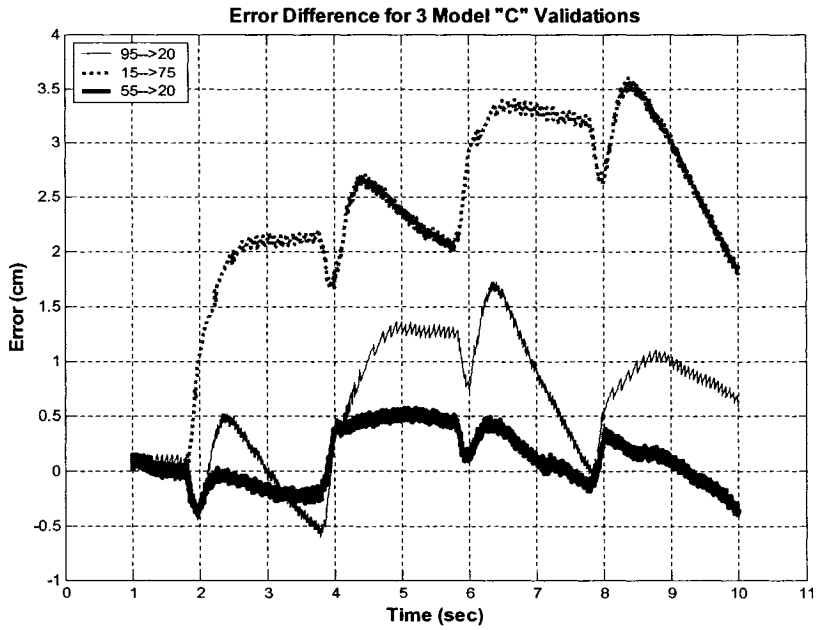

Figure 4-16: Error Comparisons for Model 'C'

Although the input signal having an h_o varying between 55% and 20% seems to be well-modeled by Model 'C', the purpose of an acceptable model is to represent a system for a large range of input signals. Clearly, from Figure 4-16, the input signal having an h_o varying between 15% and 75% is not well-modeled.

The error seen in Figure 4-16 could be explained by lack of detail in Model 'C' given to the die gap transitions. The input signals were carefully designed to vary the die gap opening at every 2 seconds. Taking a closer look at the experimental output in Figure 4-13 shows that the transition areas need particular attention. This will be the focus of the next section.

4.5 Output Abnormalities

A possible reason for the significant errors seen in Figure 4-16 is due to the die gap transition areas in the parison programs. Figure 4-17 recalls the experimental vs. the Model 'C' output for 95% → 20% with rpm = 55.

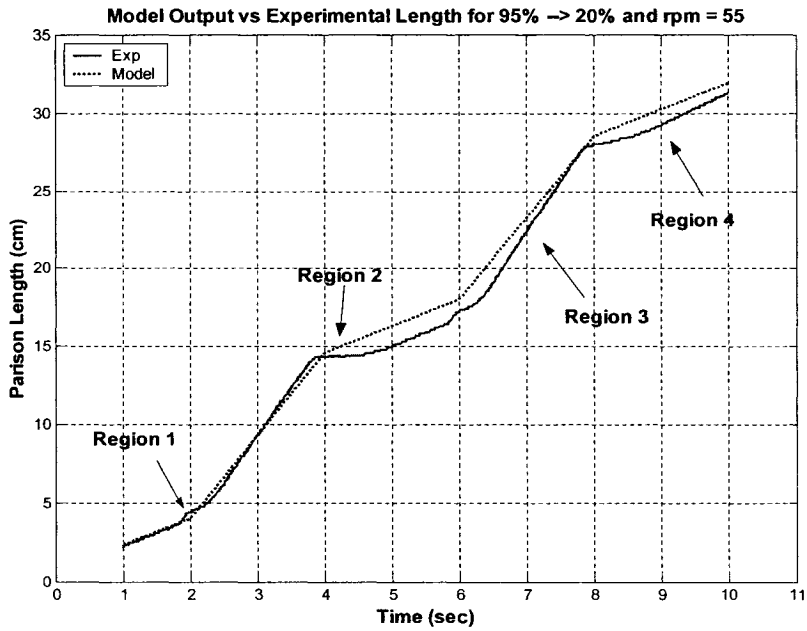

Figure 4-17: Experimental Output for 95% → 20% with rpm = 55

The model output can be divided into four distinct regions, each defined by an abnormality. Each of these abnormalities will be investigated in turn.

4.5.1 Abnormality in Region 1

Region 1 in Figure 4-17 is difficult to see, therefore in Figure 4-18, a close-up is shown.

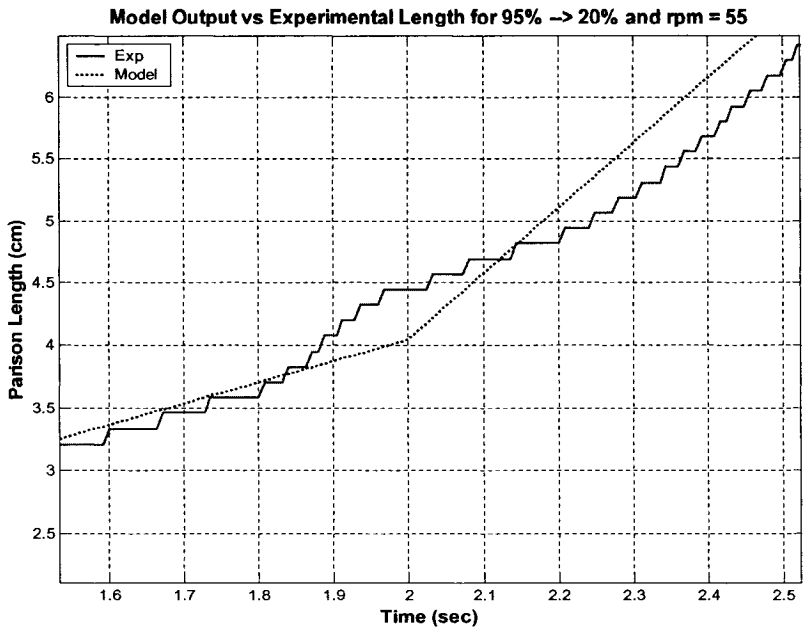

Figure 4-18: Region 1 Abnormality (Close-up)

There are two specific areas that are of interest in Figure 4-18. The first is between 1.8 and 2 seconds where the slope of the parison length curve increases suddenly. In other words, the parison is extruding at a faster rate for these 0.2 seconds. The second time interval is between 2 and 2.2 seconds where the parison seems to be slowing down immediately before it once again tracks the slope of the model.

Recall that the die gap is varying from a larger opening (95%) to a narrower one (20%) at t = 2 seconds. This change in die gap opening creates an increase in pressure. As explained in Chapter 2, reducing the die gap opening is analogous to putting one's thumb in front of a running water hose. The water will travel further or in this case, the melted resin will flow out of the die head at a faster rate.

Similarly, there is a particular machine-related pattern that needs to be investigated. This machine-related conclusion is drawn from the many films produced throughout the experiment. Suppose that the extruder is turned off and there is a short parison hanging from the die head. Please note that the knife that usually cuts the parison during the EBM process was removed for safety purposes. Although the knife was removed, the button on the operator panel that triggers the cut still operates normally. It is this knife-trigger

button that initiates the parison programming profile to begin its sequence. Once the pre-programmed profile changed the die gap from 95% to 20% at t = 2 seconds, an interesting phenomenon occurred. At t = 2 seconds, the length of the parison seemed to decrease. Filming and analyzing this machine-related phenomenon produced the graph seen below. Once again, the extruder is turned off therefore the only action affecting the pre-determined parison length is the change in die gap. Figure 4-19 shows the parison length relative to its starting length before the knife button was triggered.

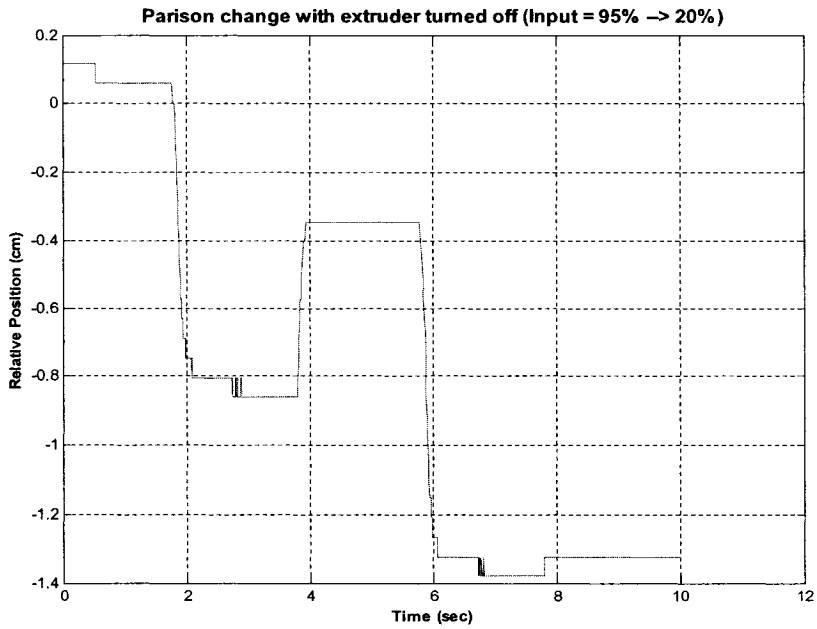

Figure 4-19: Machine Recoil for Input of 95% → 20% while Extruder Turned Off

Figure 4-19 clearly shows the parison recoil and 'lose' length (up to 8mm-10mm) at times where the die gap opening decreases (at t = 2 sec and t = 6 sec). Similarly, the inverse in true where the parison increases its length as the die head increases its gap.

These machine-related changes in length are due to the vertical displacement of the mandrel pin within a fixed bushing via a hydraulic system. Since the change in die gap for this example is large (75% difference), the diverging die attached to the mandrel pin physically lifts the free-hanging parison to the new, smaller die gap position thus 'decreasing' its overall length. Figure 4-20 shows the difference between a 95% (left) and a 20% (right) die gap opening with a fixed bushing.

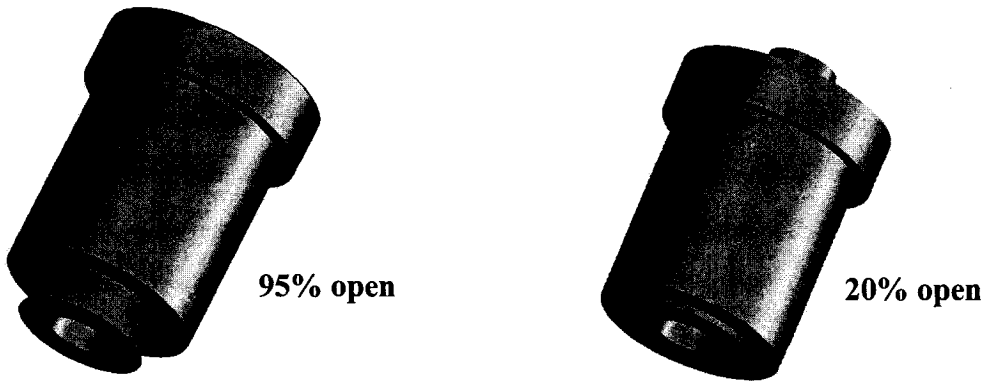

Figure 4-20: Die Gap Differences

This 'recoil' phenomenon could explain the decrease in extruded resin speed seen in the second interval between t_{ext} = 2 and 2.2 seconds. It is the pressure caused by the extrusion in the die head that prevents any 'loss' of parison length. The evolution of the parison length continues to behave normally once steady state is reached at t_{ext} = 2.2 seconds.

4.5.2 Abnormality in Region 2

Unlike to the previous subsection, the Region 2 abnormality is solely due to a pressure difference between die gap openings. Figure 4-21 shows a close-up view of Region 2.

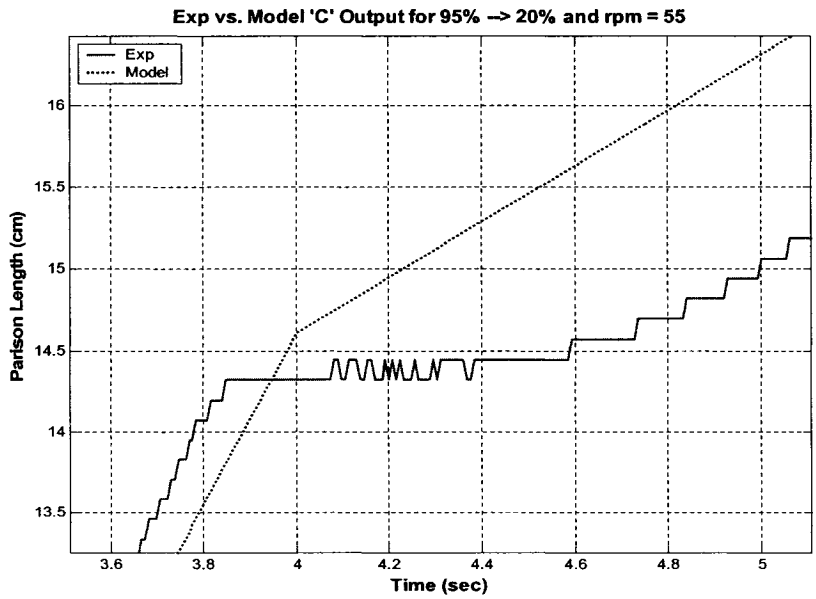

Figure 4-21: Region 2 Abnormality (Close-up)

Recall that at t_{ext} = 4 seconds, the parison programming profile informs the mandrel pin to increase the die gap from 20% to 95%. The die gap increase leads to an increase in volume inside the die head. As a result, for a very brief period of time, the melted resin must fill the void inside the die head before the parison can continue to increase in length. The pressure within the die head returns to normal once the void is no longer. Beyond this point, the model seems to track the experimental result adequately. This small plateau can be seen in all cases where the die gap increases significantly.

4.5.3 Abnormalities in Region 3 and 4

The abnormalities in Regions 1 and 2 cover the discrepancies between the experimental result and the Model 'C' output specifically during transition times. The abnormalities in Regions 3 and 4 occur in the later stages of the extrusion process. Figure 4-22 shows the close-up view of Region 3 while the die gap is 20% open.

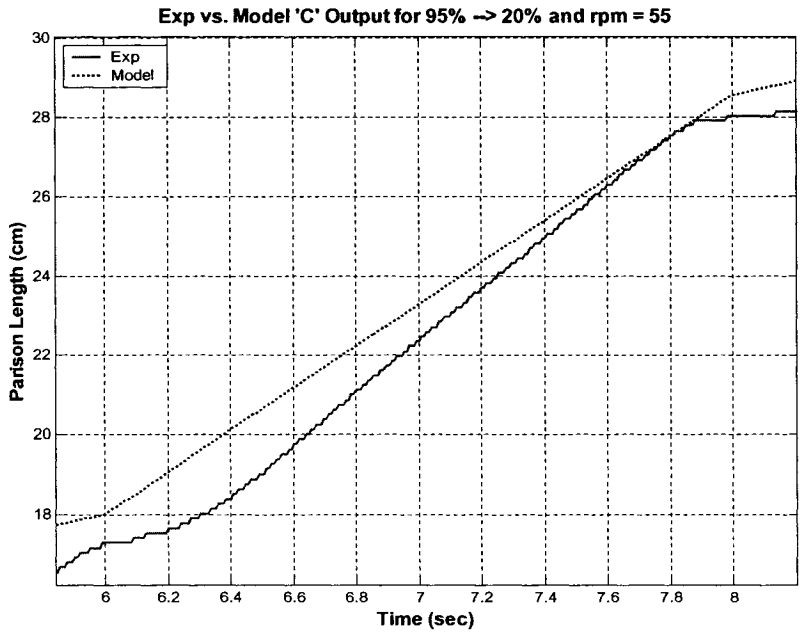

Figure 4-22: Region 3 Abnormality (Close-up)

Between t = 6.2 seconds and t = 7.8 sec, the slopes of the experimental result and the Model 'C' output are clearly different. The experimental slope is steeper than the slope from the model. On the Battenfeld, this relates to the melted HDPE flowing out of the die head faster than the modeled version. The difference in slopes is explained by a rheological property called sag. The effect of sag is proportional to extrusion time. The weight of the parison pulls down and stretches the parison due to gravity, therefore increasing its length. Note that the Region 1 abnormality also occurs at t = 6 seconds.

Figure 4-23 shows another example of sag when the die gap is opened at 95%.

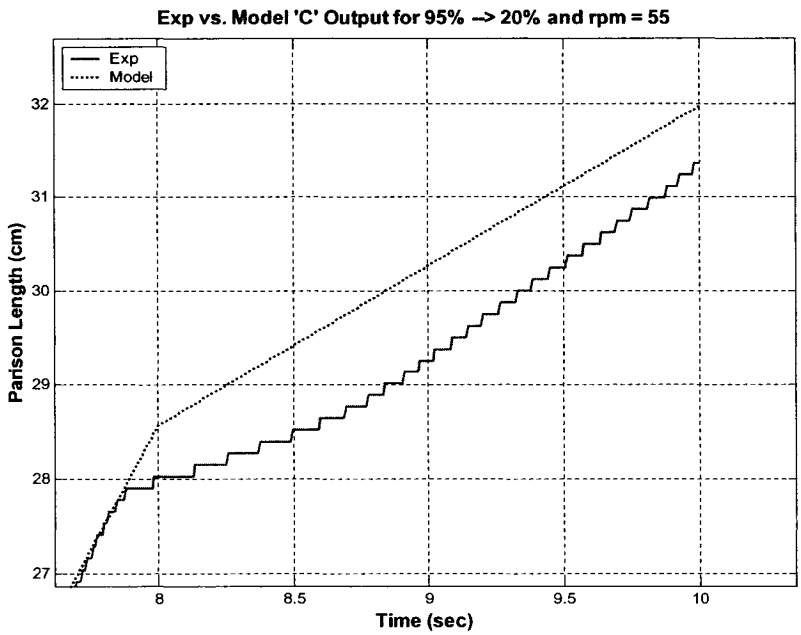

Figure 4-23: Region 4 Abnormality (Close-up)

Figure 4-23 shows the final 2 seconds of the evolution of the parison length for a die gap opening h_o = 95%. The slopes between t_{ext} = 8 and 10 seconds are comparable but the experimental curve (solid line) is still slightly steeper than the Model 'C' output. This can once again be attributed to the sag effect of the parison. However, since the die gap is large, the thicker extruded parison will be less subject to sag.

This section proves that Model 'C' needs to be altered to take into effect the transition periods of the die head and the rheological properties of the polymer. The next sections will provide improvements to Model 'C'.

4.6 Input Signal Changes

Before any improvements to the actual model are made, the input signal entering the model must be modified to better represent the system. Figure 4-24 once again shows the original input signal for Models 'B' and 'C'.

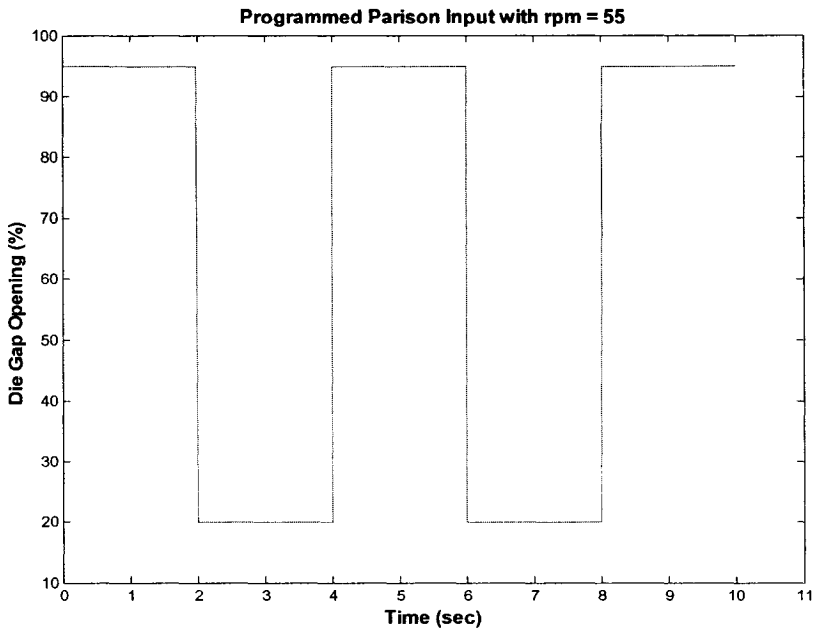

Figure 4-24: Input parison programming profile for 95% → 20% and rpm = 55

This input signal represents instantaneous changes in the die gap opening. However, perfect transitions do not exist in industry. There are always delays due to the mechanical restrictions of the machine. Other than show the abnormalities, Figures 4-18, 4-21, 4-22 and 4-23 clearly indicate that the Battenfeld machine starts its transitions a few tenths of a second *before* the ideal $t_{transition}$. Similarly, these same figures show that the steady state of the resin flow occurs a few tenths of a second *after* $t_{transition}$. In all, there is about 0.4 or 0.5 seconds of transition time before steady-state is reached. As a result, the input signal seen in Figure 4-24 needs to be modified to include these mechanical delays. This is done by including a 'Slew Rate Limiter' block from the Simulink Library after the 'Pulse Generator' block as seen in Figure 4-25. Figure 4-26 shows the resulting adjusted input signal compared to the original square wave input.

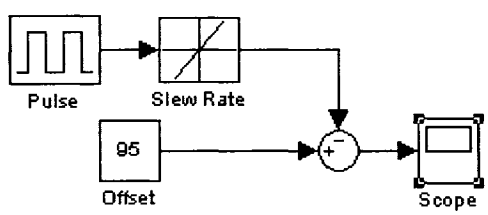

Figure 4-25: Slewed Input for 95% → 20%

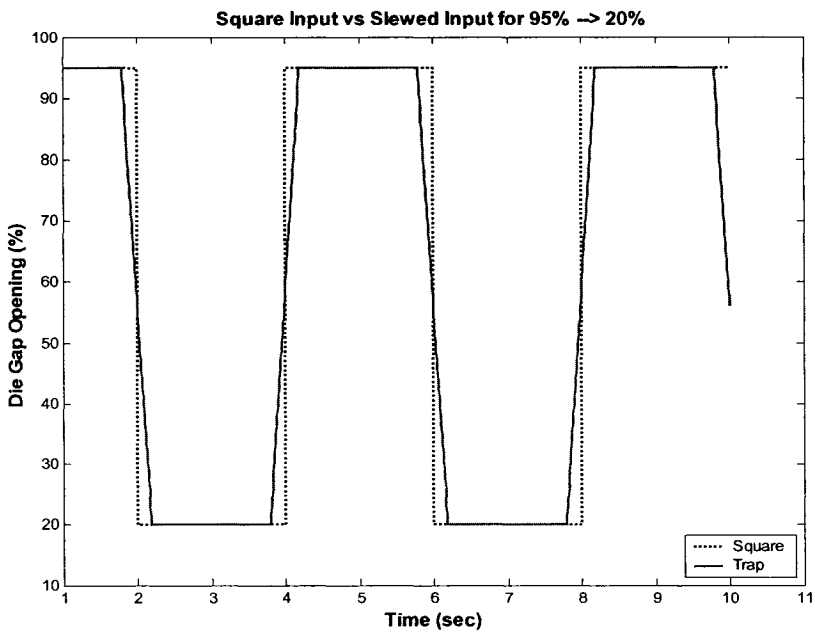

Figure 4-26: Slewed vs. Square Input Signal for 95% → 20%

The solid line in Figure 4-26 is a more realistic representation of the input due to mechanical delays when displacing the mandrel pin. Having a more realistic input will lead to designing a better model and consequently a better controller.

4.7 Model 'D'

4.7.1 Simulink

The focus of this section is to better model the periods of die gap opening transitions. Model 'D' will attempt to better track the experimental results for the 0.4-0.6 second transition periods throughout the parison programming profile. The easiest way to track the transition is to include more elements inside the LUT. Rather than have two elements and interpolate between them, adding more elements will allow for a better fitting of the experimental curve. Figure 4-27 shows a LUT block with more elements in the input and output vectors.

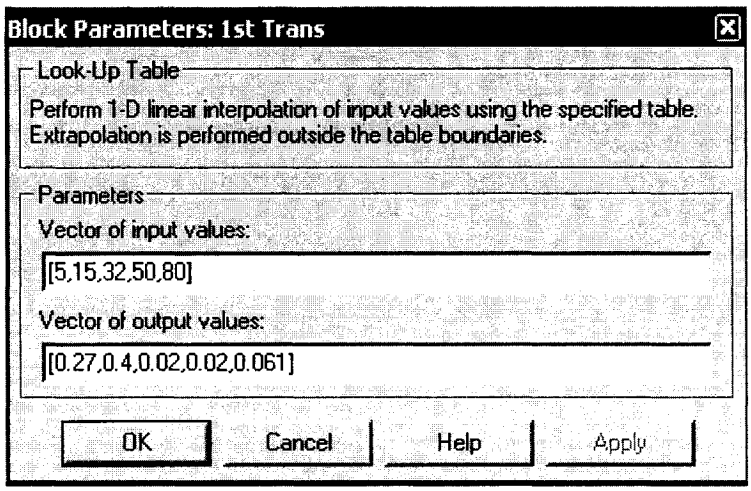

Figure 4-27: More detailed LUT

There is a disadvantage in adding more elements to the LUT. The gain values between those determined by Table 4-1 are found by trial and error which could potentially be very time consuming.

Another disadvantage to adding more elements in the LUT is based on the abnormalities shown in Sections 4.5.1 and 4.5.2, where transition behaviours depend on whether h_o is increasing or decreasing. The consequence of this is that the LUT seen in Figure 4-25 cannot be used for the next h_o transition at $t_{ext} = 4$ seconds where the die gap increases from 20% to 95%. A second LUT is therefore required to take into account the abnormality in the second transition.

Section 4.5.3 also suggests that more LUTs are recommended. This is due to the sag effect. Although the die gap openings repeat throughout the parison profile, the gains in the latter part of the extrusion need to be slightly increased to take into account the sag phenomenon. In all, since there are a total of four die gap transitions in the parison profile (see Figure 4-26), there will be a total of four LUTs in Model 'D'. These LUTs will each be triggered by a switch at the appropriate times. Figure 4-28 shows Model 'D' in Simulink.

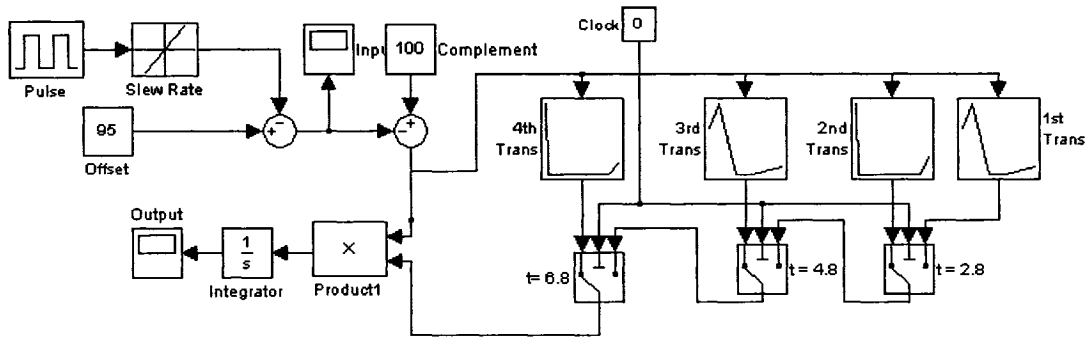

Figure 4-28: Model 'D' in Simulink

The next sub-section will verify whether Model 'D' classifies as a good model.

4.7.2 Model 'D' Validation

This section will analyze the same three parison programming profiles, or input signals, as the Model 'C' Validation Section 4.4.2 which requires each signal to be adjusted with the slew factor explained in Section 4.7.1. Table 4-2 recaps the input signals seen previously in this chapter.

Table 4-2: Input Signals Analyzed

Input Signal #	Starting h_o (%)	Next h_o (%)	RPM	# of Transitions	Slew Rate (sec)	Extrusion Time (sec)
1	95	20	55	4	0.4	10
2	15	75	45	4	0.4	10
3	55	20	50	4	0.4	10

For each of the parison profiles in Table 4-2, there will be a diagram that compares the Model 'D's output to the experimental result, a diagram showing the error between the two curves and a last diagram comparing the errors signals from Models 'C' and 'D'. The following three figures are for Signal #1.

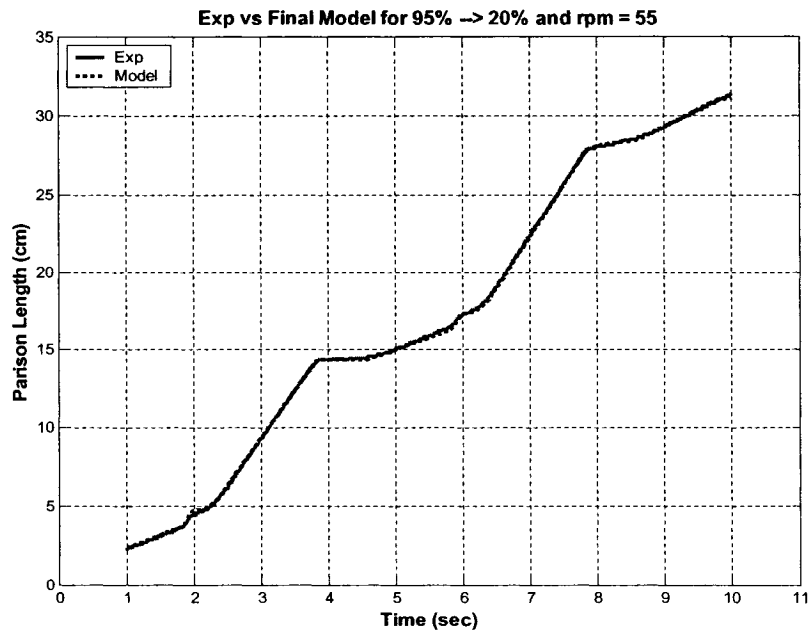

Figure 4-29: Exp vs. Model 'D' for 95% → 20% and rpm = 55

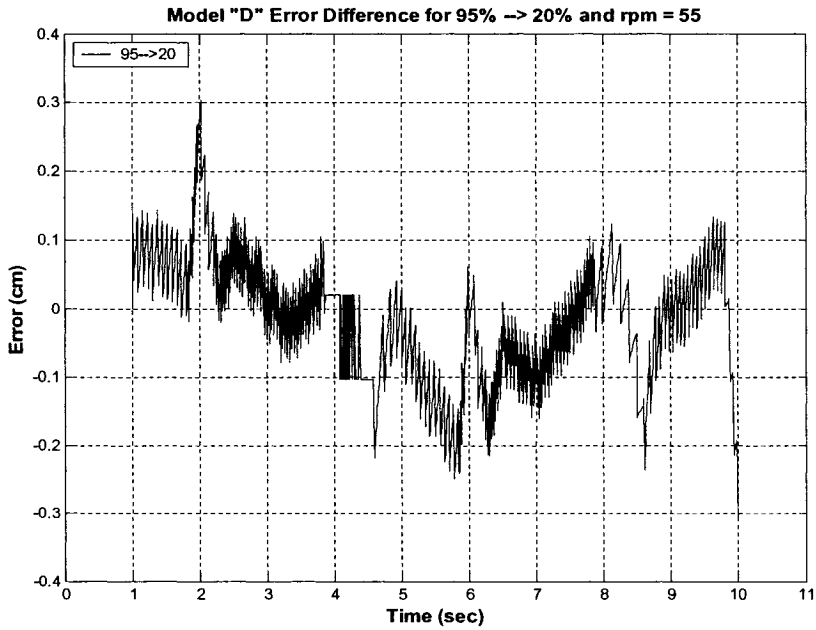

Figure 4-30: Model 'D' Error Signal for 95% → 20% and rpm = 55

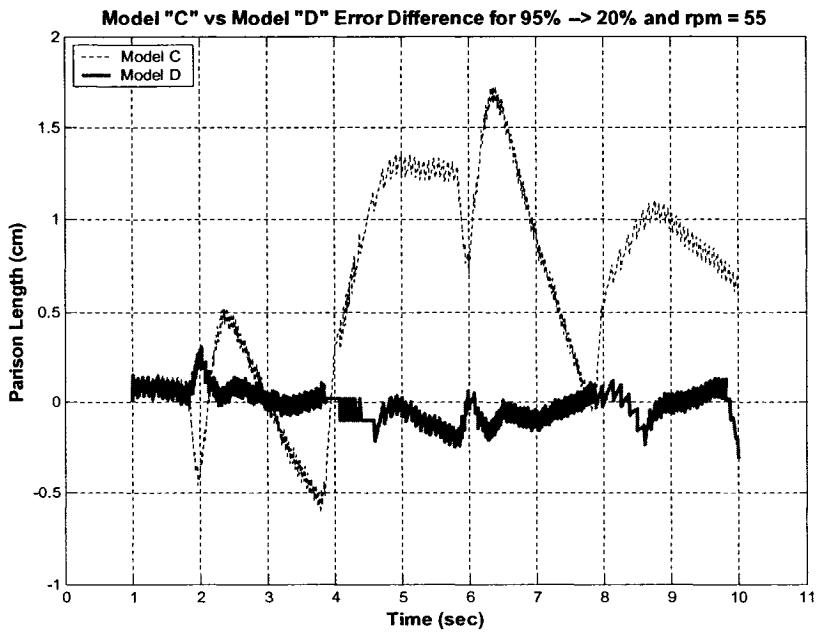

Figure 4-31: Model 'C' and Model 'D' Errors for 95% → 20% and rpm = 55

Figures 4-32, 4-33 and 4-34 are for Signal #2.

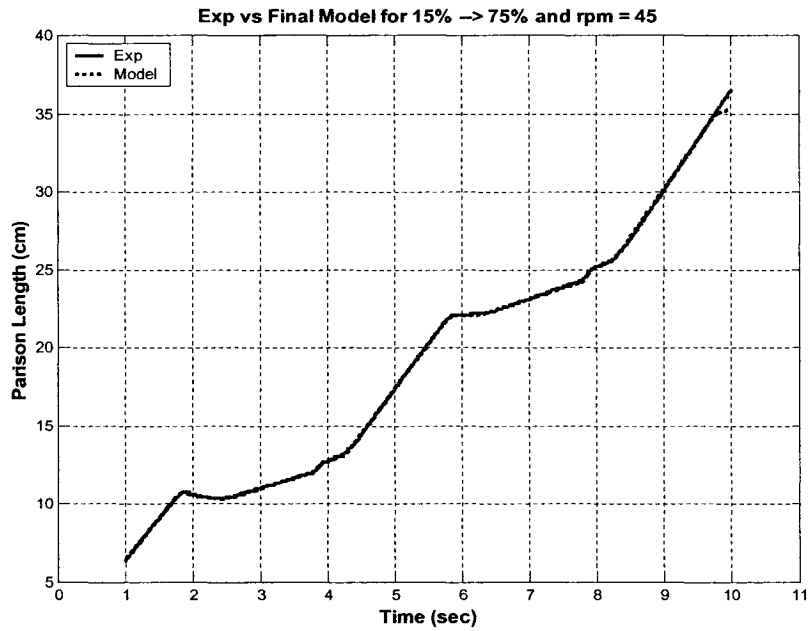

Figure 4-32: Exp vs. Model 'D' for 15% → 75% and rpm = 45

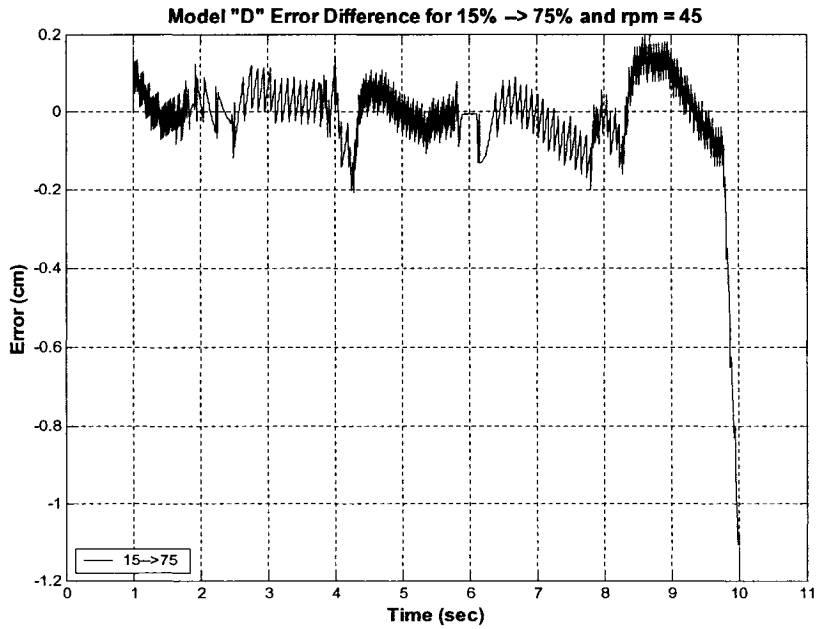

Figure 4-33: 'D' Error Signal for 15% → 75% and rpm = 45

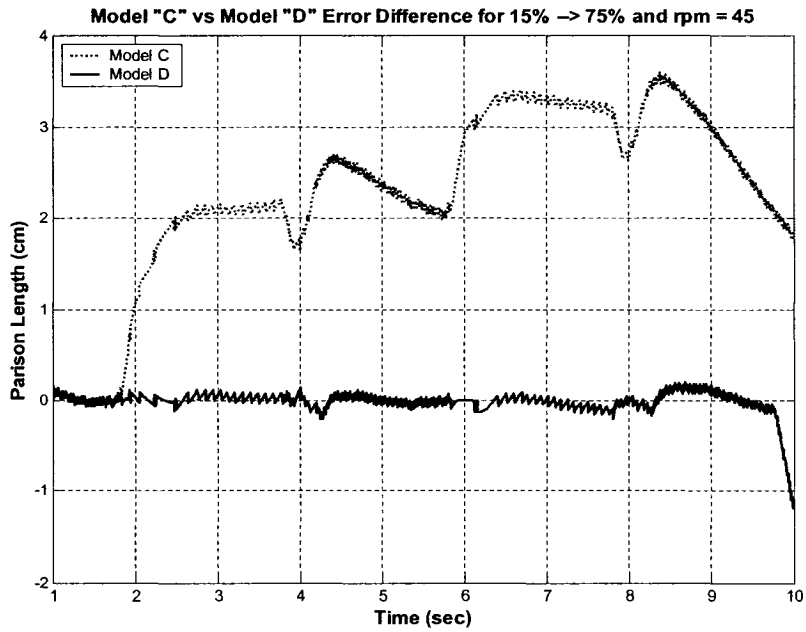

Figure 4-34: Model 'C' and Model 'D' Errors for 95% → 20% and rpm = 55

Finally, Figures 4-35, 4-36 and 4-37 are for Signal #3.

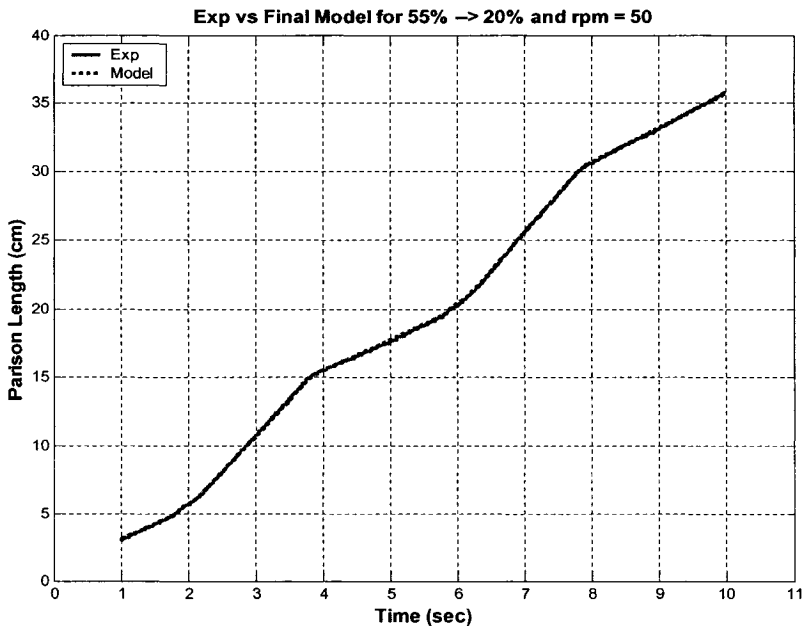

Figure 4-35: Exp vs. Model 'D' for 55% → 20% and rpm = 50

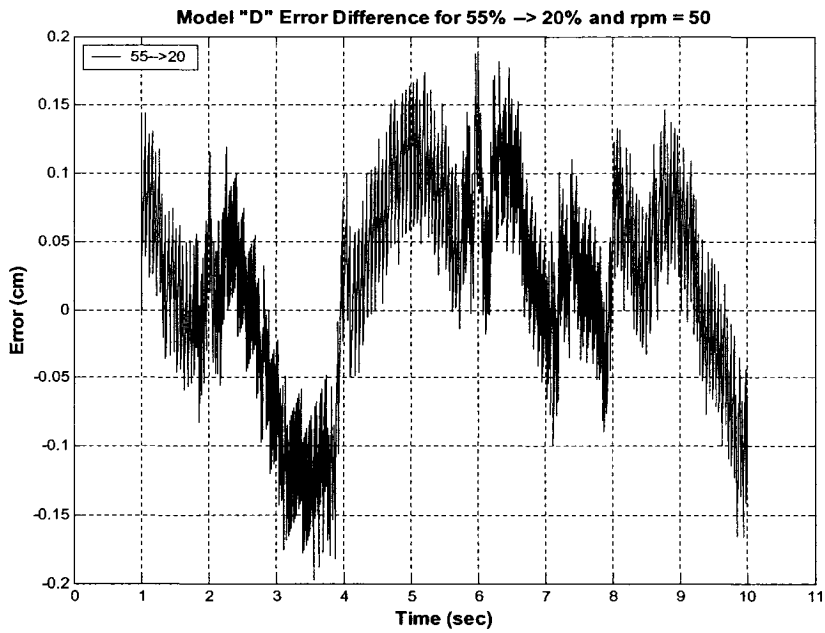

Figure 4-36: Model 'D' Error Signal for 55% → 20% and rpm = 50

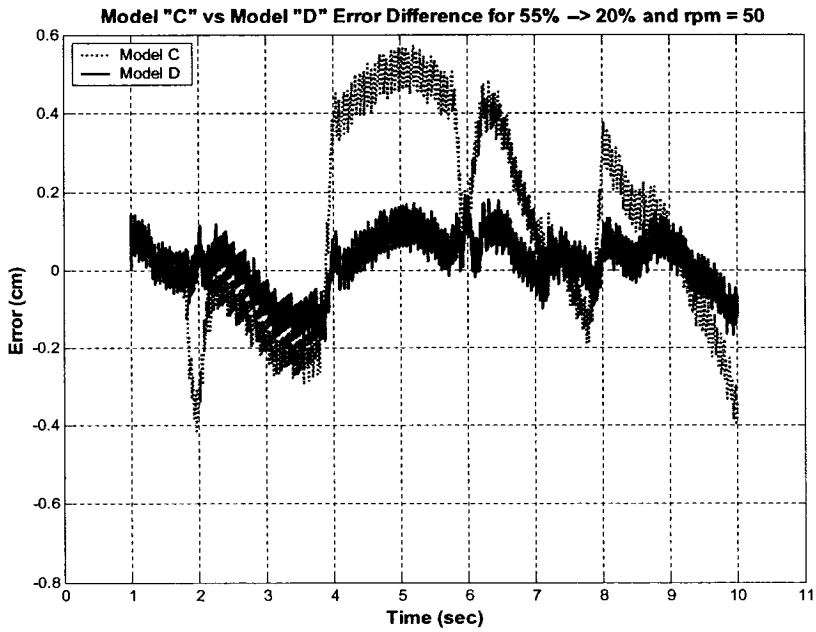

Figure 4-37: Model 'C' and Model 'D' Errors for 95% → 20% and rpm = 55

Whereas Model 'C' was able to predict the correct parison length for only one out of the three signals analyzed (55% → 20%, rpm = 50), Model 'D' is able to track all three of the parison programming profiles. This is shown in Figures 4-31, 4-34, and 4-37 where Model 'D' consistently produced a smaller error than Model 'C'. In fact, with some minor tuning of the LUT gains, Model 'D' is able to predict the parison length for any of the seventy-two input signals studied in this research (see Appendix D) within 1mm as shown in Figures 4-30, 4-33, and 4-36.

4.8 RPM Gains

Although Model 'D' seems to be developed enough to start the design of the controller, there is still one last modification required. Recall in Chapter 3 that the EBM MISO in-cycle controller to be designed has two inputs ($rpm \& h_o$) and a single output (parison length). Model 'D' developed in the previous sections takes into account the effects of die gap change on the system but does not consider the effect of extruder speed. Therefore, this section will focus on understanding how a change in the extruder speed

affects the dynamics of the system. Consequently, the modifications made due to rpm effects will be represented in Model 'E'.

4.8.1 'Family' of Inputs

For the purpose of this thesis, a 'family' of inputs is defined as a group of identical parison programming profiles each extruded at a different speed. Since there are four extruder speeds studied (rpm = 45, 50, 55, 60), there is a maximum of four input signals per family. For example, all parison profiles varying from 20% to 80% in the step pattern seen throughout the thesis belong to the same family. Figure 4-38 shows the experimental results for each of the four 20% → 80% family members.

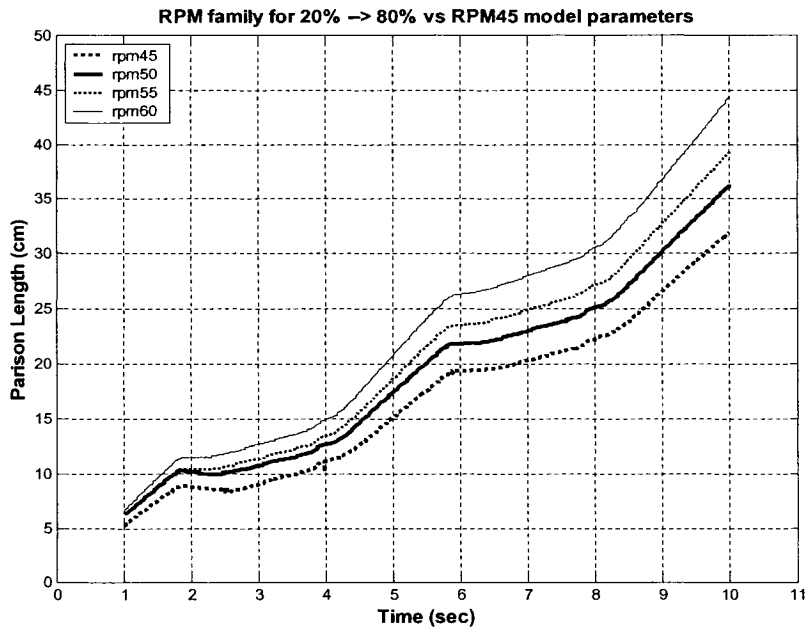

Figure 4-38: Experimental Results for 20% → 80% Input Family

Figure 4-38 seems to suggest that increasing the extruder speed from rpm = 45 to rpm = 60 does not affect the shape of the curves but rather simply amplify them. Therefore, finding a relationship of these four curves with respect to the extruder speed is crucial to reduce the number of LUTs needed to model a family. To determine this relationship, a

gain block was added after the integrator in Model 'D'. This gain block (shaded) is seen in Figure 4-39.

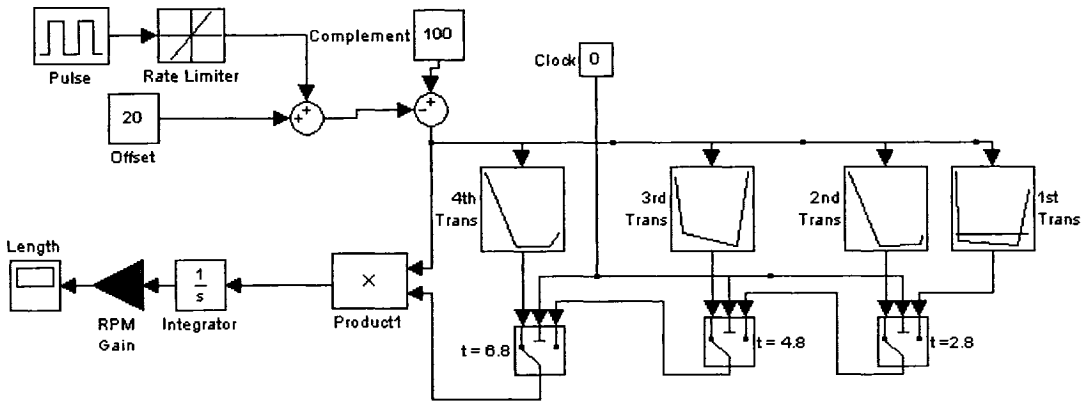

Figure 4-39: Model 'D' with an added Gain Block

The RPM Gain block having a value of 1 represents an extrusion speed of 45rpm. Figure 4-40 shows the output from Model 'D' in Figure 4-39 versus the experimental result.

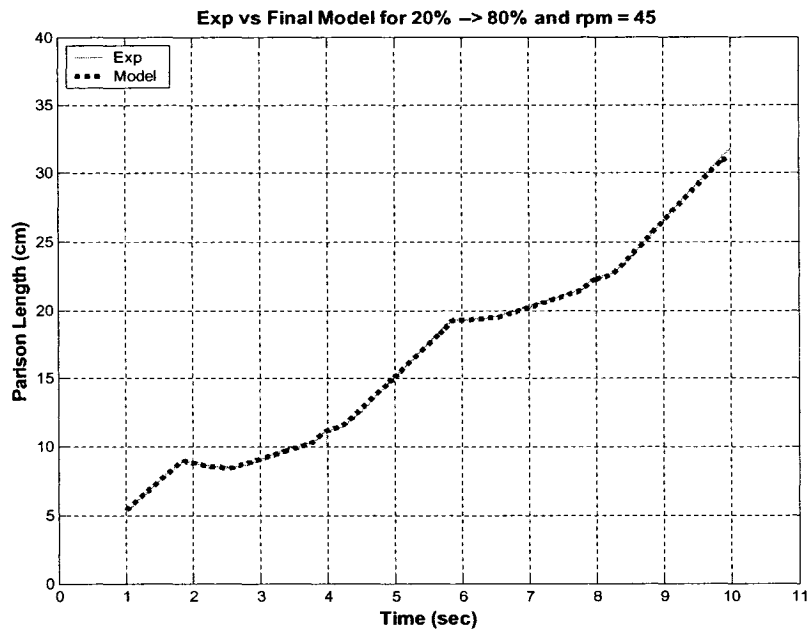

Figure 4-40: Exp (rpm = 45) vs. Model 'D' Output with RPM gain = 1

Increasing this gain value and comparing the outputs of the model with their corresponding experimental results will determine the gains for the other three extrusion speeds for the 20% → 80% family. Figure 4-41 shows the output of the model in Figure 4-39 with a RPM gain of 1.12. This curve is compared to the experimental result for the 20% → 80% input signal with rpm = 50.

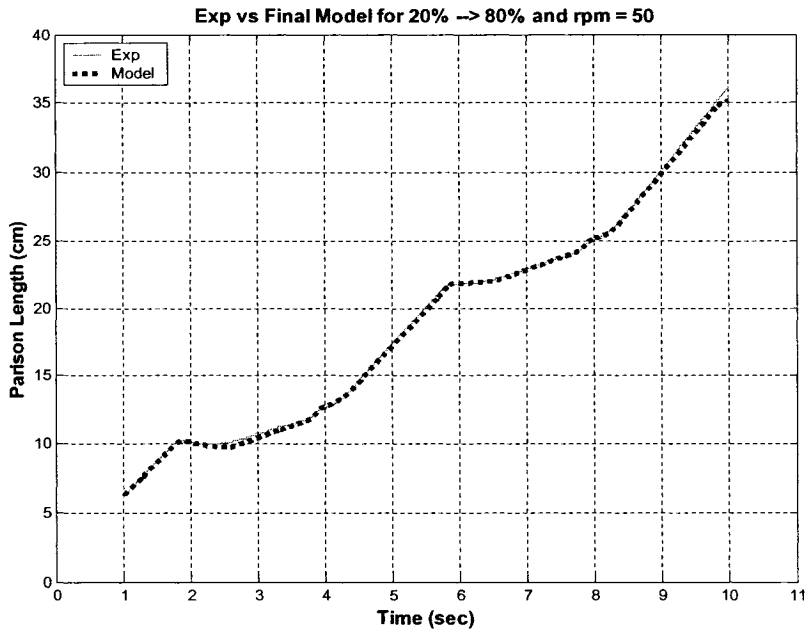

Figure 4-41: Exp (rpm = 50) vs. Model 'D' Output with RPM gain = 1.12

Similarly, Figures 4-42 and 4-43 show the results for extruder speeds of 55rpm and 60rpm respectively. The RPM gain value that best fit the 55rpm experimental curve was 1.25 while a value of 1.38 was needed for the 60rpm experimental curve.

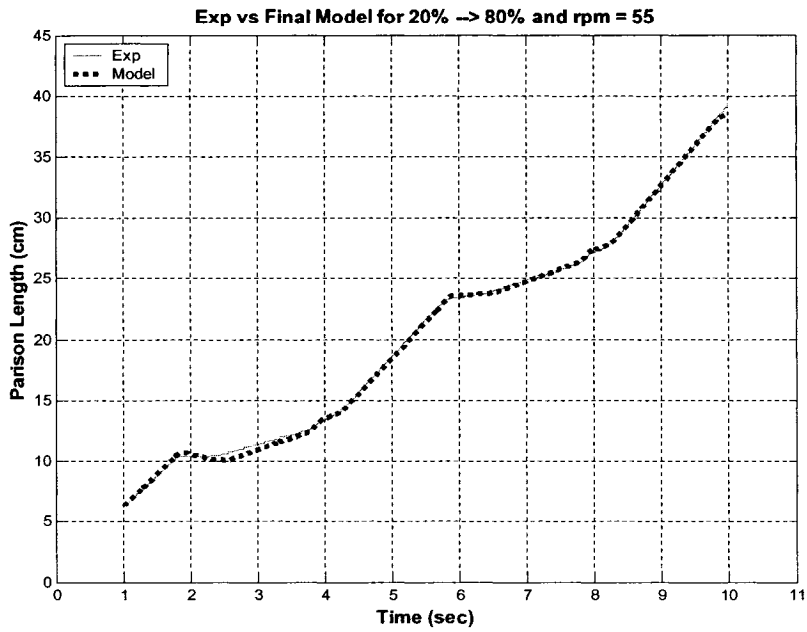

Figure 4-42: Exp (rpm = 55) vs. Model 'D' Output with RPM gain = 1.25

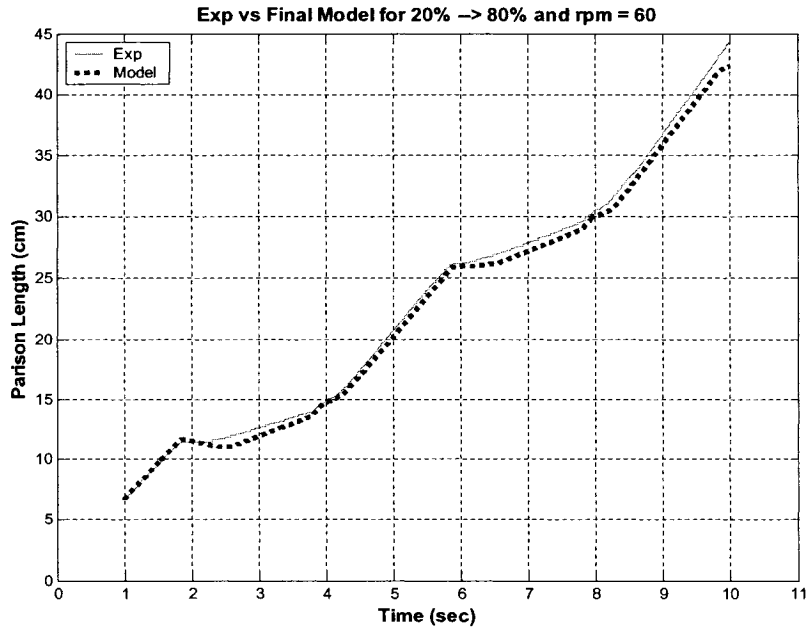

Figure 4-43: Exp (rpm = 60) vs. Model 'D' Output with RPM gain = 1.38

The next sub-section will analyze the relationship between the four RPM gain values for the 20% → 80% family of inputs. In addition, other families will be analyzed to determine a master RPM gain relationship representing all the input families.

4.8.2 RPM Gain Relationship

Figure 4-44 plots the gains needed to correctly predict the experimental result with respect to the RPM.

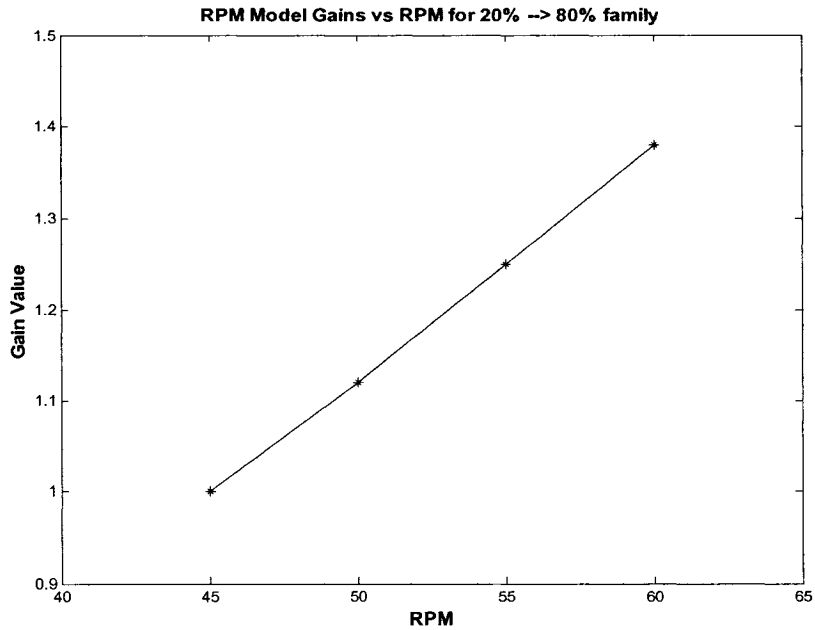

Figure 4-44: RPM gains vs. Extruder Speed

Figure 4-44 shows that the relationship between the parison lengths with respect to the extruder speed is linear. To support the last statement, four other families of inputs were considered. The families are: 95% → 20%, 45% → 90%, 10% → 90%, and 75% → 90%. These families were chosen to represent a wide range of parison programming profiles. They drastically differ in starting gaps and amplitudes. Table 4-3 displays the different input families with the gains needed to correctly predict the experimental results.

Table 4-3: RPM Gains for four (4) different Input Families

X	95%→ 20%	45%→ 90%	10%→ 90%	75%→ 90%
45	1	1	1	1
50	1.07	1.14	-	-
55	1.23	1.22	1.19	1.29
60	1.34	1.35	1.34	1.36

Figure 4-45 represents a graph similar to Figure 4-44 where the rpm gain values are plotted with respect to the extruder speed.

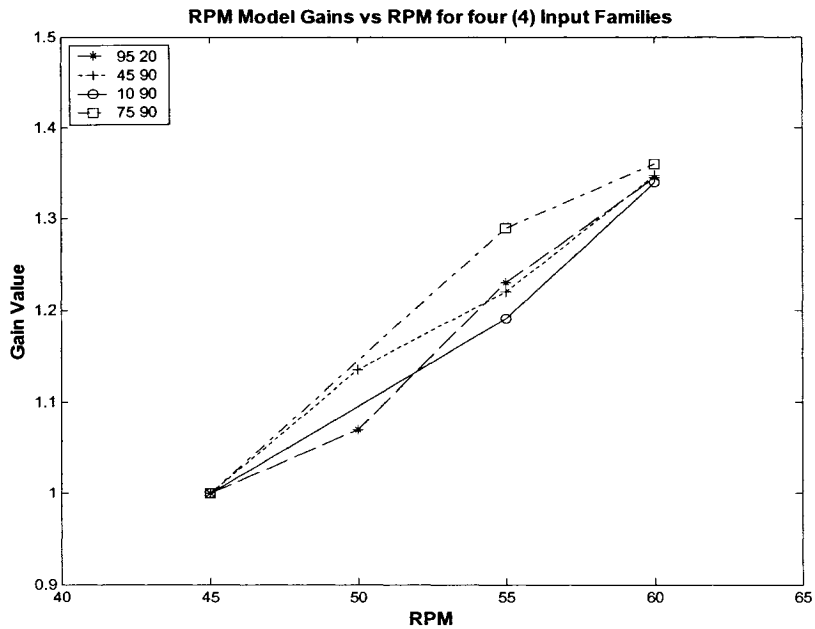

Figure 4-45: RPM gains vs. Extruder Speed for four (4) Input Families

Even though the curves in Figure 4-45 are not perfectly linear, they are close enough to assume that as the extruder speed increases, the rpm gains increase in a linear manner. Therefore, based on values from Table 4-3, the assumed equation of the rpm gain as a function of extruder speed (rpm) is shown as:

$$gain_{rpm}(rpm) = 0.024rpm - 0.08 \tag{4.1}$$

A small block configuration representing the effect of the extruder speed on the parison length will replace the 'RPM Gain' block shown in Figure 4-39. The result is shown as the Model 'E' (Figure 4-46) block diagram in the next section.

4.9 Model 'E'

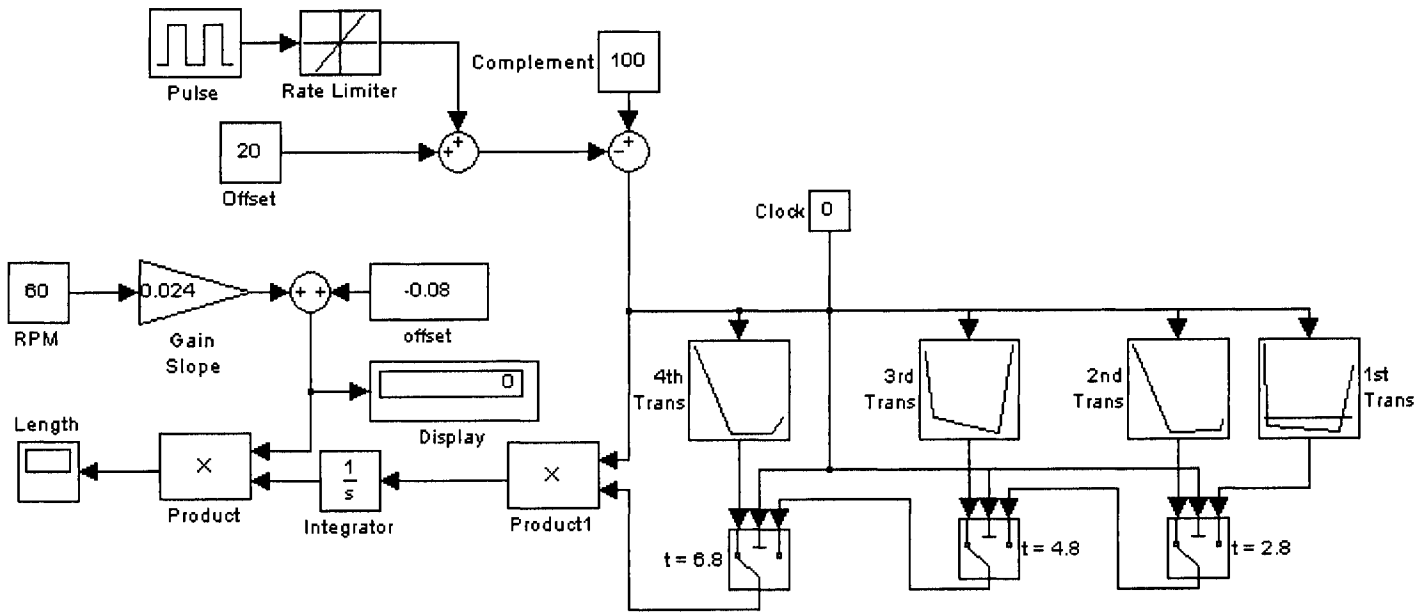

Figure 4-46: Model 'E' Block Diagram

5 Controller Design

Designing a controller for the EBM process is one of the objectives of this thesis. Model-based control design requires a plant model. Chapter 4 focused on developing a plant model using basic system identification methods. Figure 4-46 (see Section 4.9) representing Model 'E' is the result of system identification based purely on empirical results. The next step is to design a robust controller for the EBM model identified in the previous chapter. Model 'E' is able to accurately predict the experimental parison length **as long as** the four LUTs are properly tuned. A change in either the shape or the magnitudes of the signal entered in the model necessitates a change in LUT parameters. Therefore, each tuned version of Model 'E' represents one input. To represent the entire set of inputs, a set of models must be tuned. Model 'E' is but a specific example.

A control system has the property of robust stability when it is internally stable for every model in the family of perturbed models [30]. As a result, rather than design a controller based on Model 'E' which is specific to an input signal of 20% → 80%, Model 'E' will be simplified to represent, with iuncertainty, an entire set of models for the EBM process. This simpler model is shown in Figure 5-1 and will be referred to as Model 'F'.

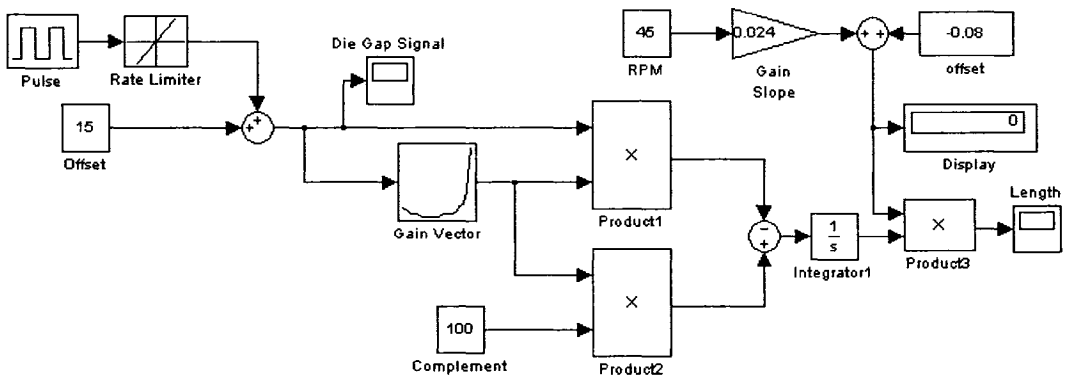

Figure 5-1: Model 'F'

The four LUTs in Model 'E' have been replaced by a single LUT in Model 'F'. The rule of thumb developed for Model 'E' in Chapter 4 states that the number of LUTs required

had to match the number of transitions in the input signal. As shown in Appendix D and seen throughout Chapter 4, the input signals studied all had four die gap transitions. Therefore, Model 'E' required a total of four LUTs. The Model 'F' LUT assigns gains for the entire range of die gap openings irrespective of the number of die gap transitions in the input signal. As a result, the clock and the switch blocks in Model 'E' are completely removed in Model 'F'. The 'Gain Vector' block in Figure 5-1 outputs the gains found in the rpm = 45 row in Table 4-1. The three remaining rows in Table 4.1 (rpm = 50, 55, and 60) are absorbed by the rpm gain configuration found in the upper right corner of Model 'F' in Figure 5-1.

Figure 5.2 shows how the output from Model 'F' compares to that of Model 'E' and the experimental result for 15% → 75% with a 45 rpm extruder speed.

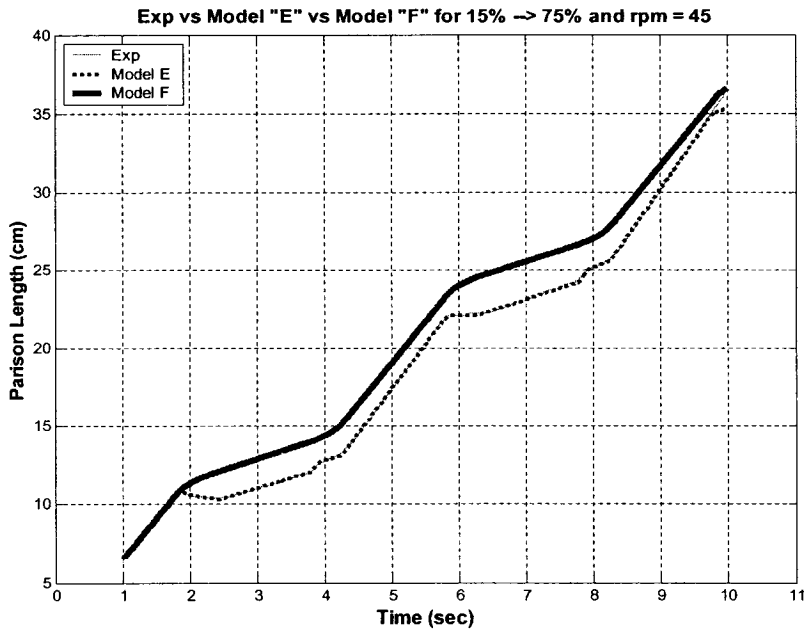

Figure 5-2: Exp vs. Model 'E' vs Model 'F' for 15% → 75% and rpm = 45

Figure 5-3 represents the error for Model 'E' and Model 'F'.

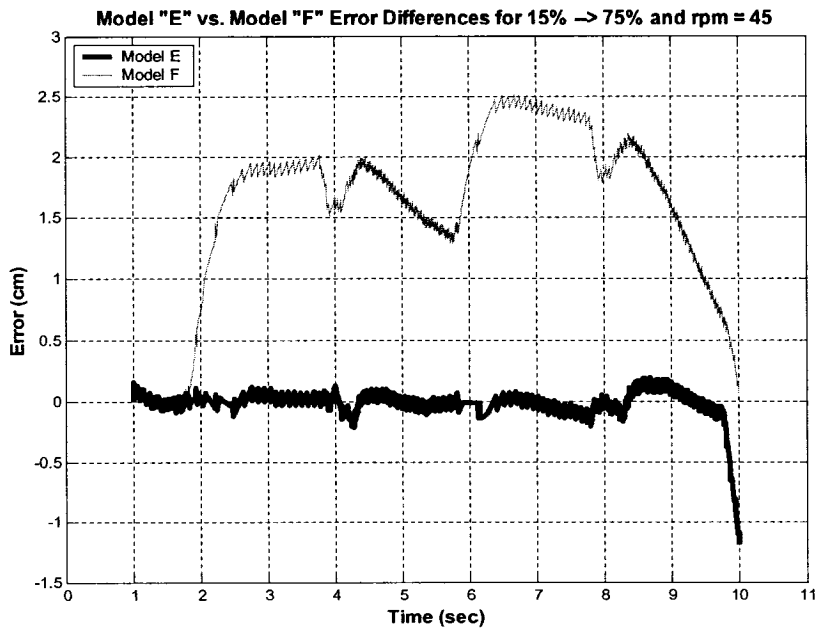

Figure 5-3: Model 'E' and Model 'F' Error Signals

Figures 5-2 and 5-3 clearly show that Model 'F' is less accurate than Model 'E'. In system identification theory, there is a trade-off between the accuracy of a model output and its complexity [31]. A perfect curve-fitting model, such as Model 'E' in Chapter 4 requires a complex structure. By reducing the number of LUTs and removing the switches in Model 'E', the accuracy is compromised but the model is simplified greatly.

In addition to being a simpler model, Model 'F' is able to output an acceptable parison length for any shaped input signal of any magnitude. This simplification eliminates the need to constantly tune the LUTs as in Model 'E' to adapt to the different parison programming profiles. Consequently, designing a robust controller will be an easier task using Model 'F', even with the loss of accuracy.

The discrepancies between the two models will be considered as uncertainties for the robust controller. The Model 'F' imprecision will represent the often seen extraneous disturbances in the EBM process. These disturbances can include irregular flow in the die head and inconsistencies in the polymer resin [2]. A well-designed robust feedback

controller will ensure that the imperfectly known EBM system will exhibit a desired length profile.

5.1 Closed-Loop Control

Currently, many polymer processes, including the EBM process, involve open-loop control. Typically, a process is controlled in open-loop when the machine operator enters a pre-determined parison programming profile, runs one cycle of the process and analyzes the final part. If the blown part is flawed, the operator must modify the parison profile until the final part is deemed acceptable. Once this step is reached, the machine is generally left to run at these settings. However, external disturbances on the process could lead to erroneous parts upon which the operator must tune the machine settings anew. These disturbances include temperature drift, uneven flow in the die head, presence of melt impurities and changes in melt characteristics [2].

Closed-loop control with an accurate plant model and a well-designed controller will prevent such machine drifts to affect the final blown part. Closed-loop control systems are achieved using feedback. Figure 5-4 shows the simplest type of feedback control [30].

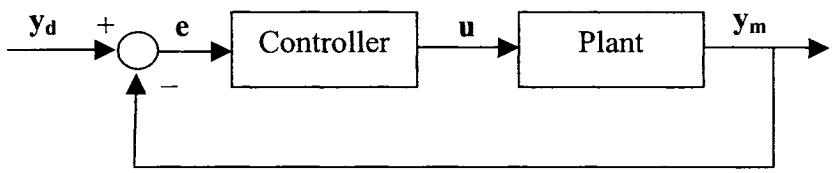

Figure 5-4: Simple Feedback Control System

The plant is driven by a control signal **u**. The feedback loop forces the controller to make a decision on how to change **u** based on the error signal **e** [32].

For the EBM process, the two factors that affect the evolution of the parison length are the die gap opening (h_o) and the extruder speed (rpm). These two factors will be inputs

to the system whereas the parison length is the lone output. The system is therefore a MISO system.

Figure 5-5 shows the design of a controller where both loops are closed.

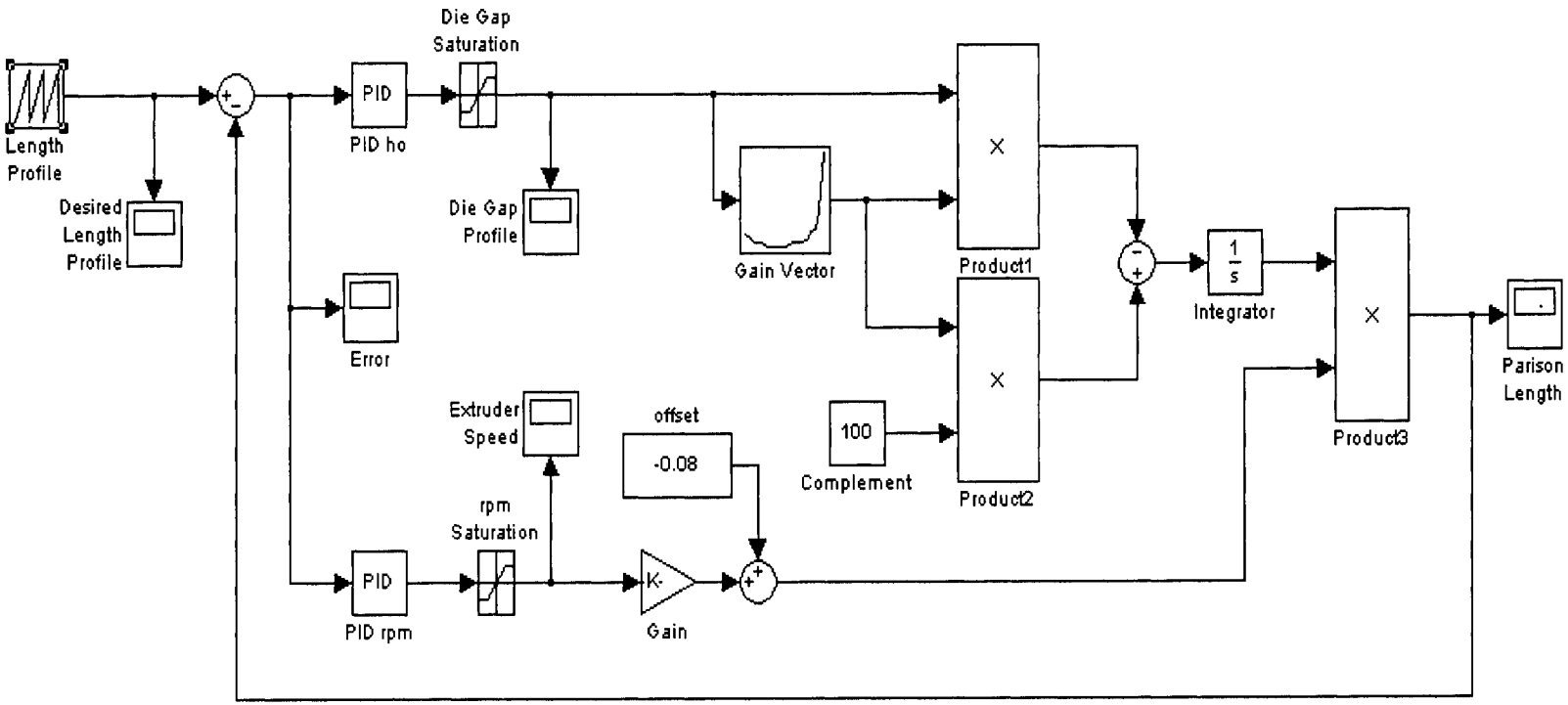

Figure 5-5: Full Controller for EBM process

The two PID-controllers, seen in the figure on the previous page, are the simplest and most widely used in industry today. The roles of the proportional gain (K_p), the integral gain (K_i) and the derivative gain (K_d) are specific within the PID-controller. The different types of PID-controllers are shown in Table 12-1 in Appendix E. The two controllers used in the design have been reduced to a PI-controller for the die gap loop and a P-controller for the rpm loop. The parameters for each controller in Figure 5-5 are shown in Figure 5-6 (for h_o input) and Figure 5-7 (for rpm input).

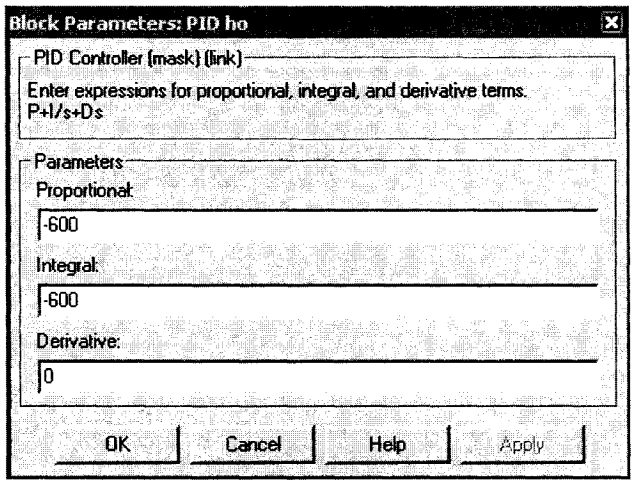

Figure 5-6: PID Gains for Die Gap Opening (h_o)

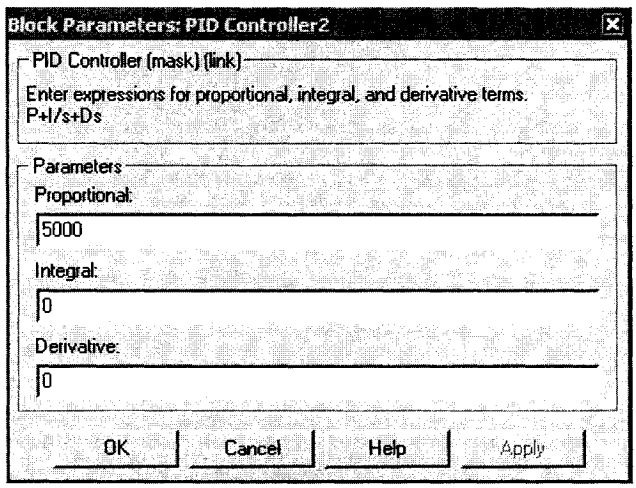

Figure 5-7: PID Gains for Extruder Speed (rpm)

Each controller was tuned using a trial and error method based on simulations to maximize the overall stability without compromising the performance of the control system.

The remainder of this section will focus on the analysis of the performance of the control system with both input loops closed. Prior to displaying the results, it is first necessary to create several different desired length profiles. The robustness of the control system will be investigated by forcing the parison length evolution to follow many different paths and magnitudes. The only condition is that these length profiles must be monotonically increasing for obvious reasons as the parison is extruded vertically downwards.

Three particular desired length profiles will be shown in this thesis. They are shown in the same Figure 5-8.

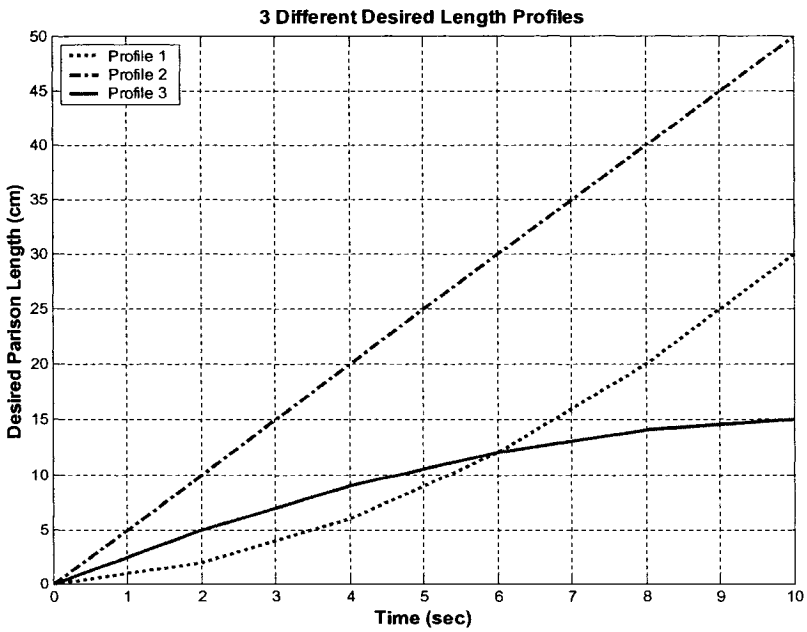

Figure 5-8: Three Desired Length Profiles

The profiles shown in Figure 5-8 each have different lengths and shapes. The desired length Profile #1 (dotted) with a final length of 30cm would be most appropriate for the molds installed on the Battenfeld. The other two profiles could be useful to create parts from other molds. In addition, each profile displays different parison behaviour. Most notably, Profile #1 is affected by the sag phenomenon as the speed of the parison increases with time. Meanwhile, Profile #2 neglects both sag and swell and resembles the length evolution of a 'steel' parison seen in Chapter 3.

For each desired length profile, the following graphs will be shown:

- Desired Length Profile vs. Plant Output
- Error Signal
- Die Gap Opening Profile
- Extruder Speed Profile

5.1.1 Desired Length Profile 1

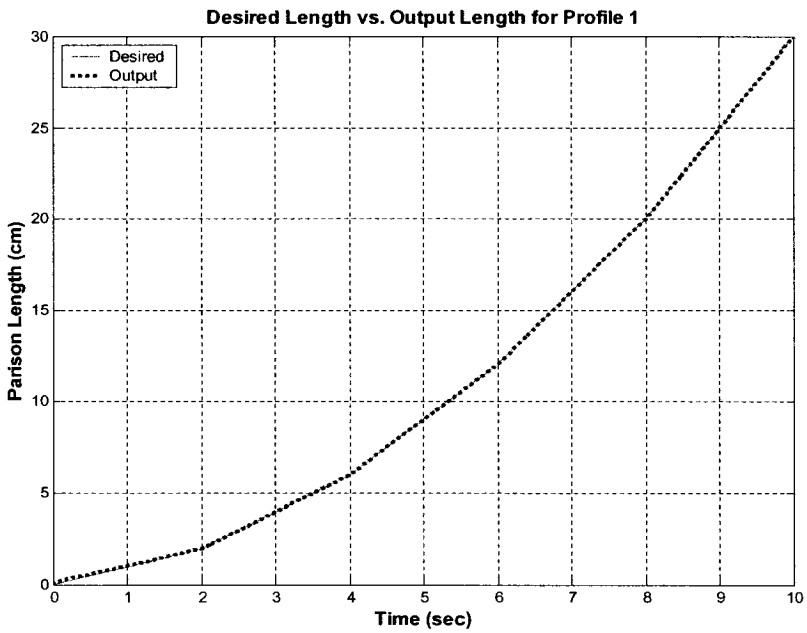

Figure 5-9: Desired vs Output Length Profile (#1)

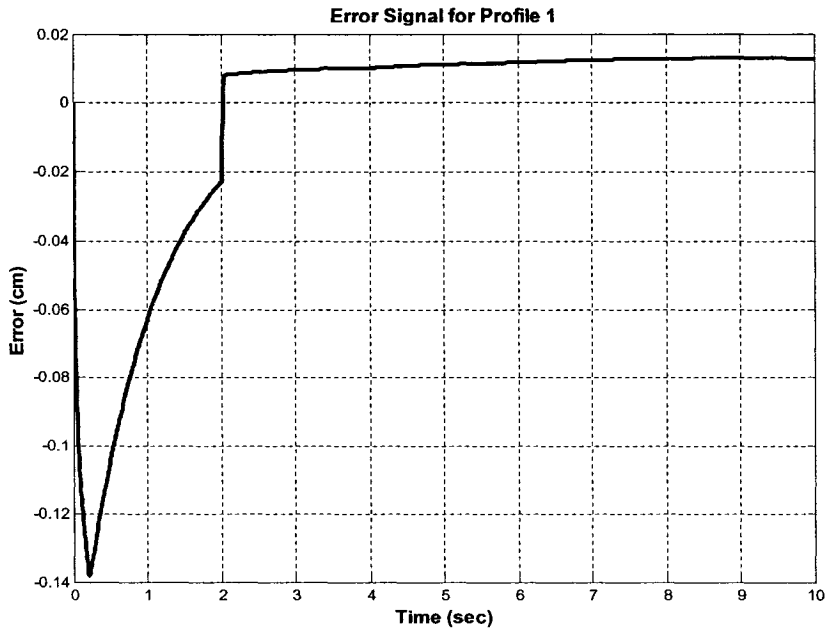

Figure 5-10: Error Signal for Profile 1

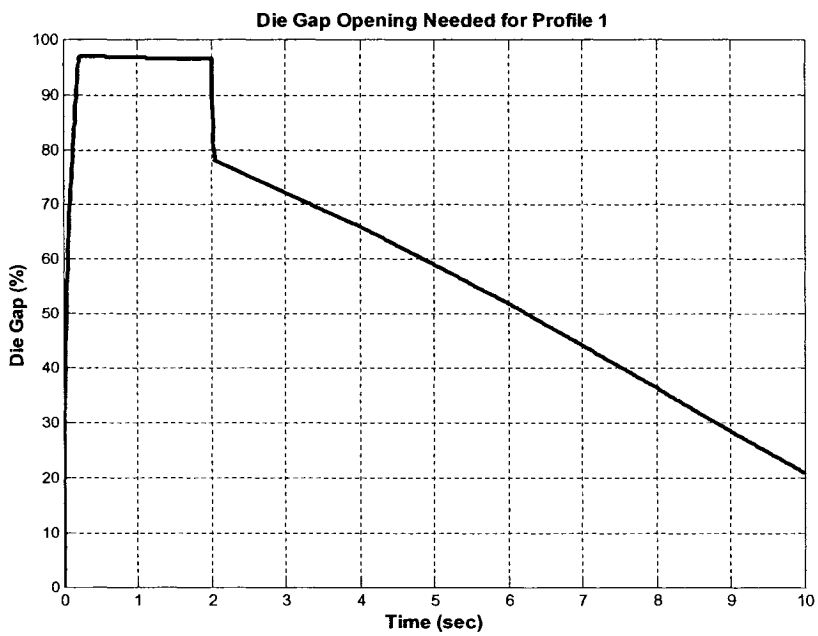

Figure 5-11: Die Gap Openings for Profile 1

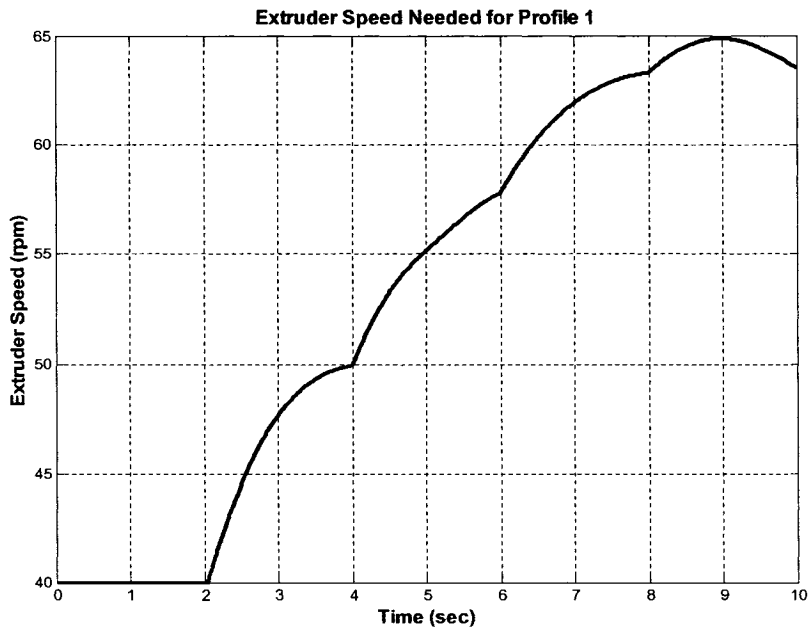

Figure 5-12: Extruder Speed for Profile 1

5.1.2 Desired Length Profile 2

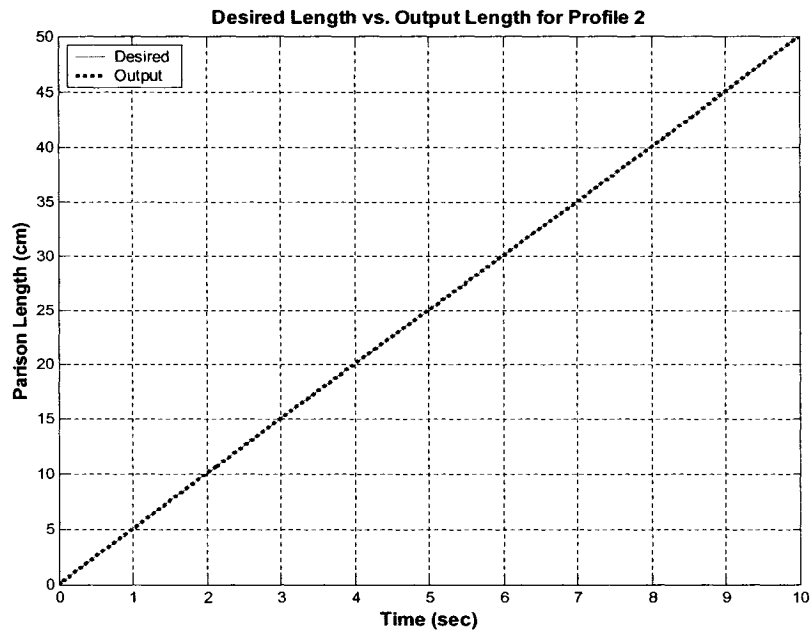

Figure 5-13: Desired vs Output Length Profile (#2)

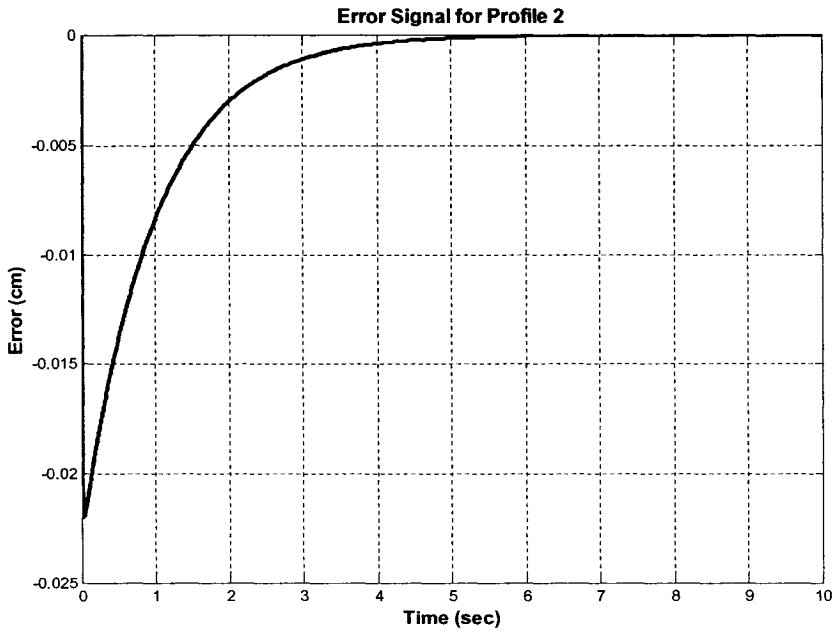

Figure 5-14: Error Signal for Profile 2

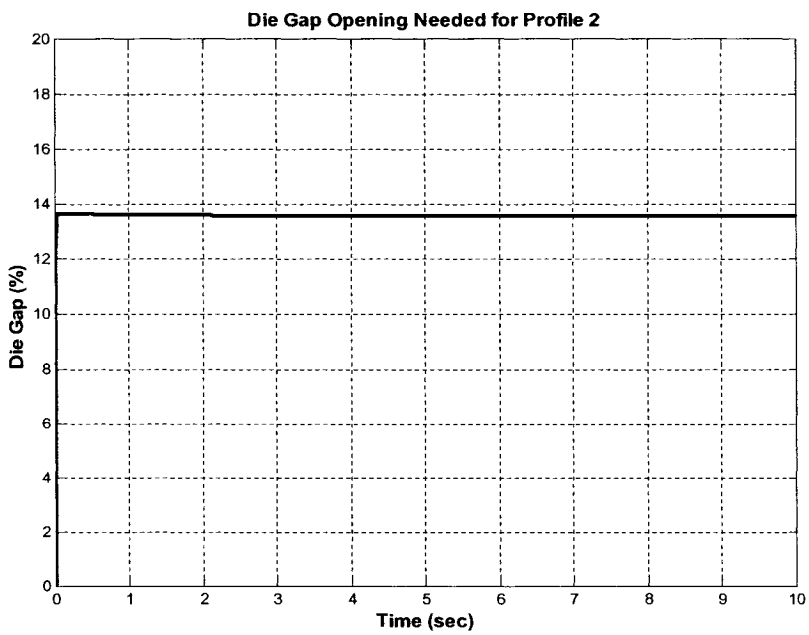

Figure 5-15: Die Gap Openings for Profile 2

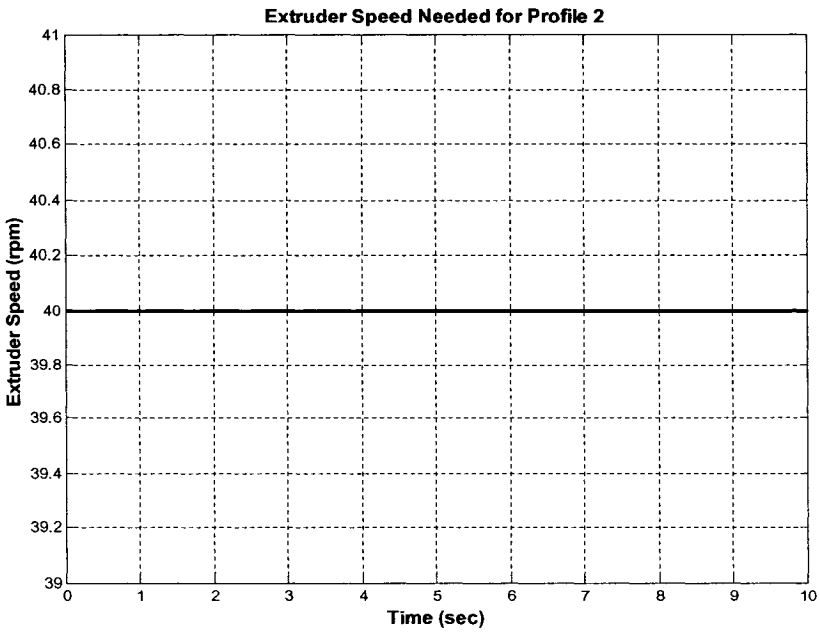

Figure 5-16: Extruder Speed for Profile 2

5.1.3 Desired Length Profile 3

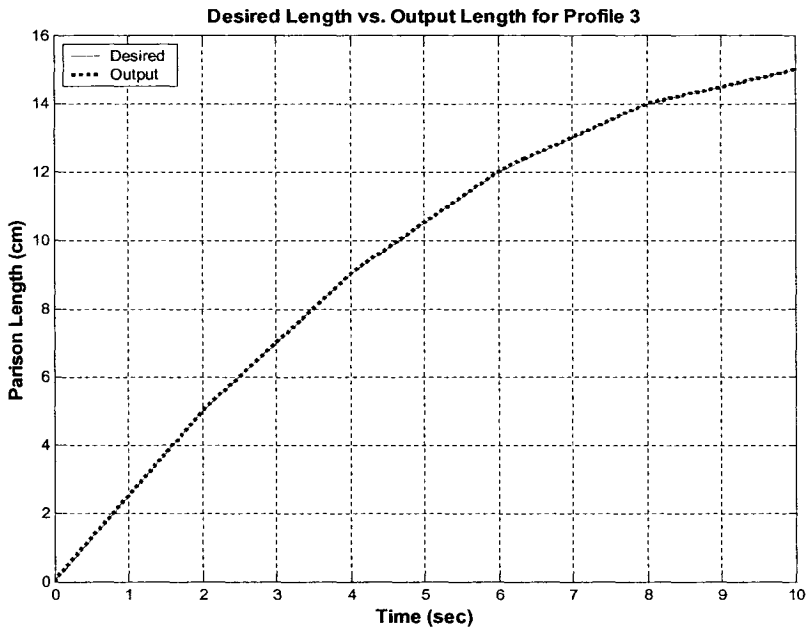

Figure 5-17: Desired vs Output Length Profile (#3)

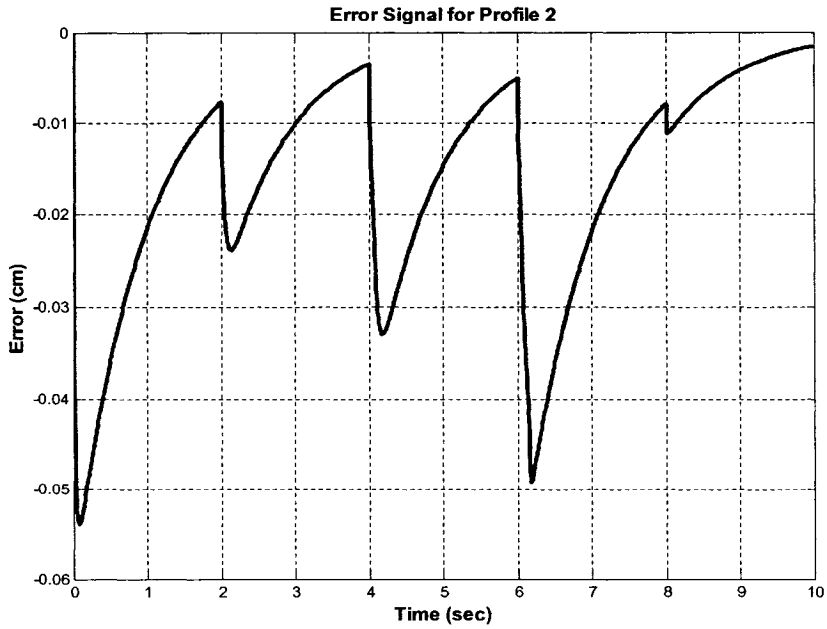

Figure 5-18: Error Signal for Profile 3

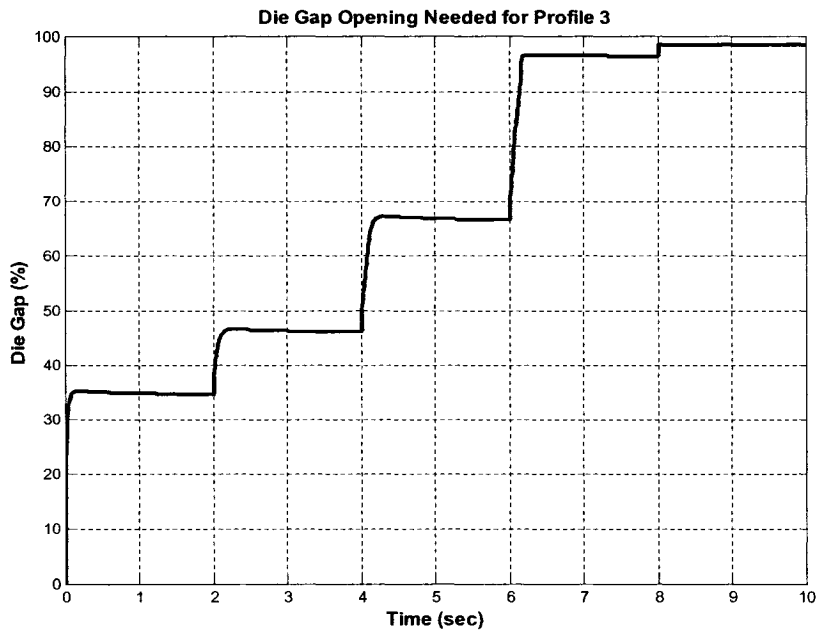

Figure 5-19: Gap Openings for Profile 3

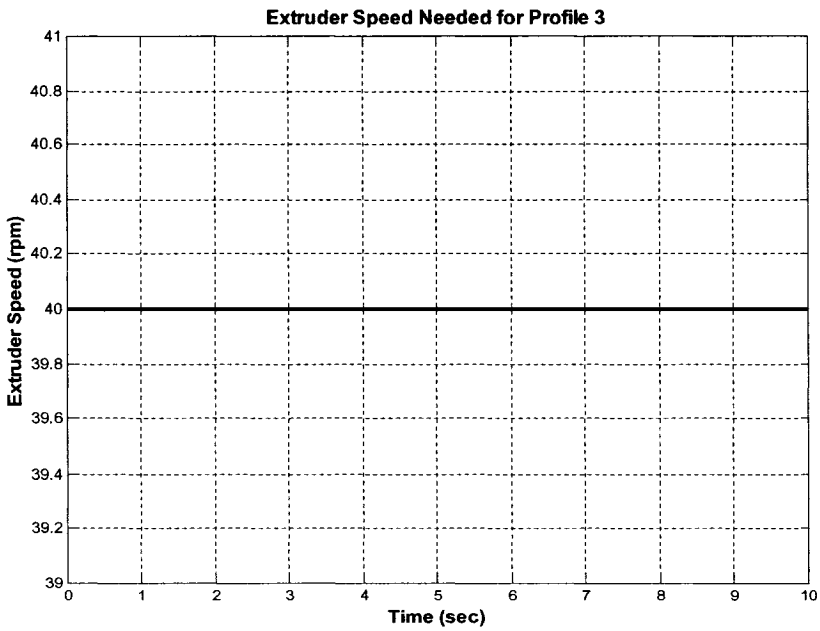

Figure 5-20: Extruder Speed for Profile 3

Included in the controller design from Figure 5-5 are two saturation blocks located immediately after the PI and P controllers. These saturation blocks are necessary to force the controller outputs to lie within a range that is physically possible for the system. Therefore, the saturation block in the die gap loop has a minimum of 0% and a maximum of 100%. Similarly, the saturation block located after the P-controller in the extruder speed loop is set to a minimum of 40rpm. This is the slowest extruder speed allowable by the Battenfeld to perform the EBM process. An arbitrary extruder speed of 100rpm was given as the maximum for the saturation block. Figure 5-21 shows the output of the P-controller in the extruder speed loop for Profile #1 before reaching the saturation block.

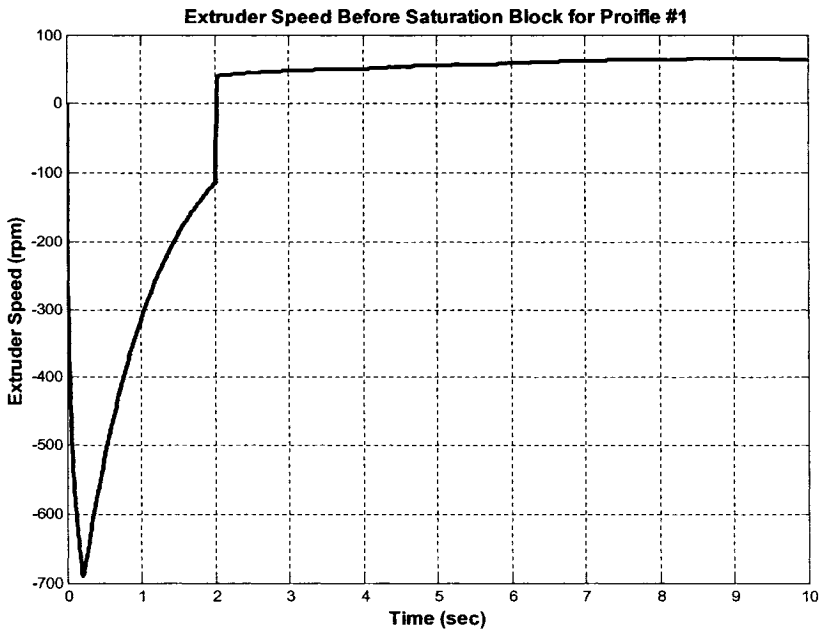

Figure 5-21: Extruder Speed Profile without Saturation Block

The shape of the extruder speed profile before the saturation block depicts the role of the P-controller. Figure 5-21 is $K_p = 5000$ times greater than the error signal in Figure 5-10. Excluding the saturation block after the P-controller would force the extruder to spin at a negative value for the first two seconds of extrusion time. Negative extruder speeds are not physically possible. After $t_{ext} = 2$ seconds, the output of the P-controller passes through the saturation block without any change. Figures 5-16 and 5-20 show that the saturation block is enforced throughout the entire cycle as it outputs a constant extruder speed of 40rpm. These results confirm that the presence of the saturation block in the extruder speed loop is required for this design of a robust in-cycle controller. The usefulness of the saturation block in the h_o loop will be shown in the next section.

5.2 Single-Loop Control Systems

The control system in the previous system is a MISO configuration. Although there are two individual feedback loops in Figure 5-5, the inputs are coupled inside the plant.

Figure 5-22 shows a simple block diagram representing the system. Due to the non-linearity of the plant, it is not possible to generate a linear transfer function.

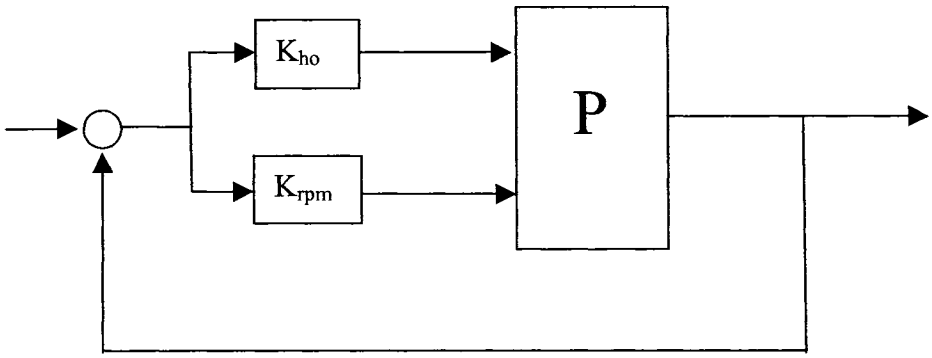

Figure 5-22: Block Diagram Representing EBM Control System

The three desired length profiles created in the previous section proved that the MISO control system was effective. It was able to control the evolution of the EBM parison length to within a few tenths of a millimetre of the desired parison length path. However, what if the MISO system became a SISO system? In other words, if one of the feedback loops was removed, how would it affect the control system as a whole? The next two subsections will study the effects of relaxing one feedback loop at a time.

5.2.1 'Relaxed' Extruder Speed Loop

Figure 5-23 shows the EBM control system with a single feedback loop controlling the die gap opening h_o. The MISO system from the previous section became a SISO system by removing the rpm feedback loop (including the P-controller) and replacing it by a constant extruder speed. Ideally, the extruder speed constant should represent a value attainable by the extruding machine. As previously mentioned, the minimum value for the Battenfeld to run the process is 40rpm. The extruder screw was set to rotate at 45rpm for the following example.

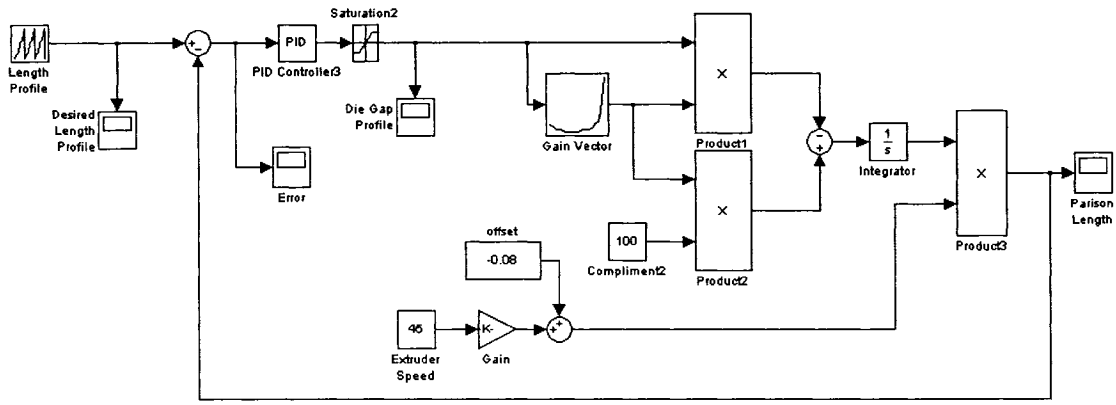

Figure 5-23: SISO Control System with Relaxed Extruder Speed Loop

Figure 5-24 shows the random length profile created to validate this controller.

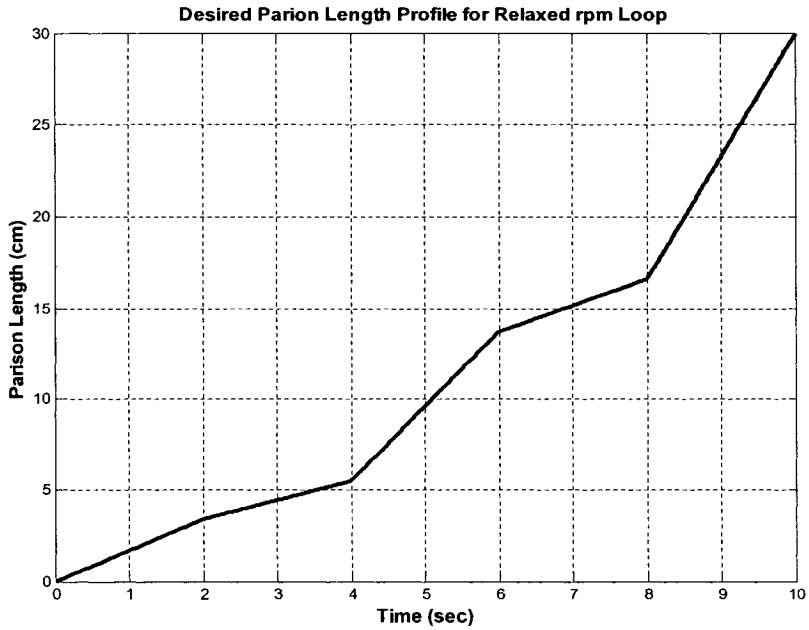

Figure 5-24: Desired Parison Length for Relaxed rpm Loop

The resulting die gap profile is shown in Figure 5-25 while the error signal is shown in Figure 5-26.

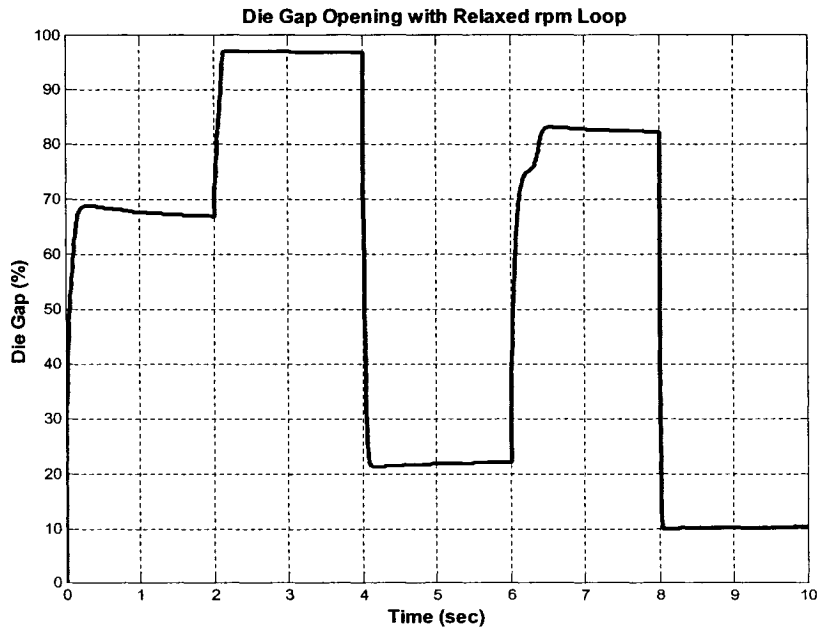

Figure 5-25: Die Gap Profile with Relaxed rpm Loop

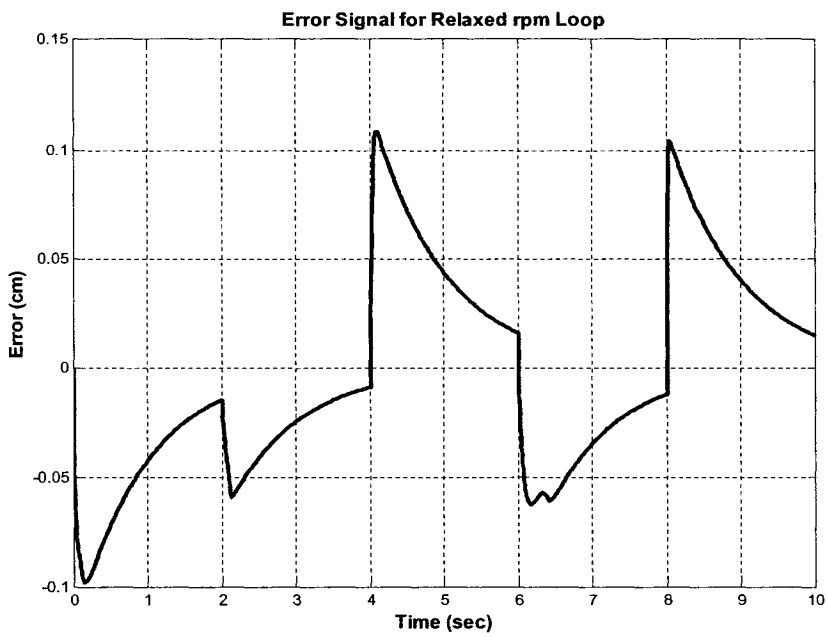

Figure 5-26: Error Signal for Relaxed rpm Loop

The example shown here proves that the SISO controller works well for an extruder speed of 45rpm. The desired versus the output parison lengths differ by a maximum of

just over 1mm. The same simulation was performed for an extruder speed of 100rpm yielding similar results. The resulting error signal is shown in Figure 5-27.

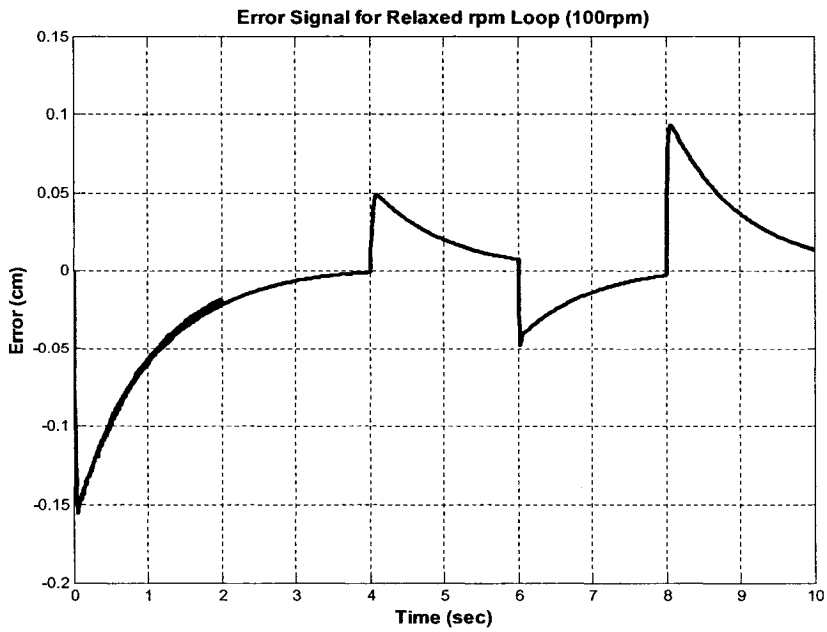

Figure 5-27: Error Signal for Relaxed rpm Loop (100rpm)

These two simulations prove that the system is stable for any extruder speed entered. Hence, for a well-designed parison length profile, the SISO controller with the relaxed rpm loop displays robust properties.

5.2.2 'Relaxed' Die Gap Loop

A similar procedure was repeated in this section except the die gap loop is relaxed rather than the extruder speed. Figure 5-28 shows the analogous version of Figure 5-23 with a constant die gap opening of 50%.

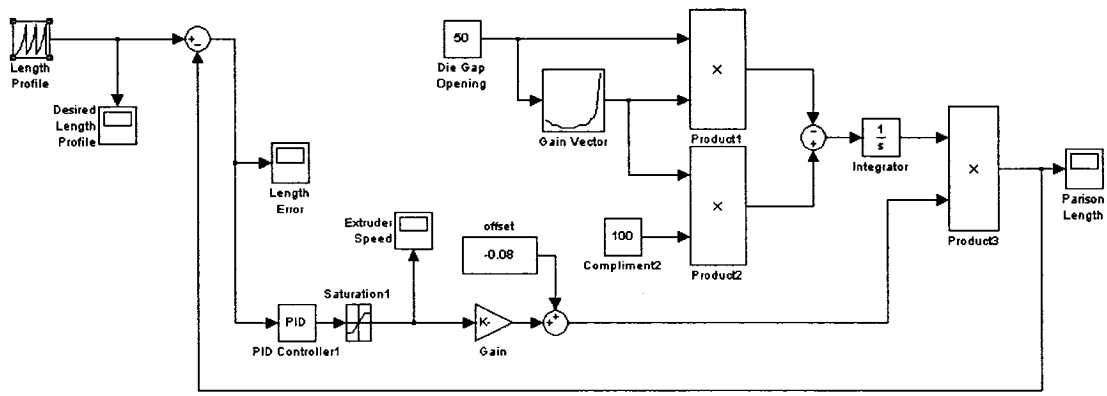

Figure 5-28: SISO Control System with Relaxed Die Gap Loop

The identical desired parison length profile shown in the previous subsection (Figure 5-24) will be used to validate this SISO controller. The resulting extruder speed profile and error signal are shown in Figure 5-29 and 5-30, respectively.

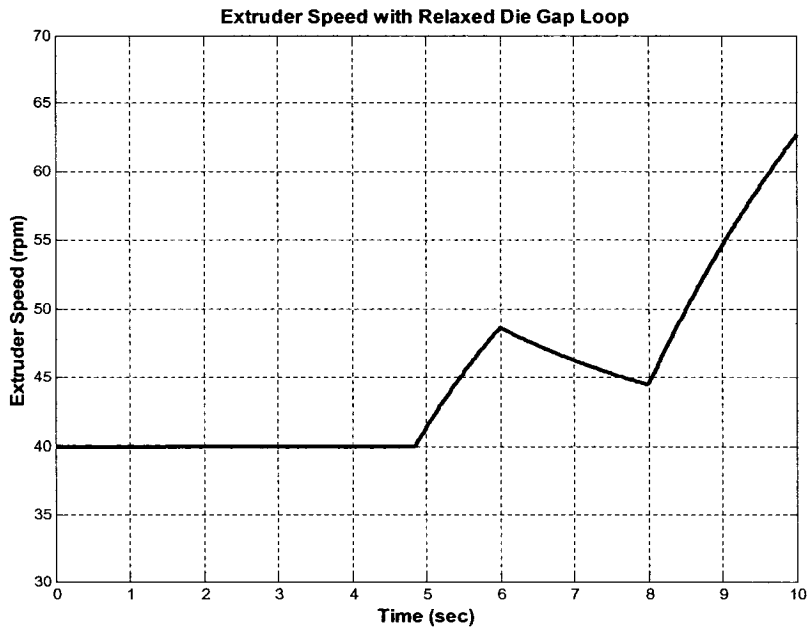

Figure 5-29: Extruder Speed Profile with Relaxed Die Gap Loop

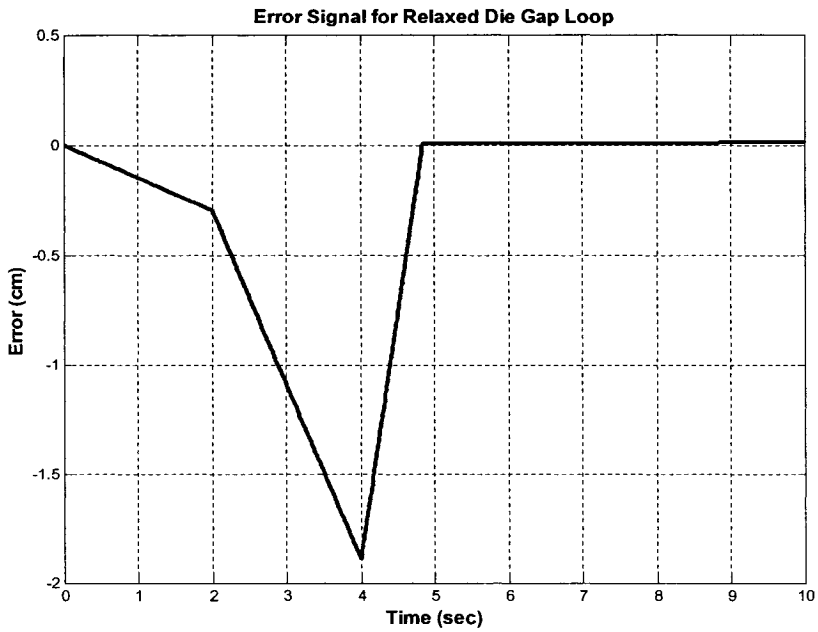

Figure 5-30: Error Signal for Relaxed Die Gap Loop

Although the signal in Figure 5-30 shows a larger error at t_{ext} = 4 seconds, the rest of the extrusion process seems to be well controlled. This statement is misleading. The constant value of h_o entered in the plant is able to produce a parison length profile close to that of the desired profile, making the output of this SISO controller seem tolerable. Unlike the previous SISO controller where drastically varying the rpm block has little effect on the overall system, any change in the h_o block can lead to an unstable system. Figure 5-31 shows the error signal of a simulation with a h_o = 10%.

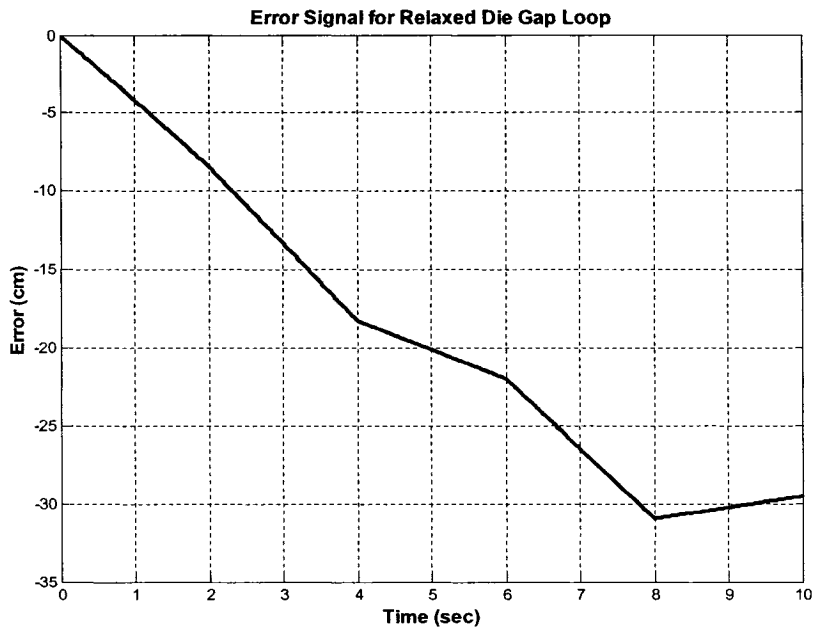

Figure 5-31: Error Signal for 10% Die Gap Opening

This result is not surprising considering the role the extruder speed played in Models 'E' and 'F'. Recall that the extruder speed simply scaled the output of the LUT(s). As a result, it is **not** strong enough to control a parison length profile on its own **unless** the die gap profile is well-designed. This will be explained further in the next section.

The last two subsections clearly demonstrate that the SIMO controller designed in Section 5.1 can be simplified to a SISO controller.

5.3 Battenfeld EBM Machine

The SIMO in-cycle controller design in Section 5.1 could be implemented on any extruding machine where the die gap openings are adjustable during a cycle of the EBM process. Should this feature not be available to the EBM machine, the user is restricted to implementing the SISO controller shown in Figure 5-28 with a relaxed die gap loop. Results have shown that implementing this type of SISO controller severely limits the control capabilities. Error divergence in this SISO controller can only be avoided if the die gap signal entering the plant resembles the parison programming profile that

produced the initial desired evolution of the parison length. In other words, the operator must have a prior knowledge of the parison programming profile before starting the EBM process. The block diagram representing the SISO controller is shown in Figure 5-32.

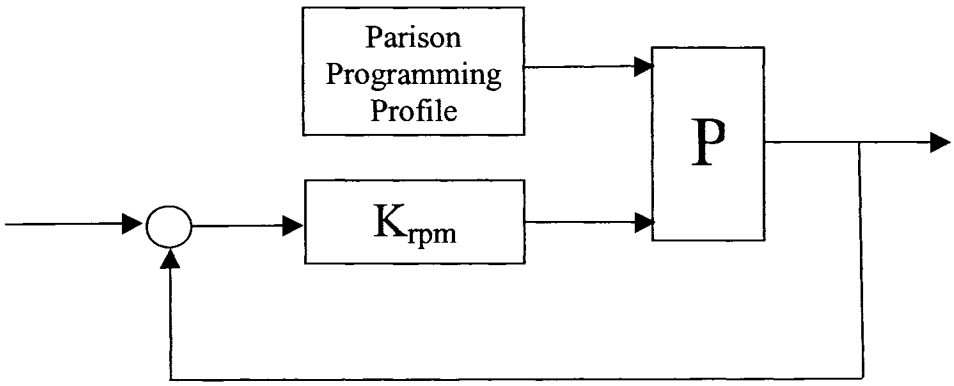

Figure 5-32: SISO rpm-controller Block Diagram

For example, suppose the operator is given a parison programming profile similar to Figure 4-4 (bottom) in Section 4.1.2 where the die gap alternates between 80% → 20%. Based on the corresponding experimental parison length evolution for such an input, the following desired length profile was created and shown in Figure 5-33.

Figure 5-33: Desired Parison Evolution based on Initial Programming Profile

Running the simulation in Simulink gives the error signal as well as the necessary extruder speed profile shown in Figures 5-34 and 5-35 respectively.

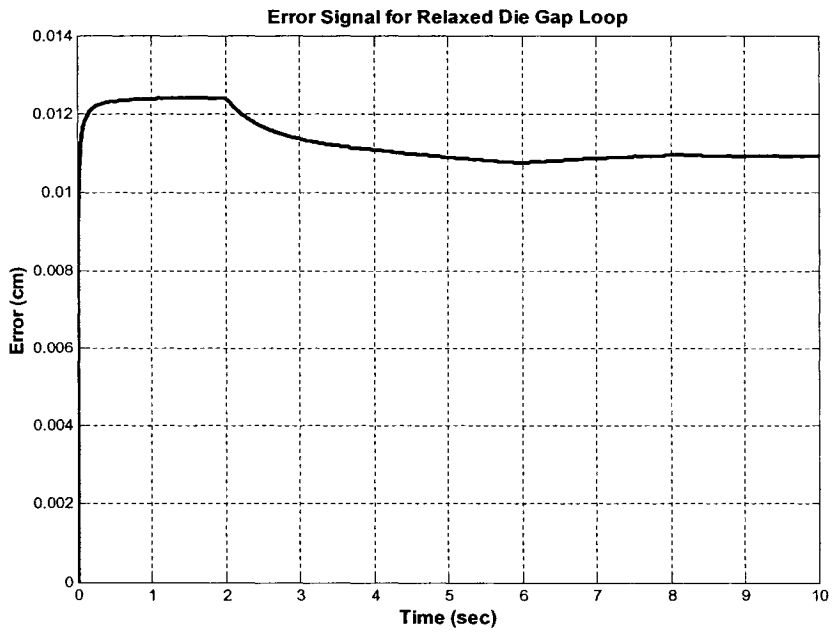

Figure 5-34: Error Signal for SISO rpm-controller

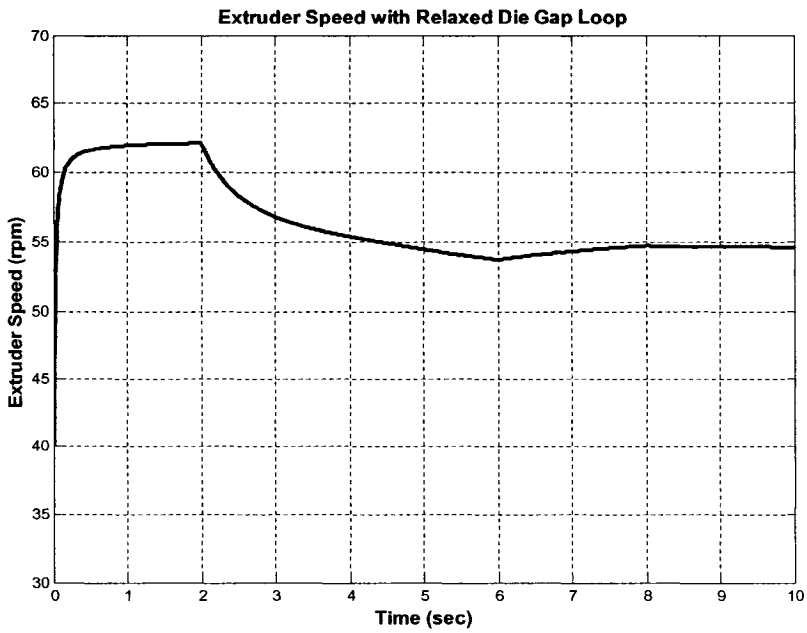

Figure 5-35: Extruder Speed Profile for SISO rpm-Controller

The Battenfeld EBM machine located at the CNRC-NRC IMI can only implement the SISO controller explained in this section. As mentioned previously in Section 2.5.1, the operator can only modify the parison programming profile between cycles. Therefore, the only possible in-cycle controller that can control the evolution of the parison length is the rpm-SISO controller shown in Figure 5-32. However, the last example shows that if the parison programming profile is well designed, then the SISO rpm-controller works to within tenths of a millimetre. The goal of controlling the evolution of the parison length is ultimately achieved.

6 Conclusion

6.1 Summary

The purpose of this thesis was to develop an in-cycle control strategy that was able to track the evolution of the parison length. Furthermore, empirical-based models were developed to represent the parison formation stage of the EBM process. The benefits to developing this control strategy are three-fold. The first benefit of a closed-loop controller is to minimize the effect of process disturbances and machine drift to consistently produce repeatable parison melts. Another benefit is a financial one. An in-cycle parison length controller will minimize the parison tail and flash thus reducing scrap and lowering cycle time. Lastly, the control of a specific process variable such as the parison length can lead to design of controllers of other process variables. A *Multiple Input/Multiple Output* (MIMO) system model could be developed with its objective to control both the length and thickness of an extruded parison for example. Considering the lack of in-cycle parison length control systems for the EBM process, a brief literature review followed illustrating parison length models, closed-loop controllers for other EBM process variables and cycle-to-cycle parison length controllers.

Chapter 2 offered the reader a brief background of the EBM process. Extrusion, injection and stretch are all different blow molding processes. The history and market share were described showing the influence of EBM over time and its importance in the industrial world of today. The remainder of Chapter 2 focused on explaining the different stages of EBM and equipment employed throughout the research.

Chapter 3 presents a theoretical derivation of the evolution of the parison length excluding any rheological properties of the resin. The theoretical model outputs were compared to experimental tests yielding poor results. Improvements to the first model were suggested for models in the next chapter.

Chapter 4 proposed several models predicting the evolution of the parison length. These models were developed using basic system identification methods based purely experimental data. Over seventy extruded parisons were filmed with a high-speed

camera and analyzed using pixel-tracking software. Abnormalities brought forth by changing the die gap opening during the extrusion were also discussed in great detail. These discrepancies in the die gap transition required the presence of more detailed LUTs in the model. Finally, the last model in the chapter produced precise predictions of the evolution of the parison length.

A robust in-cycle controller was designed in Chapter 5 for a simpler, more general plant shown in Model 'F'. Three examples of desired parison length profile were simulated generating very precise control. Relaxing one loop in turn of the MISO system produced two individual SISO controllers. These SISO systems were simulated using the same desired parison profile. The results showed that one of the SISO controllers remained robust while the other displayed severe control limitations. Finally, the last section in Chapter 5 explained the controllers which were suitable for the Battenfeld EBM machine used throughout this work.

6.2 Recommendations and Future Work

The next logical step following this research is the implementation and testing of the designed controllers on an extruding machine. Unfortunately, due to the restrictions of the parison programming feature on the console, the MISO in-cycle system cannot be used on the Battenfeld. However, a specific SISO controller for the Battenfeld was proposed in Chapter 5. A cycle-to-cycle die gap controller could still be applied in addition to the in-cycle rpm controller designed in this work. These two controllers could work in parallel to achieve complete control of the parison length. Furthermore, real-time software such as RT-Lab 6.2 by OPAL-RT can be used in conjunction with an appropriate sensor to implement the rpm in-cycle controller. Similarly, control using OPAL-RT software allows for: real-time execution of the simulation, real-time communication with the I/O devices, initialization and synchronization of the I/O devices, data acquisition from I/O devices, and data recording [33].

Future research projects could repeat the methodology described in this work for different polymer resins such as PP or PVC. This method could also be used for different dies. A database of in-cycle controllers may be created for any combination of machine or material parameters. The SIMO controller presented in this research may expand to include these aforementioned parameters as inputs. This new controller would encompass the entire parison length control for that particular EBM machine. A similar process could be performed on other EBM machines.

As previously mentioned, closed-loop control of other process variables (e.g. parison thickness and parison melt temperature) has already been attempted. Assuming these variables can be measured in a feasible manner, empirical model-based in-cycle controllers could then be designed in the same fashion. Ideally, the entire EBM parison formation process can be represented by a MIMO-control system.

7 Bibliography

[1] Ryan, M.E., *Optimization of the Blow Moulding Process*, Blow Moulding RETEC (1997), p.51.

[2] Kamal, M.R., Patterson, W.I., DiRaddo, R.W., *On-Line Measurement and Closed Loop Control of Parison Dimension Profiles in Extrusion Blow Molding*, ANTEC (1989), p.954.

[3] DiRaddo, R.W. and Garcia-Rejon, A., *In-cycle Deterministic and Stochastic Dynamics of Extrusion Blow Molding*, Intern. Polymer Processing VII (1992), p.257.

[4] Schrand, H., *Adaptive Control Loops Reduce Scrap*, ANTEC (1989), p.952.

[5] *Technical Glossary*, LNP Engineering Plastics, http://www.lnp.com/LNP/Design/Glossary/p1.html.

[6] Sheptak, N. and Beyer, C.E., SPEJ, 21 (1965), p.190.

[7] Kalyon, D.M., Tan, V. and Kamal, M.R., *The Dynamics of Parison Development in Blow Molding*, Polymer Engineering Science, 20 (1980), p.773.

[8] Ryan, M.E., and Dutta, A., *Mathematical Modeling of the Blow-Molding Process*, Polymer Engineering Science, 22 (1982), p.1075.

[9] Dormeier, S., *Model Reference System for Continous Acquisition of Parison Length*, ANTEC (1986), p.796.

[10] Dealy, J.M and Orbey, N., *A Model for Parison Behavior in the Extrusion Blow Molding Process*, AICHE (1985), p.807.

[11] Noguchi, et al., *Parison Length Control Method for Extrusion Blow Molding Machine*, United States Patent (5,399,302), 1995.

[12] Chabot Jr., Joseph F., *The Development of Plastics Processing Machinery and Methods*, John Wiley and Sons Inc., New York, NY, 1992, 196pp.

[13] Hu, C-L., *Blow Molding*, Department of Chemical Engineering, University of Connecticut, http://www.engr.uconn.edu/cheg/cheg_blow.htm.

[14] *Blow Molding*, Jobwerx Manufacturing Network, http://www.jobwerx.com/plastics/blow_molding.htm.

[15] *Extrusion Blow Molding*, British Plastics Federation, http://www.bpf.co.uk/bpfindustry/process_plastics_extrusion_blow_moulding.cfm.

[16] Lee, Norman C., *Plastic Blow Molding Handbook*, Van Nostrand Reinhold, New York, NY, 1990, 560pp.

[17] Lee, Norman C., *Blow Molding Design Guide*, Hanser Publishers, Cincinnati, OH, 1998, 212pp.

[18] Rubin, Irvin I., *Handbook of Plastic Materials and Technology*, John Wiley and Sons Inc., New York, NY, 1992, 1745pp.

[19] Wood, B., *Blow Molding's Steady Growth Will Continue*, Plastics Technology, http://www.plasticstechnology.com/articles/200410bib4.html.

[20] *Blow Molders – 2004*, Plastics News, http://www.plasticsnews.com/subscriber/rankings/listbm.html.

[21] Thedinger, B., *No Recession in Blow Molded Packaging*, Plastics Technology, http://www.plasticstechnology.com/articles/200203bib3.html.

[22] *2001 North American Blow Molding Survey*, Plastics News, http://www.plasticsnews.com/subscriber/fyi.html?id=1005174270.

[23] Thedinger, B., *Blow Molded Industrial Packaging Grows Slowly*, Plastics Technology, http://www.plasticstechnology.com/articles/200207bib2.html.

[24] *Polyethylene Summary Data (HDPE 1000)*, Petromont, http://www.petromont.com/en/FichesEng/HDPE%201000.pdf.

[25] Belcher, S.L., *Practical Extrusion Blow Molding*, Marcel Dekker Inc., New York, NY, 1999, 381pp.

[26] *Polyethylene Technical Publication #10*, BP Solvay, http://www.bpsolvaype.com/na/upload/techpub_n10.pdf.

[27] Tadmor, Z. and Gogos, C.G., *Principles of Polymer Processing*, John Wiley and Sons Inc., New York, NY, 1979, 736pp.

[28] Mathworks Inc., http://www.mathworks.com/products/simulink/.

[29] Oppenheim, A.V., Willsky, A.S., *Signals & Systems – 2nd Edition*, Prentice Hall, Upper Saddle River, NJ, 1997, 957pp.

[30] Bélanger, Pierre R., *Control Engineering: A Modern Approach*, Saunders College Publishing, Orlando, FL., 471pp.

[31] Castellano, G., *Background*, http://www.cranfield.ac.uk/wsc3/tutorial/soucek/chater14/node1.html.

[32] Barr, M., *Introduction to Closed-Loop Control*, O'Reilly Network, http://www.oreillynet.com/pub/a/network/synd/2003/08/05/closed_loop.html.

[33] *RT-LAB v6.2 User's Manual*, Opal-RT Technologies, Inc., Rev. A, January 2003, 110pp., http://support.opal-rt.com/common/docs/pdf/rt-lab_usersmanual.pdf.

[34] *PCI Fastcam Spec Sheet*, Optikon, http://www.optikon.ca/pdf/FASTCAMPCI.pdf.

[35] Lee, N.C, *Control Flash in Extrusion Blow Molding*, Plastics Technology, http://www.plasticstechnology.com/articles/200209ts1.html.

8 Appendix A: Blow Molding Time Line

- 1937: LDPE patented in the UK
- 1940: Plax Corp. first blow molds LDPE
- 1947: Custom blow molded packaging
- 1950: Kautex, Bekum, Fisher – First commercial blow molding machine
- 1951: Phillips Petroleum develops PP and HDPE
- 1957: Plax Corp. manufactures first HDPE bottle (baby nurser)
- 1957: HDPE and PP come to market
- 1969: Proctor and Gamble Labs. develops electronic parison programming based on mandrel position feedback
- 1980: Volkswagen (Passat) is the first car to use a blow molded fuel tank
- 1989: Placo Machinery (Japan) introduces 3D blow molding
- 1991: Johnson Controls introduces its UNILOY coextrusion blow molding machine (individual concentricity adjustment rings for each layer)

9 Appendix B: HDPE 1000 Properties (Petromont)

Table 9-1: HDPE 1000 Properties

PROPERTIES	UNITS S.I.	UNITS ENG	TEST METHOD	TYPICAL VALUES S.I.	TYPICAL VALUES ENG
CLASSIFICATION	-	-	ASTM D 4976	PE 234	
Melt Index, I_2	dg/min		ASTM D 238	0.33	0.33
Flow Index, I_{21}	dg/min		ASTM D 238	29	29
Density	g/cm^3		ASTM D 505	0.9550	0.955
Tensile Strength at Yield	MPa	(PSI)	ASTM D 638	26.9	3,90(
Ultimate Elongation	%		ASTM D 638	>800	>80(
Flexural Modulus	MPa	(PSI)	ASTM D 790	1,325	192,0(
Brittleness Temperature	°C	(°F)	ASTM D 746	<-76	<-10
IZOD Impact Strength	J/m	(ft-lb/in)	ASTM D 256	160	3.0
Hardness - SHORE D	--		ASTM D 2240	67	67
ESCR, 50% failure (F_{50}) @ 100% Igepal Solution	hours		ASTM D 1693 (Condition B)	33	33
VICAT Softening Temperature	°C	(°F)	ASTM D 1525	128	262
Heat Deflection Temperature - 455 KPa/66 psi Load	°C	(°F)	ASTM D 648	74	165
Melting Point	°C	(°F)	Pétromont	134	273
Crystallization Point	°C	(°F)	Pétromont	111	232
Coefficient of Linear Expansion	cm/cm/°C	(in/in/°F)	ASTM D 696	1.3 x 10^{-4}	7 x 1(

10 Appendix C: Optikon PCI Fastcam

Specifications PCI

PHOTRON™

Frame Rates in frames per second

30	60	125	250	500	1,000	2,000	3,000	5,000	10,000

Resolution 8-bit monochrome, 24-bit color.

Frame Rate (fps)	Resolution Max H	Resolution Max V	Available Shutter Range
250	512	480	4 ms to 16.7 µs
500	512	240	2 ms to 16.7 µs
1,000	256	240	1 ms to 16.7 µs
2,000	256	120	0.5 ms to 16.7 µs
3,000	128	120	0.33 ms to 16.7 µs
5,000	128	80	20 µs to 8.33 µs
10,000	128	34	100 µs to 8.33 µs

Record Time in seconds (and frames)

Frame Rate (fps)	Record Duration
250	8.7s (2,176)
500	8.7s (4,352)
1,000	8.7s (8,704)
2,000	8.7s (17,408)
3,000	11.6s (34,816)
5,000	10.4s (52,224)
10,000	12.3s (122,880)

Playback Speeds in frames per second

1	2	3	4	5	10	15	30	60	125	250

Sensor	7.4µm square pixel, progressive-scan CCD
Shutter	Global electronic shutter from 4ms to 8.33µs
Saved Image Formats	JPEG, AVI, TIFF, BMP, RAW (compressed or uncompressed)
PC Control	Live image during record, camera control, digital data transfer, file management and image analysis
Phase Lock	Enables cameras to be synchronized precisely together to a master camera or external source
Triggering	Switch closure, open collector and TTL
Lens Mount	C-mount standard, CS optional
Camera Cable	20' (6m) standard, 50' (16m) optional
Data Display	Frame Rate, Shutter Speed, Trigger Mode, Date or Time (can be switched), Status (Playback/Record), Real Time, Frame Count and Resolution
PC Specifications	**CPU:** Pentium3 750 Mhz recommended; Pentium2 333 Mhz minimum. 128 MB or more of RAM. 16 MB or more of V-RAM recommended **OS:** 2000/XP, 98SE/98, ME and NT 4.0
Dimensions and Weight	**Camera Head:** 2" (51mm) H x 2" (51mm) W x 4.5" (114mm) D **Weight:** 1.8 lb (0.82kg).

Specifications subject to change without notice.

PHOTRON USA, INC.
9520 Padgett Street, Suite 110
San Diego, CA 92126-4446
858.684.3555
800.585.2129
fax 858.684.3558
email: image@photron.com
www.photron.com

PHOTRON (EUROPE) LIMITED
Willowbank House
84 Station Road
Marlow
Bucks. SL7 1NX
United Kingdom
+44 (0) 1628 894353 fax +44 (0) 1628 894354
email: image@photron.com
www.photron.com

Canadian Distributor
The OPTIKON Corporation Ltd.
1099 Guelph Street
Kitchener, Ontario N2B 2E4 CANADA
Tel. (519) 745-4115 Fax (519) 745-6922
Email info@optikon.ca
Website www.optikon.ca

11 Appendix D: Complete List of Input Signals

Table 11-1: List of Input Signals Filmed

Input Signal #	Starting h_o (%)	Next h_o (%)	RPM
1	50	100	50
2	100	50	50
3	20	50	50
4	20	80	50
5	80	20	50
6	10	90	50
7	15	75	50
8	30	80	50
9	35	80	50
10	40	80	50
11	45	90	50
12	55	20	50
13	60	20	50
14	65	20	50
15	70	20	50
16	85	20	50
17	90	20	50
18	95	20	50
19	10	90	45
20	10	90	55
21	10	90	60
22	15	75	45
23	15	75	55
24	15	75	60
25	20	80	45
26	20	80	55
27	20	80	60
28	25	75	45
29	25	75	55
30	25	75	60
31	30	75	45
32	30	75	55
33	30	75	60
34	35	75	45
35	35	75	55
36	35	75	60

Input Signal #	Starting h_o (%)	Next h_o (%)	RPM
37	40	75	45
38	40	75	55
39	40	75	60
40	45	90	45
41	45	90	55
42	45	90	60
43	50	90	45
44	50	90	55
45	50	90	60
46	55	90	45
47	55	90	55
48	55	90	60
49	60	90	45
50	60	90	55
51	60	90	60
52	65	90	45
53	65	90	55
54	65	90	60
55	70	90	45
56	70	90	55
57	70	90	60
58	75	90	45
59	75	90	55
60	75	90	60
61	80	20	45
62	80	20	55
63	80	20	60
64	85	20	45
65	85	20	55
66	85	20	60
67	90	20	45
68	90	20	55
69	90	20	60
70	95	20	45
71	95	20	55
72	95	20	60

Notes:

1. All input signals have t_{ext} = 10 seconds.
2. All input signals have four (4) die gap transitions
3. All input signals have a shape similar to Figure (any input signal)

12 Appendix E: PID Controllers

Table 12.1 shows the advantages and disadvantages of each type of controller. Using these guidelines, it would be easier to tune the PID-controllers in the EBM system.

Table 12-1: List of Controllers

Control Type	Advantages	Disadvantages
P	• Feedback makes system stable • Feedback increases natural frequency of system (ie makes it faster)	• No control when length first reaches the desired output • As soon as the system is past this point, it begins to correct the error • Only one degree of freedom (Kp) • Does not fix steady-state error
PD	• Before reaching the final value of the step input for the first time, the derivative controller (speed controller) already knows that it needs to slow down • 2 degrees of freedom (Kp, Kd) which means that both the roots and the damping factors can be adjusted to increase the speed of the system	• Does not fix steady-state error • Decreases bandwidth of system • Only controls the system when there is a speed
PI	• Increases type of system by 1 by adding a pole at zero • Eliminates steady-state error, because it controls the system when there is no speed (ie better than PD controller)	• When Ki gets too big, the system becomes unstable because the poles get too close to the imaginary axis • A large Ki also leads to saturation of the system (ie casusing large overshooot)
PID	• Combines all advantages of the previous examples: faster rise time (Kd, and Kp), with no steady-state error (Ki)	• Same observation as for PI controller, the Integral gain is not needed since the steady state error is minimal for the P case. This means that all the Ki is doing is adding instability to the system